NTNU
Norwegian University of
Science and Technology

Modeling and Model Predictive Control of a Conveyor-Belt Dryer

Applied to the Drying of Fish Feed

Tord Johansen van Delft

Master of Science in Engineering Cybernetics
Submission date: June 2010
Supervisor: Morten Hovd, ITK

Norwegian University of Science and Technology
Department of Engineering Cybernetics

Problem Description

Field of study:
Industrial process control

Purpose:
To optimize the control of a conveyor belt dryer for the drying of fish feed.

Prerequisites:
The project is a continuation of
1. The project and diploma work of John Paul Salvador from 2007/2008.
2. The project work of Tord van Delft in 2009.

The student will be supplied with a model of a conveyor-belt dryer.

Main content:
1. Model development
   a. Verification of the existing model
   b. Further development of the model to account for noise and disturbances.
   c. Model simplifications for MPC.
   d. Simulation and evaluation of the process dynamics (open-loop)
2. Development of MPC for the conveyor-belt dryer.
   a. MPC design based on the simplified model.
   b. The MPC algorithm should be computationally efficient and the computational requirements should be realistic for a real implementation..
3. Evaluation of the controller
   a. Nominal stability analysis
   b. Compare the MPC to basic/existing control configurations
4. Optional tasks (if time allows):
   a. Compare the model to the real conveyor-belt dryer.
   b. Evaluate implementation of the controller.
   c. Implementation of controller.

Assignment given: 11. January 2010
Supervisor: Morten Hovd, ITK

Abstract

Moisture control of industrial processes is often difficult and complex. The product composition and moisture content changes as disturbances affect the upstream production processes. When there are changes in the product content, simple control configurations may not work due to changes in the drying characteristics of the product.

This thesis presents a general conveyor-belt dryer model describing a six-zone multiple-pass dryer, accounting for the falling rate drying period, input disturbances, conveyor-belts with different belt speeds and product bed heights. In addition, a description is presented of how linear input dynamics can be included in the dryer model. Furthermore, open loop simulations are performed in order to investigate the behavior of the model.

The model is linearized and reduced, in order to be utilized in a model-based control solution (MPC), where stability and feasibility is ensured through an algorithm based on known techniques within the field of model predictive control (e.g. infinite horizon optimalization, target optimalization routine, soft constraints and a Kalman filter). Several closed loop simulation examples are presented, illustrating reference steps and disturbance rejection. Furthermore, a modeling error is introduced in order to investigate the limitations imposed by model uncertainty. Finally, a basic control solution (PI control) is compared to the model-based control.

Preface

The way toward this thesis has been interesting, exciting and challenging. I have learned much about modeling, simulations and control; both general and of drying processes.

The background for this thesis is based on the previous thesis of John Paul Salvador, regarding the modeling of conveyor-belt dryers, applied on the drying of fish feed. As with his thesis, mine has also been done in cooperation with Goodtech Solutions. And just like he was reqruited in Goodtech after his thesis, so was I.

Goodtech has supplied me with my own office, a laptop, guidance and inspiration. Thanks to Goodtech, and specially John Paul for his invaluable input. I hope this research will be valuable for Goodtech as well as the academia.

I would also like to thank Professor Morten Hovd. His ability to quickly adapt to my current problems and his input of how to approach them has been essential and has guided me through this thesis.

Beyond that, I would like to thank my family for their support and at all times belief in me managing different challenges.

Tord Johansen van Delft
Oslo, Norway - June 7, 2010

Contents

List of Figures

List of Tables

Abbreviations

CV	Controlled Variable
FDA	Finite Difference Approximation
LQR	Linear Quadratic Regulator
MPC	Model Predictive Control
MV	Manipulated Variable
$NTNU$	Norwegian University of Science and Technology
ODE	Ordinary Differential Equation
PDE	Partial Differential Equation
PI	Proportional-Integral (control)
PID	Proportional-Integral-Derivative (control)
PV	Process Variable
QP	Quadratic Programming

Chapter 1

Introduction

Drying processes are complex and moisture control is often difficult. The product composition and moisture changes as disturbances affect the upstream production processes. When there are changes in the product content, simple control configurations may not work due to changes in the drying characteristics of the product. In addition the type of instrument used for moisture measurement is often only compatible or calibrated to some product compositions, and may not work when the product content changes.

The feedstocks to be dried are vast and the methods for drying are many. According to [ASM07], over 400 types of dryers have been reported whereas over 100 distinct types are commonly available. The specifications of these can vary by

- Drying time ranging from 0.25s to 5 months.
- Product size ranging from microns to tens of centimeters.
- Product porosity ranging from 0 to 99.9%.
- Product capacities ranging from 0.1 kg/h to 100 tons/h.
- Product speeds ranging from 0(stationary) to 2000 m/min.
- Heat may be transferred continuously or intermittently by convection, conduction, radiation and electromagnetic fields.

Therefore no single dryer configuration, process model or measurement principle can cover all dryer variants. Specialized applications are needed in order to automatically control the specific dryer. And it is essential to use the knowledge of the material properties coupled with the fundamentals of heat and mass transfer, when modeling an existing dryer.

If a model for the dryer in study is obtained, then model based control could be used on the dryer. In this thesis, model predictive control (MPC) is used to control a conveyor-belt dryer, applied on the drying of fish feed. Even

though the focus of this thesis is on the drying of fish feed, much of the theory used is applicable on other feedstocks as well. Furthermore, the presented control theory is general and can therefore be applied on other processes as well.

1.1 Previous Work

This thesis is a continuation of my final year project [vD09].

A mathematical model of a conveyor-belt dryer zone was first modeled by J.P Salvador in [Sal08a]. Then in [vD09], by using the single zone model, a framework on linearly combining several zones was developed. This framework covered the modeling of multiple-pass conveyor-belt dryers, which included mixing of the product between zones.

In [vD09], a function describing the falling rate was also developed. An attempt to include this function in Salvadors model was done, but it will in this thesis be shown that this model extension was performed with errors.

As this thesis is a continuation of the final year project, some of the content is taken from it. What is used from the project will be stated in advance.

1.2 Motivation

Moisture control is critical for several reasons. When focusing on the drying of fish feed, the moisture content has to be accurately controlled for reasons like product quality, sinking depth, preservation and storage. Further, most products need a proper drying procedure which do not damage the product while drying. High product temperatures influence the nutrition quality, and high product temperature gradients may lead to shrinking and therefore structural changes within the product. Improper drying may lead to irreversible damage to the product quality resulting in a waste of the product.

If a model could be developed for the general conveyor-belt dryer, then the model could be used for moisture and temperature estimation, among others. If, in addition, a MPC was designed for the conveyor-belt dryer, then it could control the product moisture content while simultaneously maintaining a proper drying procedure.

1.3 Scope

The main goal for this thesis is to use MPC on a conveyor-belt dryer, in the drying of fish feed. Further, the thesis will answer how or if the MPC can maintain the following requirements of accuracy, speed of response, stability, robustness and efficiency:

- The exit product moisture content must be close to the desired value at steady state.
- Changes in the desired values should be quickly reached and disturbances should be quickly offset by the controller.
- Oscillations due to controller design are not acceptable.
- The controller should be able to operate successfully under the influence of model uncertainty and large disturbances.
- The computational requirements should be realistic for a real implementation.

And in addition, how will MPC perform compared to PID-control?

Furthermore, if a dryer model differs significantly from a genuine dryer, then even with perfect MPC design, control would be poor. The modeling is therefore emphasized and here are several questions that will be discussed in the thesis: Is it possible to successfully extend the model developed in [Sal08a] to account for the falling rate, input disturbances and input dynamics? If so, is it possible to linearize the nonlinear model and still have an accurate model? Moreover, when simulating the dryer model, will the simulation show a realistic behavior compared to the laws of physics and dryer configuration?

1.4 Thesis Outline

Chapter 2 accounts for the variety of readers, by introducing them to both conveyor-belt dryers and drying theory.

Chapter 3 contains the control theory necessary for MPC design.

Chapter 4 derives the model for the general-conveyor belt dryer.

Chapter 5 considers some model properties through simulations and comparisons.

Chapter 6 is the core of the thesis, where a conveyor-belt dryer is configured, modeled and simulated in both open and closed loop.

Chapter 7 presents the conclusion and suggestions on future work.

Chapter 2

Background Theory

The theory presented in this chapter considering conveyor-belt dryers, dew point temperature, drying basics and drying rate was first presented in [vD09]. But in order to account for the variety of readers, introductions to conveyor-belt dryers and drying theory are given. In addition, because the model has its origin in the production of fish feed, a short overview of the production process is given.

2.1 The Production Process

When modeling and controlling the drying process, knowledge of the overall production process is important. When there are changes in raw material composition, raw material quality, and so on, it influences the drying of the product. And therefore drying of the fish feed is just one of several important steps in the overall production process. The product in this thesis is the same as in [Sal08a]. Therefore the production process is the same, and a illustration of the overall production process is shown in Figure 2.1.

2.2 Conveyor-Belt Dryers

The principle of the conveyor belt dryer is very simple. The product is dropped onto perforated conveyor-belts on which it is transported through several drying chambers. While traveling through a chamber, hot air is forced through the bed of product. The hot air temperature is typically the *manipulated variable* of the dryer. An illustration of one chamber in a conveyor-belt dryer is shown in Figure 2.2.

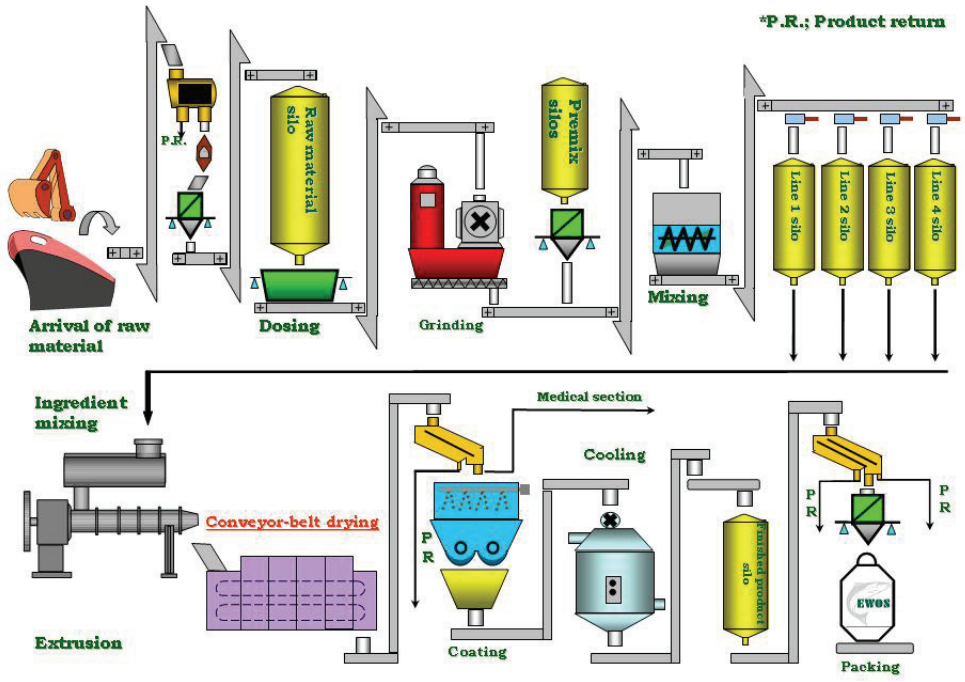

Figure 2.1: Illustration of the overall production process

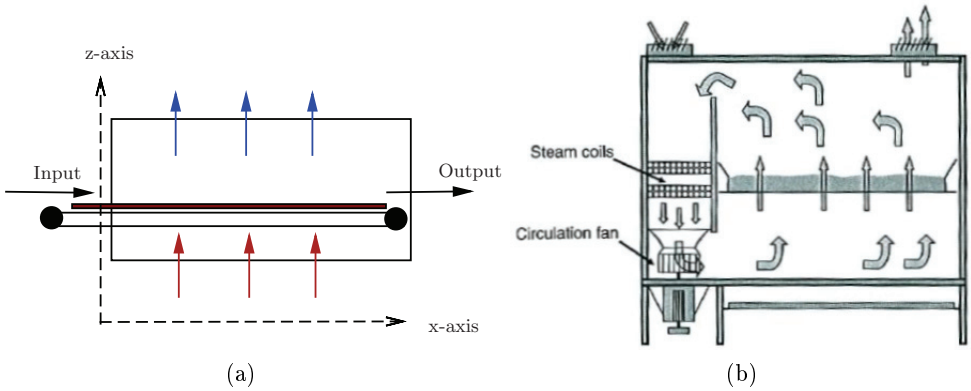

Figure 2.2: Illustration of a drying chamber seen from the side (a) and as a cross-section (b).

2.2.1 Distribution Pattern

Distribution pattern is how the product is distributed on the belt. For the product to dry uniformly throughout the conveyor-belt, the product has to be evenly distributed. A product feeder/spreader is used to distribute the product evenly on the belt. Figure 2.3 illustrates how the airflow follows the path of least resistance, which can give an unevenly distributed drying of the product.

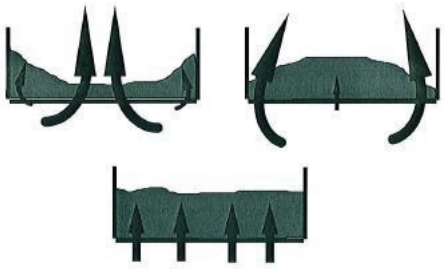

Figure 2.3: Effect of product distribution on the airflow

2.2.2 Dryer Configurations

Typically a conveyor-belt dryer consist of several interconnected chambers (multiple stage dryers). The configuration of the dryers varies in both number of chambers, as well how the chambers are interconnected. In this thesis the terms chamber and zone means the same.

2.2.2.1 Single Pass

In Figure 2.4 a single pass/multiple-stage dryer is shown. This is a configuration where the product simply travels from one chamber to the next until the desired product moisture is reached. It is also possible to vary the bed depth between the chambers. *Single pass* implies that the air used for drying only passes the product once before being dehumidified and reheated.

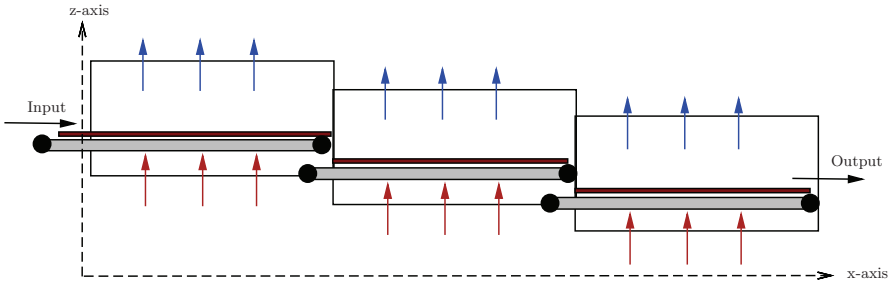

Figure 2.4: Illustration of a single pass/multiple-stage dryer

2.2.2.2 Multiple Pass

In Figure 2.5 a configuration of a multiple pass dryer is shown. The multiple pass dryer offers many of the same benefits as the single pass dryer, but with a much smaller footprint. As seen in the figure, the beds are arranged one above the other, running in opposite directions. The product enters the dryer in the top bed, and cascades down to the lower beds. As the product cascades down to the lower beds, the product often is mixed such that the overall product humidity becomes more uniform. At the same time clumped products also are unclumped. Although the multiple pass dryers have advantages over single pass dryers, zoning of the dryer are more difficult. It is not uncommon that the air used for drying passes the product two or three times. This complex airflow arrangement makes the control of the dryer more complicated. Also, it is not unusual that the final chamber is used for cooling the product.

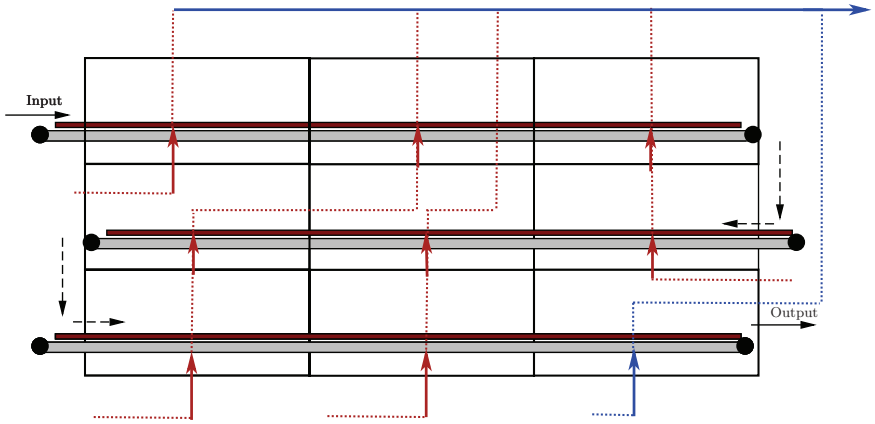

Figure 2.5: Illustration of a multiple pass dryer

2.2.3 Drying Techniques

It is possible to vary both the bed depth and the retention time of the different chambers. Therefore a choice of retention time/bed depth must be made. In order to maximize production at the lowest possible air temperature, the conveyor beds must be run as slowly as possible without allowing the product to get excessively deep. With an excessively deep product, a loss of airflow may increase the drying time of the product, and with some products, excessive depths can cause product clumping or product damage. Multiple-stage conveyor-belt dryers are better suited to cope with these problems, since products leaving the early chambers have a partial dry surface, and therefore typically can be stacked deeper in the later chambers without clumping, product damage or even without a loss of airflow.

In multiple-stage dryers the product often is mixed between some of the chambers such that the overall product humidity becomes more uniform while at the same time clumped products also are unclumped. This mixing can be very simple, where the product is dropped from an elevated chamber to a lower one, or there could be a more mechanical mixing involved.

2.3 Drying Theory

2.3.1 Medium Definitions

The product moisture content is defined as a combination of dry solid and water. When the expression *solid* is used it is referring to the *dry solid* within the product. Furthermore the indexes for the product and solid, are 'p' and 's' respectively.

As with the product, the gas mixture used for drying the product is defined as a combination of dry air and vapor. When the expression *air* is used it is referring to the *dry air* within the gas mixture. Furthermore the indexes for the gas and air, are 'g' and 'a' respectively.

2.3.2 Drying Basics

In conveyor belt dryers, heat transfer occurs by convection between the product and the air. *Convection* is heat transfer that occurs as a result of the movement of fluid in contact with a material. Heat for evaporation is supplied by convection to the exposed surface of the material and the evaporated moisture carried away by the drying air.

When a wet solid is subjected to thermal drying, two processes occur simultaneously:

1. Transfer of energy (mostly as heat) from the surrounding environment to evaporate the surface moisture.

2. Transfer of internal moisture to the surface of the solid and its subsequent evaporation due to process 1

Process 1, the removal of water as vapor from the material surface, depends on the external conditions of:

- temperature of both product and gas
- air humidity and air flow
- area of exposed surface
- pressure.

Process 2, the movement of moisture internally within the solid, is primarily a function of:

- the physical nature of the solid
- the temperature
- the moisture content of the solid.

When the product is saturated with moisture, the internal moisture flow is so high that the entire surface of the solid is covered with water. This period is named the *constant rate drying period*, and what characterizes this period is that process 1 dominates the drying rate of the solid. As the moisture content of the solid decreases, the drying rate is continuously getting more dominated by process 2.

2.3.3 Humidity Ratio

Defining the moisture is important since there are several definitions used both in academia and in the industry. When the expression moisture or humidity is used in this report, it is referring to the humidity ratios defined in (2.1) and (2.2).

Humidity ratio γ is the unit mass of water per unit mass of dry air:

$$\gamma = \frac{m_v}{m_a} \tag{2.1}$$

where m_v is the total mass of vapor, while m_a is the total mass of air not including the vapour.

The humidity ratio α for the solid is defined as:

$$\alpha = \frac{m_w}{m_s} \tag{2.2}$$

where m_w is the total mass of water, while m_s is the total mass of solid not including the water.

Further by utilizing (2.1) and (2.2) the total mass of the product m_p and the air m_a can now be stated as

$$\begin{aligned} m_p &= m_s + m_w \\ &= m_s + m_w \frac{m_s}{m_s} \\ &= m_s(\alpha + 1) \end{aligned} \tag{2.3}$$

$$\begin{aligned} m_g &= m_g + m_v \\ &= m_a + m_v \frac{m_a}{m_a} \\ &= m_a(\gamma + 1) \end{aligned} \tag{2.4}$$

furthermore the total mass M_p[kg/m^3] and M_g[kg/m^3] for each volume unit is given by

$$M_p = \rho_s(\alpha + 1) \tag{2.5}$$

$$M_g = \rho_a(\gamma + 1) \tag{2.6}$$

2.3.4 Dew Point Temperature

The dew point temperature is the temperature at which the gas is saturated with vapor. As a gas is cooled, the dew point temperature is the temperature at which condensation first will occur.

In [Sal08a] it is stated: *The dew point temperature is an important and fundamental property of the air mixture used for drying. For parts of the process, this temperature is proportional to the rate of drying. The temperature of the product will rise toward the air temperature, but will halt at the dew point temperature. While the rate is constant the boundary temperature between liquid water and water vapor equals the dew point temperature. Eventually the product moisture will fall below the critical moisture content, and the product temperature will consequently continue to increase toward the gas temperature.*

By utilizing the ideal gas law and the Clausius-Clapeyron equation, an expression for the dew point temperature can be developed. [Sal08a] states the expression for the dew point temperature T_{dp} as a function of the air moisture γ as

$$T_{dp}(\gamma) = \left[\frac{1}{T_0} - \frac{R_v}{\lambda_0} ln\left(\frac{P_{atm}\gamma}{p_{s,0}(\beta + \gamma)}\right)\right]^{-1} \tag{2.7}$$

where

$$P_{atm} = p_v + p_a \tag{2.8}$$

γ = humidity ratio, air [kg/kg]
T_{dp} = temperature, dew point [°C]
T_0 = reference temperature, gas [K]
p_a = partial pressure, air [hPa]
p_v = partial pressure, vapor [hPa]
$p_{s,0}$ = saturated partial pressure at reference temperature [hPa]
R_v = specific gas constant [J/kg K]
λ_0 = heat of vaporization, water [J/kg]
β = spesific mass ratio, steam/dry air [1]

2.3.5 Drying Rate

The drying rate determines the rate of which moisture evaporates from product to air. It is in this thesis defined as the amount of moisture per volume unit that is evaporated to air per second.

2.3.5.1 Basics

The factors governing the rates of the two processes, heat transfer and mass transfer, determine the drying rate. These factors are primary product temperature, product humidity, air velocity, air temperature, product characteristics, and product size and distribution pattern. The rate of surface evaporation from the product is proportional to the velocity of air passing over it. In general, the higher the air velocity and temperature, the higher is the rate of evaporation.

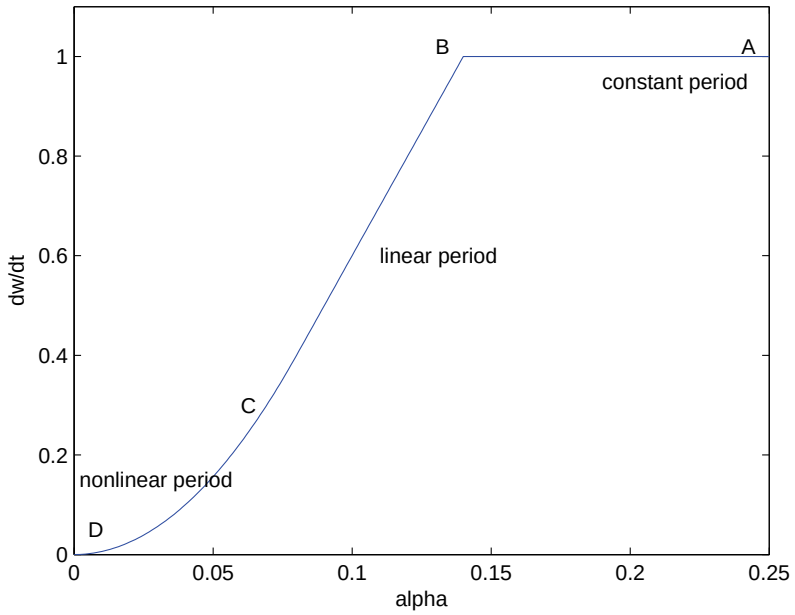

Figure 2.6: Rates of drying as a function of the humidity.

The drying rate of wet solids can typically be categorized in two or three periods. In Figure 2.6 these periods are illustrated. The first period is when the solid is saturated with moisture, and therefore the surface of the solid is also covered with water. We call this periods the *constant-rate drying period*. What characterizes this period is that the rate of drying is independent of the moisture of the solid.

The next period is when the solid is no longer able to completely cover the surface with water. Dry spots on the surface of the solid are appearing, thereby reducing the drying rate of the solid while at the same time the temperature of the solid increases. We call this period the *falling-rate drying period*. The start of this period is known as the *critical product moisture content* α_{crit}. The falling rate can be illustrated as a linear function of humidity.

If the drying rate of the solid has three periods, then the final period is

when the internal product moisture movement controls the rate of drying. The internal moisture movements are caused by mechanisms such as diffusion, capillary flow, and flow due to shrinkage and pressure gradients. The modeling of this period is complex, which results in a nonlinear function of humidity.

2.3.5.2 Modeling The Drying Rate

It is in this thesis assumed that the drying rate with respect to the humidity has the graph illustrated in Figure 2.6. This graph is specific for each product composition, and is chosen as realistic as possible. It is assumed that the critical moisture content B is at $\alpha = 0.14$[kg/kg], and that drying rate has been decreased with a factor of 0.14 when the moisture content is $\alpha = 0.05$[kg/kg].

A smooth function can be obtained by fitting a polynomial to this non-smooth function. This can be done by several methods, the polynomial fit is here done in MATLAB by the use of a least squares approximation. The conveyor-belt dryer in this thesis is assumed to have a product input/output humidity of 25% and 8%, respectively. Therefore a good polynomial fit is only required in this range. In figure 2.7 the polynomial fit is illustrated.

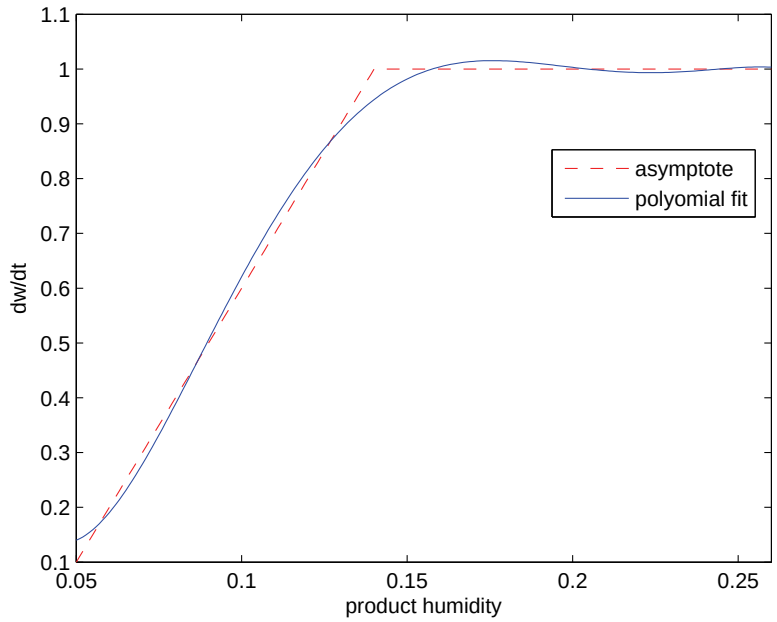

Figure 2.7: Polynomial fit of the rates of drying

The rate of drying as a function of product humidity can now be described by the function

$$\zeta(\alpha) = p_\theta \alpha^\theta + p_{\theta-1}\alpha^{\theta-1} + \cdots + p_1\alpha + p_0 \tag{2.9}$$

where θ is the order of the polynomial approximation

2.4 Energy Theory

The energy theory presented in this section is later used while balancing the energy in the dryer, which further results in evaporization and condensation of the water/vapor, and heat transfer between the product and the air. In [MGV01] it is stated: *to correctly model the physics involved in a conveyor-belt dryer, the model must consider both the specific and latent heat of the product, thereby taking into account the effects of both evaporation and condensation.*

2.4.1 Energy in General

All substances have an internal energy due to the motion and relative position of the constituent atoms and molecules. Absolute values of the internal energy, u, are unknown, but numerical values relative to an arbitrarily defined baseline at a particular temperature can be computed.

In any steady flow system there is an additional energy associated with forcing streams into a system against a pressure and in forcing streams out of the system. This flow work per unit mass is PV, where P is the pressure and V is the specific volume. The internal energy and the flow work per unit mass have been conveniently grouped together into a composite energy called the enthalpy H. The enthalpy is defined by the expression

$$H = u + PV \tag{2.10}$$

Therefore, when doing energy considerations, it is important to define a reference level, where the relative energy is equal zero, from where the energy either increases or deacreases. In this thesis, the modeling is simplified by assuming constant pressures and volumes. Further, to analyze the energy in solids and liquids, it is common to choose the reference level at the *triple-point* of water. The zero enthalpy is now at the water triple-point temperature (0.01°C), where the energy is defined as zero.

2.4.2 Latent Heat of Vaporization

With the reference at the triple-point temperature, the relative energy of water at this temperature is zero. By adding energy to the water the temperature of the water reaches 100°C. Here the water temperature cannot increase anymore at atmospheric pressure. At this point the added energy goes into evaporization of water into vapor. The phase of the water will change from liquid to gas, to fulfill this phase-change energy is needed, and there is a fixed amount of energy required to fulfill this transition. For the case of vaporization the energy required is called the *latent heat of vaporization*. A phase diagram that

shows two phase-changes and how the temperature increases for pure water is illustrated in Figure 2.8

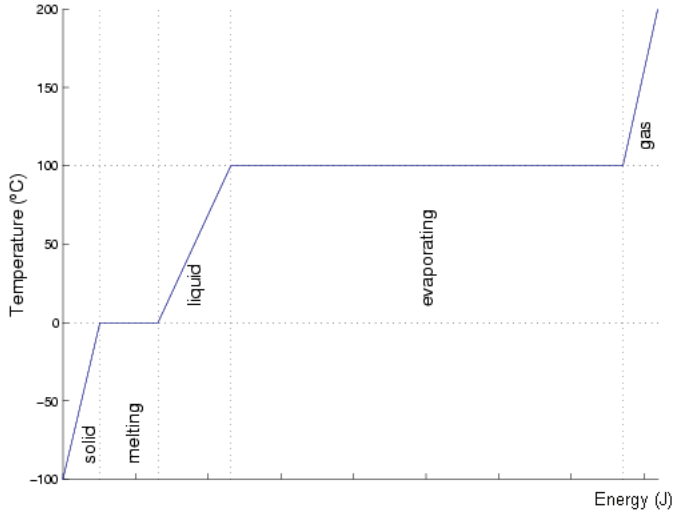

Figure 2.8: Phase diagram for pure water

2.4.3 Product and Air Energies

The relative internal energy for a medium of a fixed volume is given as

$$E = mc_pT \tag{2.11}$$
$$= \rho V c_p T \tag{2.12}$$

where the reference temperature is chosen at the triple-point temperature. To simplify the modeling, the energy is considered per product volume.

2.4.3.1 Product Energy

The energy contained in the product is given as

$$E_p = m_p c_{pp} T_p \tag{2.13}$$

where c_{pp} is the *bulk* specific heat capacity of the composition of water and dry solid. c_{pp} is not directly known, therefore an assumption that the product is a combination of dry solid and water must be made. The energy for the product can now be written as the sum of the dry solid energy and the water

energy:

$$\begin{aligned} E_p &= (m_s c_{ps} + m_w c_{pw}) T_p \\ &= (m_s c_{ps} + m_s \alpha c_{pw}) T_p \\ &= m_s (c_{ps} + \alpha c_{pw}) T_p \\ &= m_s h_p \end{aligned} \tag{2.14}$$

where h_p is known as the enthalpy of the solid and is given as

$$h_p = (c_{ps} + \alpha c_{pw}) T_p \tag{2.15}$$

The same enthalpy is commonly used when modeling conveyor-belt dryers, this is confirmed in both [ASM07] and [CTK94].

In order to inspect the energy balance, the equation describing the change of energy in the product must be defined. In [EG03] the energy equation for a fixed volume is stated as

$$\frac{dE_p}{dt} = V \frac{d}{dt}(u_p \rho_p) = [u_p A_p \rho_p v_p]_{in} - [u_p A_p \rho_p v_p]_{out} \tag{2.16}$$

$$= [u_p w_p]_{in} - [u_p w_p]_{out} \tag{2.17}$$

$$= [w_p c_{pp} T_p]_{in} - [w_p c_{pp} T_p]_{out} \tag{2.18}$$

where u_p is the product internal energy, A_p is the product cross-section area, ρ_p is the product density, v_p is the belt-speed and w_p is the product mass flow given in [kg/s]. Just like (2.13) was decomposed, the terms in (2.18) can be decomposed into

$$w_p c_{pp} T_p = w_s (c_{ps} + \alpha c_{pw}) T_p \tag{2.19}$$

which is obtained by utilizing the definition of α in (2.1). Finally the change of energy can be stated as

$$\frac{dE_p}{dt} = [w_s (c_{ps} + \alpha c_{pw}) T_p]_{in} - [w_s (c_{ps} + \alpha c_{pw}) T_p]_{out} \tag{2.20}$$

where w_s is the mass flow of solid [kg/s] given by

$$w_s = \rho_s v_p A_p \tag{2.21}$$

2.4.3.2 Gas Mixture Energy

The energy of the air has an energy equation very similar as the product energy equation (2.14), but now the *latent heat of vaporization* must be accounted for. The energy of the gas mixture can be formulated as follows

$$E_g = (m_a c_{pa} + m_v c_{pv}) T_g + m_v \lambda_0 \tag{2.22}$$

where the final term in (2.22) is the energy required to convert m_w kg of water into m_v kg of vapor. The term can be interpreted as a form of potential energy, where the potential energy increases as the amount of vapor increases, or vice versa. λ_0 is the fixed amount of energy required to fulfill the transition of 1 kg water into 1 kg of vapor. In this thesis, it is assumed that the vaporization occurs at 100°C at the pressure of 1.014 Bar. Furthermore (2.22) can be expressed as

$$\begin{aligned} E_g &= (m_a c_{pa} + m_a \gamma c_{pv}) T_g + m_a \gamma \lambda_0 \\ E_g &= m_a \big[(c_{pa} + \gamma c_{pv}) T_g + \gamma \lambda_0 \big] \\ E_g &= m_a h_g \end{aligned} \tag{2.23}$$

where h_g is known as the enthalpy of the gas and is given by

$$h_g = (c_{pa} + \gamma c_{pv}) T_g + \gamma \lambda_0 \tag{2.24}$$

where the same enthalpy is commonly used when modeling conveyor-belt dryers, this is confirmed in both [CTK94] and [ASM07]. In the latter, it is stated that (2.24) is not recommended above a humidity of 0.05 [kg/kg]. In the case that the humidity exceeds this limit, then more general and complex equations are to be used.

Further the equation describing change of energy in the air is defined. Similar to (2.20) the equation for a fixed volume of gas is derived to

$$\frac{dE_g}{dt} = \big[w_a [(c_{pa} + \gamma c_{pv}) T_g + \gamma \lambda_0] \big]_{in} - \big[w_a [(c_{pa} + \gamma c_{pv}) T_g + \gamma \lambda_0] \big]_{out} \tag{2.25}$$

where w_a is the mass flow of air [kg/s] given by

$$w_a = \rho_a v_g A_g \tag{2.26}$$

Chapter 3

Control Theory

This chapter contains the theory necessary for designing the conveyor-belt dryer control. The theory is general and does not focus on the conveyor-belt dryer control. Later on, in chapter 6, the theory from this chapter is set in context with the control of conveyor-belt dryers.

3.1 Terminology

- *Inputs* are mediums entering the process. Inputs can be divided into two terms, manipulated variables(MVs) and disturbances.
- *Manipulated variables* are those process inputs which are manipulated by the controller.
- *Disturbances* are those process inputs which are not manipulated by the controller.
- *Outputs* are mediums exiting the process.
- *Process variables*(PVs) are variables residing inside the process.
- *Controlled variables*(CVs) are those PVs and outputs which are controlled and have set points associated with them. These are either measured or estimated.
- *Measurements* are measured PVs and outputs. These are always subjected to measurement noise, and are therefore never completely accurate.

3.2 Linear Stability Concepts

A linear system is said to be *marginally stable* if all the poles of the system have a real part less than or equal to zero. If the system is in discrete form,

the poles of the system must be within or at the edge of the unit disc. In either case, this results in, that for every finite initial state x_0, there exists a bounded response.

A linear system is said to be *asymptotically stable* if all the poles of the system have a real part less than zero. If the system is in discrete form, the poles of the system must be within the unit disc. In either case, the result is, that for every finite initial state x_0 there exists a bounded response, which, in addition, approaches zero as time moves towards infinity.

In [Che99], Chen defines the concepts of controllability and observability as:

- A linear system is said to be *controllable* if for any initial state $x(0) = x_0$ and any final state x_1, there exists an input that transfers x_0 to x_1 in a finite time. Otherwise the system is said to be uncontrollable.

- A linear system is said to be *observable*, if for any unknown initial state $x(0)$, there exist a finite $t_1 > 0$ such that the knowledge of the input u and the output y over $[0, t_1]$ suffices to determine uniquely the initial state $x(0)$. Otherwise the system is said to be unobservable.

Furthermore, weaker definitions than those defined above are also used in this thesis:

- An uncontrollable system can be *stabilizable*, given that all the uncontrollable states in the state vector x, are asymptotically stable states. This means that the system is controllable to some degree: All controllable states can be moved to their desired locations in finite time and the states that are uncontrollable approaches zero in a finite time.

- An unobservable system can be *detectable*, given that all the unobservable states in the state vector x, are asymptotically stable states. This means that the system is observable to some degree: All initial states which are observable can be determined in finite time and the states that are unobservable approaches zero in a finite time.

3.3 Model Simplification

Modern controller design methods such as H_∞, LQG, and MPC produce controllers of order at least equal to that of the plant. These control laws may be to complex with regards to practical implementation, and simpler models are then sought. This section describes a method for reducing the order of a plant or controller model. There are many different methods for simplifying a model, but in this thesis the best results were obtained with the method *balanced residualization*.

3.3.1 Balanced Realization

A balanced realization is an asymptotically stable minimal realization in which the controllability and observability Gramians are equal and diagonal, [SP05]. A rational, stable and minimal realization $G(s)$ is called balanced if the solutions to the Lyapunov equations

$$AP + PA^T + BB^T = 0 \tag{3.1}$$
$$A^TQ + QA + C^TC = 0 \tag{3.2}$$

are $P = Q = diag(\sigma_1, \sigma_2, ..., \sigma_n) = \sum$ where $\sigma_1 \geq \sigma_2 \geq .. \geq \sigma_n > 0$. P and Q are the controllability and observability Gramians. The σ_i's are the ordered Hankel singular values of G(s). In a balanced realization the value of each σ_i is associated with a state x_i of the balanced system. And the size of σ_i is a relative measure of the contribution that x_i makes to the input-output behavior of the system. This property is fundamental to many model reduction methods, which work by removing states having little effect on the system's input-output behavior.

3.3.2 Residualization

Let (A,B,C,D) be a minimal realization of a stable system G(s), and partion the state vector x, of dimension n, into $\begin{bmatrix} x_1 \\ x_2 \end{bmatrix}$ where x_2 is the vector of $n-k$ states which we wish to remove. With appropriate partioning of A,B and C, the state-space equations become

$$\dot{x}_1 = A_{11}x_1 + A_{12}x_2 + B_1u \tag{3.3}$$
$$\dot{x}_2 = A_{21}x_1 + A_{22}x_2 + B_2u \tag{3.4}$$
$$y = C_1x_1 + C_2x_2 + Du \tag{3.5}$$

In residualization x_2 is removed by setting $\dot{x}_2 = 0$, then by solving x_2 in terms of x_1 and u, (3.3)-(3.5) becomes

$$\dot{x}_1 = (A_{11} - A_{12}A_{22}^{-1}A_{21})x_1 + (B_1 - A_{12}A_{22}^{-1}B_2)u \tag{3.6}$$
$$y = C_1 - C_2A_{22}^{-1}A_{21}x_1 + D - C_2A_{22}^{-1}B_2u \tag{3.7}$$

Here A_{22} must be invertible. Furthermore we can define the reduced model $G_r(s) = (A_r, B_r, C_r, D_r)$ as

$$\dot{x}_r = A_rx_r + B_ru \tag{3.8}$$
$$y = C_rx_r + D_ru \tag{3.9}$$

where

$$A_r = (A_{11} - A_{12}A_{22}^{-1}A_{21}) \tag{3.10}$$
$$B_r = (B_1 - A_{12}A_{22}^{-1}B_2) \tag{3.11}$$
$$C_r = C_1 - C_2A_{22}^{-1}A_{21} \tag{3.12}$$
$$D_r = D - C_2A_{22}^{-1}B_2 \tag{3.13}$$

An important property of residualization is that it preserves the steady state gain of the system, $G_r(0) = G(0)$. This is because the residualization process sets the derivatives to zero, which at steady state are zero anyway. The reduced model $G_r(s)$ is accurate at low frequencies, at higher frequencies the poles of $G_r(s)$ differs from $G(s)$ and it is therefore recommended to use techniques as truncation for high frequency modeling. More details about truncation and residualization can be found in [SP05].

3.3.3 Balanced Residualization

Balanced residualization is obtained by finding a balanced realization of G(s), then by using residualization on the balanced equation, a reduced model is obtained where the states having little effect on the input/output behavior are removed. A more detailed approach is explained in the algorithm below:

1. Obtain $G_{bal}(s)$, and g by balancing $G(s)$ where $g = [\sigma_1, \sigma_2, ..., \sigma_n]^T$.
2. Find a tolerance that decides which states should be removed from the balanced model.
3. Every state belonging to the element in g which is below this tolerance should be a part of the x_2 vector of states defined in (3.4)
4. Because (3.3)-(3.5) is balanced and x_1 and x_2 is known, the reduced model is given by equations (3.8)-(3.13)

3.4 Model Predictive Control

Model predictive control (MPC) can account for constraints in the input, output and process states. These constraints are meet while simultaneous either maximizing the throughput, minimizing the input or by combinations of these. The controller uses mathematical programming for optimizing predicted future performance and handles constraints on inputs as well as states and outputs.

The most common type of MPC is the *linear MPC*, which uses linear process models for prediction and convex quadratic programming (QP) for optimization of a quadratic objective function. The objective function is a

quadratic weighting of future manipulated variables and set points errors. Although the first MPC applications optimized performance on a finite horizon, it is just as easy to optimize performance on the infinite horizon.

3.4.1 Structure Choice

All model predictive controllers have different configurations. The controller used in this thesis, optimizes over the *infinite horizon*, where it uses the linear quadratic regulator (LQR) after the input horizon. This is allowed by assuming that the controller, by the end of the input horizon, has steered the plant to a region in which the constraints are passive. The infinite horizon optimization is actually a finite horizon optimization, where the weight on the terminal 'state' $\bar{Q}$ is calculated in such a way that it contributes the same to the objective function, as would have been obtained with a LQR from the input-horizon to infinity.

Further, in order to ensure that the controller finds a feasible solution within the constraints, a *reference target* is calculated. For example, due to disturbances, the plant can be pushed into a region in which the desired value cannot be reached without violating the constraints. Then by calculating the closest point the controller can achieve without constrain violation, the optimal target for the situation is calculated.

In order for the controller to calculate the optimal input sequence, the states of the plant must be known, even the unmeasured ones. This is only possible by estimating them, which brings up *estimator design*. Now, by applying a Kalman filter, optimal estimates for the plant is obtained by correcting the model with online measurements from the plant. The model update law is important in order to estimate the effects of disturbances and modeling errors[1], making the model diverge from the plant.

The MPC algorithm should be computationally efficient and the computational requirements should be realistic for a real implementation. Therefore, the MPC algorithm does not use the nonlinear model for optimizing; instead it uses a linear model reduced by *balanced residualization*. In addition to this, the algorithm is only optimizing with future inputs as optimization variables. Choosing future inputs as optimization variables decreases the number of optimization variables drastically, depending on how many states the reduced model consists of.

The structure of the MPC is illustrated in Figure 3.1. It can be seen that by measuring the inputs and outputs, the estimator supply the target calculation with the estimated disturbances. The main optimizing routine is supplied with the desired trajectories and model estimates.

[1] Modeling errors can sometimes affect the estimates the same way disturbances could, and the estimator can therefore compensate for modeling errors by assuming artificial disturbances affecting the plant.

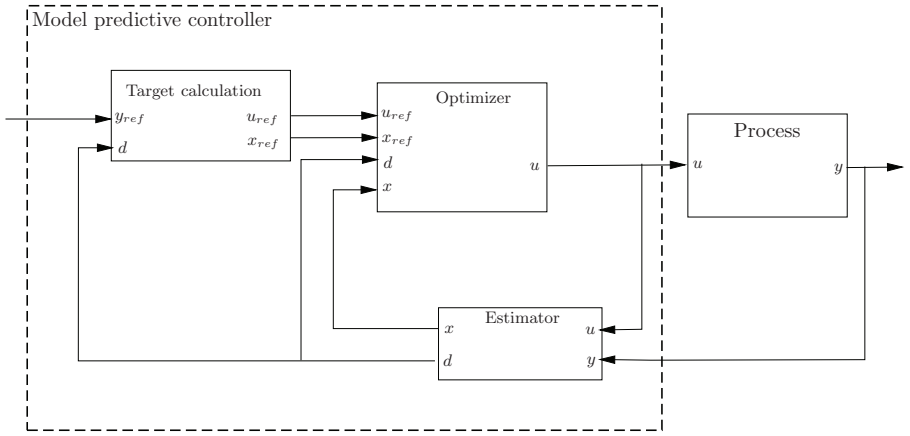

Figure 3.1: Illustration of the MPC structure

3.4.2 The MPC QP Formulation

The process which is to be controlled is described by the discrete state space model

$$x_{k+1} = Ax_k + Bu_k + B_d d_k \tag{3.14}$$
$$y_k = Cx_k + Du_k + Ed \tag{3.15}$$

The objective we want to obtain by control, is to optimize performance by minimizing the cost function

$$V_k = \sum_{i=1}^{\infty} ||\hat{y}_{k+i|k} - t_{k+i|k}||_Q^2 + \sum_{i=0}^{H_u-1} ||\hat{u}_{k+i|k} - \tilde{t}_{k+i|k}||_R^2 \tag{3.16}$$

where the norm is defined as

$$||Z||_M^2 = Z^T M Z \tag{3.17}$$

The matrices Q and R are tuning parameters which must fulfill the conditions

$$Q \geq 0 \tag{3.18}$$
$$R > 0 \tag{3.19}$$

in order for the QP problem to be convex.

In most MPC applications there are constraints which are not to be violated (and if there are no constraints, there is probably little reason to use MPC in the first place). These constraints can be on the states, the inputs or the outputs. In this thesis the constraints are on the inputs and outputs (the states are indirectly affected tough):

$$Y_l \leq y_k \leq Y_u \tag{3.20}$$
$$U_l \leq u_k \leq U_u \tag{3.21}$$

The optimization criteria can now be summarized as

$$\min V_k \tag{3.22}$$

$$s.t$$

$$x_{k+1} = Ax_k + Bu_k + B_d d_k \tag{3.23}$$
$$y_k = Cx_k + Du_k + Ed \tag{3.24}$$

$$Y_l \leq y_k \leq Y_u \qquad 1 \leq k \leq H_u - 1 \tag{3.25}$$
$$U_l \leq u_k \leq U_u \qquad 0 \leq k \leq H_u - 1 \tag{3.26}$$

This optimization criterion can be somewhat explained with words:

The objective is to minimize the distance between the output-trajectory and output while minimizing the use of the input, without violating the constraints imposed by physical process limitations or user specific needs. By doing this minimization, the controller is predicting the optimal input sequence by using the model equations (3.14) and (3.15).

3.4.3 Infinite Horizon

To ensure stability an infinite prediction horizon is chosen. If the objective function (3.16) had a finite horizon, then the controller would have no knowledge of the process after time step $k = H_u$, and the process output could approach infinity.

At first, the objective function stated in (3.16) is split into

$$\begin{aligned} V_k = \sum_{i=1}^{H_u-1} ||\hat{y}_{k+i|k} - t_{k+i|k}||_Q^2 + \sum_{i=0}^{H_u-1} ||\hat{u}_{k+i|k} - \tilde{t}_{k+i|k}||_R^2 \\ + \sum_{i=H_u}^{\infty} ||\hat{y}_{k+i|k} - t_{k+i|k}||_Q^2 \end{aligned} \tag{3.27}$$

The desired target is given by

$$t_{k+i|k} = C\bar{t}_{k+i|k} + D\tilde{t}_{k+i|k} + Ed_{\infty|k} \tag{3.28}$$

where

$$t_{k+i|k} = \text{trajectory for } y_{k+1} \tag{3.29}$$
$$\bar{t}_{k+i|k} = \text{trajectory for } x_{k+1} \tag{3.30}$$
$$\tilde{t}_{k+i|k} = \text{trajectory for } u_{k+1} \tag{3.31}$$

are the steady state targets for the infinite horizon, and $d_{\infty|k}$ is the estimated disturbance at timestep k, which is assumed constant for all $t \geq k$. By substituting (3.15) and (3.28) into the final sum in (3.27), the sum can be stated as

$$\begin{aligned}\sum_{i=H_u}^{\infty} ||\hat{y}_{k+i|k} - t_{k+i|k}||_Q^2 = \sum_{i=H_u}^{\infty} ||C(x_{k+i|k} - \bar{t}_{k+i|k}) \\ +D(u_{k+i|k} - \tilde{t}_{k+i|k}) + E(d_{k+i|k} - d_{\infty|k})||_Q^2\end{aligned} \tag{3.32}$$

Then, by assuming that all constraints are respected after the control horizon H_u, a stabilizing controller[2] $u_k = K(\bar{t}_k - x_k)$ for $i \geq H_u$ is used. Furthermore, by assuming that the disturbances d_k are constant and that the inputs follows their desired targets (which is the case since the constraints are within their bounds), then the sum (3.32) is rewritten as

$$\sum_{i=H_u}^{\infty} ||\hat{y}_{k+i|k} - t_{k+i|k}||_Q^2 = \sum_{i=H_u}^{\infty} ||C(x_{k+i|k} - \bar{t}_{k+i|k})||_Q^2 \tag{3.33}$$

Futher, the state equation (3.14) can be stated as

$$x_{k+1} = [A - BK]x_k + BK\bar{t}_k + B_d d_k \tag{3.34}$$

where the desired target is given by

$$\bar{t}_{k+1} = [A - BK]\bar{t}_k + BK\bar{t}_k + B_d d_{\infty|k} \tag{3.35}$$

The future states can now be expressed as

$$\begin{aligned}x_{k+H_u+1|k} - \bar{t}_{k+H_u+1|k} &= [A - BK](x_{k+H_u|k} - \bar{t}_{k+H_u|k}) \\ x_{k+H_u+2|k} - \bar{t}_{k+H_u+2|k} &= [A - BK]^2(x_{k+H_u|k} - \bar{t}_{k+H_u|k}) \\ &\vdots \\ x_{k+H_u+j|k} - \bar{t}_{k+H_u+j|k} &= [A - BK]^j(x_{k+H_u|k} - \bar{t}_{k+H_u|k})\end{aligned}$$

[2]The stabilizing controller used in this thesis, is the linear quadratic regulaor (LQR), designed with the same tuning matrices as the MPC

which will converge to zero given that [A-BK] has all eigenvalues within the unit disc. The sum (3.33) is furter rewritten as

$$\sum_{i=H_u}^{\infty} ||\hat{y}_{k+i|k} - t_{k+i|k}||_Q^2 = (x_{k+Hu|k} - \bar{t}_{k+Hu|k})^T \bar{Q} (x_{k+Hu|k} - \bar{t}_{k+Hu|k}) \quad (3.36)$$

where

$$\bar{Q} = \left[\sum_{i=0}^{\infty} ([A - BK]^T)^i C^T Q C [A - BK]^i \right] \quad (3.37)$$

According to [Mac02], given that $Q \geq 0$, and that [A-BK] has all its eigenvalues iniside the unit disc, the Lyapunov equation

$$[A - BK]^T \bar{Q} [A - BK] = \sum_{i=1}^{\infty} ([A - BK]^T)^i C^T Q C [A - BK]^i \quad (3.38)$$

$$= \bar{Q} - C^T Q C \quad (3.39)$$

can be solved for $\bar{Q}$.

3.4.4 Future Inputs as Optimization Variables

It is here shown how the optimization criteria can be expressed with future inputs as optimization variables. First it is shown how to substitute the future states into the objective function, then into the constraints equations.

3.4.4.1 Stacking the Future Inputs

By defining the input $v_k = u_k - \tilde{t}_k$ and state $\chi_k = x_k - \bar{t}_k$ deviations, and by stacking the state references $\bar{t}_k$, input references $\tilde{t}_k$, input deviations v_k, state deviations χ_k, and predicted disturbances d_k in vectors $\bar{t}$, $\tilde{t}$, v, χ, d:

$$\tilde{t} = \begin{bmatrix} \tilde{t}_0 \\ \tilde{t}_1 \\ \vdots \\ \tilde{t}_{H_u-2} \\ \tilde{t}_{H_u-1} \end{bmatrix}; \qquad \bar{t} = \begin{bmatrix} \bar{t}_1 \\ \bar{t}_2 \\ \vdots \\ \bar{t}_{H_u-1} \\ \bar{t}_{H_u} \end{bmatrix} \quad (3.40)$$

$$v = \begin{bmatrix} v_0 \\ v_1 \\ \vdots \\ v_{H_u-2} \\ v_{H_u-1} \end{bmatrix}; \qquad \chi = \begin{bmatrix} \chi_1 \\ \chi_2 \\ \vdots \\ \chi_{H_u-1} \\ \chi_{H_u} \end{bmatrix}; \qquad d = \begin{bmatrix} d_0 \\ d_1 \\ \vdots \\ d_{H_u-2} \\ d_{H_u-1} \end{bmatrix} \quad (3.41)$$

the future state target can be expressed as

$$\chi + \bar{t} = \begin{bmatrix} A \\ A^2 \\ \vdots \\ A^{H_u-1} \\ A^{H_u} \end{bmatrix} x_0 + \begin{bmatrix} B & 0 & \cdots & 0 & 0 \\ AB & B & \ddots & \vdots & \vdots \\ \vdots & \vdots & \ddots & 0 & 0 \\ A^{H_u-2}B & A^{H_u-3}B & \cdots & B & 0 \\ A^{H_u-1}B & A^{H_u-2}B & \cdots & AB & B \end{bmatrix} (v + \tilde{t}) \tag{3.42}$$

$$+ \begin{bmatrix} B_d & 0 & \cdots & 0 & 0 \\ AB_d & B_d & \ddots & \vdots & \vdots \\ \vdots & \vdots & \ddots & 0 & 0 \\ A^{H_u-2}B_d & A^{H_u-3}B_d & \cdots & B_d & 0 \\ A^{H_u-1}B_d & A^{H_u-2}B_d & \cdots & AB_d & B_d \end{bmatrix} d \tag{3.43}$$

$$= \Psi x_0 + \Theta(v + \tilde{t}) + \Xi d \tag{3.44}$$

$$\Downarrow$$

$$\chi = \Psi x_0 + \Theta(v + \tilde{t}) + \Xi d - \bar{t} \tag{3.45}$$

3.4.4.2 The objective function

The first two terms in the objective function (3.27) can now be stated as

$$\sum_{i=1}^{H_u-1} ||\hat{y}_{k+i|k} - t_{k+i|k}||_Q^2 + \sum_{i=0}^{H_u-1} ||v_{k+i|k}||_R^2 \tag{3.46}$$

Then by substitution of the measurement (3.15) and target (3.28) equations the terms is rewritten as

$$\sum_{i=1}^{H_u-1} ||C\chi_{k+i|k} + Dv_{k+i|k}||_Q^2 + \sum_{i=0}^{H_u-1} ||v_{k+i|k}||_R^2 \tag{3.47}$$

$$= \sum_{i=1}^{H_u-1} \left[\chi_{k+i|k}^T C^T Q C \chi_{k+i|k} + v_{k+i|k}^T D^T Q D v_{k+i|k} + 2\chi_{k+i|k}^T C^T Q D v_{k+i|k} \right] \tag{3.48}$$

$$+ \sum_{i=0}^{H_u-1} v_{k+i|k}^T R v_{k+i|k}$$

$$= \sum_{i=1}^{H_u-1} \left[\chi_{k+i|k}^T C^T Q C \chi_{k+i|k} + v_{k+i|k}^T [D^T Q D + R] v_{k+i|k} + 2\chi_{k+i|k}^T C^T Q D v_{k+i|k} \right] \tag{3.49}$$

$$+ v_0^T R v_0$$

$$= \sum_{i=1}^{H_u-1} \left[\chi_{k+i|k}^T \tilde{Q} \chi_{k+i|k} + v_{k+i|k}^T \tilde{R} v_{k+i|k} + \chi_{k+i|k}^T \tilde{G} v_{k+i|k} \right] + v_0^T R v_0 \tag{3.50}$$

where

$$\tilde{Q} = C^T Q C; \qquad \tilde{R} = D^T Q D + R \qquad \tilde{G} = 2C^T Q D \tag{3.51}$$

Now, by introducing the matrices

$$\hat{Q} = \begin{bmatrix} \tilde{Q} & 0 & \cdots & 0 & 0 \\ 0 & \tilde{Q} & \ddots & \vdots & \vdots \\ 0 & 0 & \ddots & 0 & 0 \\ \vdots & \vdots & \ddots & \tilde{Q} & 0 \\ 0 & 0 & \cdots & 0 & \bar{Q} \end{bmatrix}; \qquad \hat{R} = \begin{bmatrix} R & 0 & \cdots & 0 & 0 \\ 0 & \tilde{R} & \ddots & \vdots & \vdots \\ 0 & 0 & \ddots & 0 & 0 \\ \vdots & \vdots & \ddots & \tilde{R} & 0 \\ 0 & 0 & \cdots & 0 & \tilde{R} \end{bmatrix} \tag{3.52}$$

$$G = \begin{bmatrix} \tilde{G} & 0 & \cdots & 0 & 0 \\ 0 & \tilde{G} & \ddots & \vdots & \vdots \\ 0 & 0 & \ddots & 0 & 0 \\ \vdots & \vdots & \ddots & \tilde{G} & 0 \\ 0 & 0 & \cdots & 0 & \tilde{G} \end{bmatrix} \tag{3.53}$$

and by using (3.36) and (3.50) the objective function for the infinite horizon (3.27) can be stated as

$$V = \chi^T \hat{Q} \chi + v^T \hat{R} v + \chi'^T G v' \tag{3.54}$$

where

$$\chi' = \begin{bmatrix} \chi_1 \\ \chi_2 \\ \vdots \\ \chi_{H_u-2} \\ \chi_{H_u-1} \end{bmatrix} = \begin{bmatrix} I & 0 & \cdots & 0 & 0 & 0 \\ 0 & I & \ddots & \vdots & \vdots & \vdots \\ 0 & 0 & \ddots & 0 & 0 & 0 \\ \vdots & \vdots & \ddots & I & 0 & 0 \\ 0 & 0 & \cdots & 0 & I & 0 \end{bmatrix} \chi = I_\chi \chi; \tag{3.55}$$

$$v' = \begin{bmatrix} v_1 \\ v_2 \\ \vdots \\ v_{H_u-2} \\ v_{H_u-1} \end{bmatrix} = \begin{bmatrix} 0 & I & 0 & \cdots & 0 & 0 \\ 0 & 0 & I & \ddots & \vdots & \vdots \\ 0 & 0 & 0 & \ddots & 0 & 0 \\ \vdots & \vdots & \vdots & \ddots & I & 0 \\ 0 & 0 & 0 & \cdots & 0 & I \end{bmatrix} v = I_v v, \tag{3.56}$$

Finally by substituting (3.45), (3.55) and (3.56) into (3.54), and by removing the terms which does not affect the solution, the objective function becomes

$$\boxed{V = v^T H v + f v} \tag{3.57}$$

where

$$H = H_1 + H_2 + \hat{R} \qquad f = f_1 + f_2 \tag{3.58}$$

$$H_1 = \Theta^T \hat{Q} \Theta \qquad f_1 = 2\left[\Psi x_0 + \Theta\tilde{t} + \Xi d - \vec{t}\right]^T \hat{Q}\Theta \tag{3.59}$$

$$H_2 = \Theta^T I_\chi^T \hat{G} I_v \qquad f_2 = \left[\Psi x_0 + \Theta\tilde{t} + \Xi d - \vec{t}\right]^T I_\chi^T \hat{G} I_v \tag{3.60}$$

3.4.4.3 Constraints

By introducing the vectors

$$\hat{Y}_l = \begin{bmatrix} Y_l \\ \vdots \\ Y_l \end{bmatrix}; \qquad \hat{Y}_u = \begin{bmatrix} Y_u \\ \vdots \\ Y_u \end{bmatrix}; \qquad \hat{U}_l = \begin{bmatrix} U_l \\ \vdots \\ U_l \end{bmatrix}; \qquad \hat{U}_u = \begin{bmatrix} U_u \\ \vdots \\ U_u \end{bmatrix}, \tag{3.61}$$

the constraints over the horizon can be stated as

$$\hat{Y}_l \leq y \leq \hat{Y}_u \tag{3.62}$$

$$\hat{U}_l \leq u \leq \hat{U}_u \tag{3.63}$$

The future outputs are given by

$$y = \begin{bmatrix} y_1 \\ y_2 \\ \vdots \\ y_{Hu-1} \end{bmatrix} = \underbrace{\begin{bmatrix} C & 0 & \cdots & 0 \\ 0 & C & \cdots & 0 \\ \vdots & \vdots & \ddots & \vdots \\ 0 & 0 & \cdots & C \end{bmatrix}}_{\hat{C}} \begin{bmatrix} x_1 \\ x_2 \\ \vdots \\ x_{Hu-1} \end{bmatrix} \tag{3.64}$$

$$+ \underbrace{\begin{bmatrix} D & 0 & \cdots & 0 \\ 0 & D & \cdots & 0 \\ \vdots & \vdots & \ddots & \vdots \\ 0 & 0 & \cdots & D \end{bmatrix}}_{\hat{D}} \begin{bmatrix} u_1 \\ u_2 \\ \vdots \\ u_{Hu-1} \end{bmatrix} \tag{3.65}$$

$$+ \underbrace{\begin{bmatrix} E & 0 & \cdots & 0 \\ 0 & E & \cdots & 0 \\ \vdots & \vdots & \ddots & \vdots \\ 0 & 0 & \cdots & E \end{bmatrix}}_{\hat{E}} \begin{bmatrix} d_1 \\ d_2 \\ \vdots \\ d_{Hu-1} \end{bmatrix} \tag{3.66}$$

and by simple manipulation of the x,u and d vectors, the future outputs can be stated as

$$y = \hat{C}x' + \hat{D}u' + \hat{E}d' \tag{3.67}$$

$$= \hat{C}I_x x + \hat{D}I_u u + \hat{E}I_d d \tag{3.68}$$

$$= \hat{C}I_x(\chi + \bar{t}) + \hat{D}I_u(v + \tilde{t}) + \hat{E}I_d d \tag{3.69}$$

where $I_x = I_\chi$, $I_u = I_v$, are defined by equations (3.55) and (3.56), respectively. I_d is given by

$$d' = \begin{bmatrix} d_1 \\ d_2 \\ \vdots \\ d_{H_u-2} \\ d_{H_u-1} \end{bmatrix} = \begin{bmatrix} 0 & I & 0 & \cdots & 0 & 0 \\ 0 & 0 & I & \ddots & \vdots & \vdots \\ 0 & 0 & 0 & \ddots & 0 & 0 \\ \vdots & \vdots & \vdots & \ddots & I & 0 \\ 0 & 0 & 0 & \cdots & 0 & I \end{bmatrix} d = I_d d, \tag{3.70}$$

Furthermore substitution of (3.45) for χ gives

$$y = \hat{C} I_x \left[\Psi x_0 + \Theta(v + \tilde{t}) + \Xi d \right] + \hat{D} I_u (v + \tilde{t}) + \hat{E} I_d d \tag{3.71}$$

$$= \hat{C} I_x \Psi x_0 + [\hat{C} I_x \Theta + \hat{D} I_u] v + [\hat{C} I_x \Theta + \hat{D} I_u] \tilde{t} + [\hat{C} I_x \Xi + \hat{E} I_d] d \tag{3.72}$$

and the constraints over the horizon for the output can now be stated as

$$\begin{bmatrix} \hat{C} I_x \Theta + \hat{D} I_u \\ -\hat{C} I_x \Theta - \hat{D} I_u \end{bmatrix} v \leq \begin{bmatrix} \hat{Y}_u - \hat{C} I_x \Psi x_0 - [\hat{C} I_x \Theta + \hat{D} I_u] \tilde{t} - [\hat{C} I_x \Xi + \hat{E} I_d] d \\ -\hat{Y}_l + \hat{C} I_x \Psi x_0 + [\hat{C} I_x \Theta + \hat{D} I_u] \tilde{t} + [\hat{C} I_x \Xi + \hat{E} I_d] d \end{bmatrix} \tag{3.73}$$

The contraints over the horizon for the inputs are somewhat simpler, and can be stated as

$$\begin{bmatrix} I \\ -I \end{bmatrix} v \leq \begin{bmatrix} \hat{U}_u - \tilde{t} \\ -\hat{U}_l + \tilde{t} \end{bmatrix} \tag{3.74}$$

Finally by combining (3.73) and (3.74) the constraints over the horizon becomes

$$\begin{bmatrix} \hat{C} I_x \Theta + \hat{D} I_u \\ -\hat{C} I_x \Theta - \hat{D} I_u \\ I \\ -I \end{bmatrix} v \leq \begin{bmatrix} \hat{Y}_u - \hat{C} I_x \Psi x_0 - [\hat{C} I_x \Theta + \hat{D} I_u] \tilde{t} - [\hat{C} I_x \Xi + \hat{E} I_d] d \\ -\hat{Y}_l + \hat{C} I_x \Psi x_0 + [\hat{C} I_x \Theta + \hat{D} I_u] \tilde{t} + [\hat{C} I_x \Xi + \hat{E} I_d] d \\ \hat{U}_u - \tilde{t} \\ -\hat{U}_l + \tilde{t} \end{bmatrix} \tag{3.75}$$

$$\Downarrow$$

$$\Omega' v \leq \omega' \tag{3.76}$$

3.4.4.4 Including constraints in the change of measurements

In some cases, it is desirable that the change of measurement from one time step to the next is below some level. In other words, there are constraints in the change of measurements over the horizon.

Given a vector of selected measurements $y_{e,k}$ k defined by

$$y_{e,k} = C_e x_k + D_e u_k + E_e d_k \tag{3.77}$$

where C_e, D_e and E_e consists of selected rows in the matrices C, D and E from (3.15).

The constraint over the horizon can be formulated as

$$-\Delta y_e \leq y_{e,k+1} - y_{e,k} \leq \Delta y \qquad 0 \leq k \leq H_u - 1 \tag{3.78}$$

where Δy is a vector defining the maximum change from one time step to the next.

Further, by stacking the measurements over the horizon in a vector

$$y_e = \begin{bmatrix} y_{e,0} \\ y_{e,1} \\ \vdots \\ y_{e,Hu-1} \end{bmatrix} \tag{3.79}$$

the constraint over the horizon can be stated as

$$\Lambda y_e \leq \Delta Y \tag{3.80}$$

where

$$\Lambda = \begin{bmatrix} -I & I & 0 & \cdots & 0 & 0 \\ I & -I & 0 & \cdots & 0 & 0 \\ 0 & -I & I & \cdots & 0 & 0 \\ 0 & I & -I & \cdots & 0 & 0 \\ \vdots & \vdots & \ddots & \ddots & \vdots & \vdots \\ 0 & 0 & \cdots & \cdots & -I & I \\ 0 & 0 & \cdots & \cdots & I & -I \end{bmatrix} \qquad \Delta Y = \begin{bmatrix} \Delta y \\ \Delta y \\ \vdots \\ \Delta y \end{bmatrix} \tag{3.81}$$

Finally, the constraints in the change of measurements (3.80) can be included in the optimization problem. The constraints

$$Y_l \leq y_k \leq Y_u \qquad 1 \leq k \leq H_u - 1 \tag{3.82}$$

$$U_l \leq u_k \leq U_u \qquad 0 \leq k \leq H_u - 1 \tag{3.83}$$

$$-\Delta y_e \leq y_{e,k+1} - y_{e,k} \leq \Delta y \qquad 0 \leq k \leq H_u - 1 \tag{3.84}$$

can be stated, similarly to (3.76), as

$$\Omega v \leq \omega \tag{3.85}$$

where Ω and ω is given by

$$\Omega = \begin{bmatrix} \hat{C}I_x\Theta + \hat{D}I_u \\ -\hat{C}I_x\Theta - \hat{D}I_u \\ \Lambda\big[\hat{C}_eI_x\Theta + \hat{D}_eI_u\big] \\ I \\ -I \end{bmatrix} \tag{3.86}$$

$$\omega = \begin{bmatrix} \hat{Y}_u - \hat{C}I_x\Psi x_0 - [\hat{C}I_x\Theta + \hat{D}I_u]\tilde{t} - [\hat{C}I_x\Xi + \hat{E}I_d]d \\ -\hat{Y}_l + \hat{C}I_x\Psi x_0 + [\hat{C}I_x\Theta + \hat{D}I_u]\tilde{t} + [\hat{C}I_x\Xi + \hat{E}I_d]d \\ \Delta Y - \Lambda\Big[\hat{C}_eI_x\Psi x_0 + [\hat{C}_eI_x\Theta + \hat{D}_eI_u]\tilde{t} + [\hat{C}_eI_x\Xi + \hat{E}_eI_d]d\Big] \\ \hat{U}_u - \tilde{t} \\ -\hat{U}_l + \tilde{t} \end{bmatrix} \tag{3.87}$$

here the matrices $\hat{C}_e$,$\hat{D}_e$ and $\hat{E}_e$ is given by using C_e, D_e and E_e instead of C, D and E in the matrices $\hat{C}$,$\hat{D}$ and $\hat{E}$ defined by (3.64), (3.65) and (3.66), respectively.

3.4.5 Softening the Constraints

It can happen that disturbances push the states outside the feasible region, and it follows that the MPC QP problem has no feasible solution. It is therefore essential that a practical implementation have a strategy for dealing with the possibility of infeasibility. There exists several methods for dealing with infeasibility, and in this thesis, the infeasibility is dealt with by softening the constraints.

Normally input constraints are not softened, because these are often hard constraints imposed by physical limitations on the actuators etc. which means that there is no way of exceeding them.

A straightforward way of softening the constraints is to use slack variables. In [Mac02], it is suggested to use a scalar slack variable, which gives in general, a much faster algorithm compared to other slack variable methods. The trade-off is the loss of priority in the various constraints. The scalar slack variable is added to the constraints in (3.85) and objective function (3.57) and results in the optimalization problem:

$$min \qquad v^THv + fv + \rho\epsilon \tag{3.88}$$

$$s.t \tag{3.89}$$

$$\Omega v \leq \omega + \epsilon\mathbf{1}_0 \tag{3.90}$$

$$\epsilon \geq 0 \tag{3.91}$$

where ρ is a positive scalar variable used to severely punish the constrain violation. As it is stated in [Mac02]: It can be shown that, choosing ρ large

enough, gives an 'exact penalty' method, which means that constraint violations will not occur unless there is no feasible solution to the original 'hard' problem. $\mathbf{1}_0$ is given by

$$\mathbf{1}_0 = \begin{bmatrix} 1 \\ \vdots \\ 1 \\ 0 \\ \vdots \\ 0 \end{bmatrix} \tag{3.92}$$

where there are $\dim(y) \times 3$ ones, and $\dim(u) \times 2$ zeros. This impose constraint softening only on the measurements. Further by stacking the optimization variables into the vector

$$z = \begin{bmatrix} v \\ \epsilon \end{bmatrix} \tag{3.93}$$

the optimization problem can be stated as

$$\begin{aligned} min \quad & z^T \hat{H} z + \hat{f} z & (3.94) \\ s.t & \\ \hat{\Omega} z \leq \hat{\omega} & & (3.95) \end{aligned}$$

where

$$\hat{H} = \begin{bmatrix} H & 0 \\ 0 & 0 \end{bmatrix} \qquad \hat{f} = \begin{bmatrix} f & \rho \end{bmatrix} \tag{3.96}$$

$$\hat{\Omega} = \begin{bmatrix} \Omega & -\mathbf{1}_0 \\ 0 & -1 \end{bmatrix} \qquad \hat{\omega} = \begin{bmatrix} \omega \\ 0 \end{bmatrix} \tag{3.97}$$

3.4.6 Target Calculation

Achieving the desired values for the CVs may be impossible due to constraints or one may wish to keep the inputs close to specific values. Different methods exist for finding targets close to the desired values while maintaining a feasible solution. Direct or pseudo inverse of the system matrices can be impossible or may lead to poor solutions. Therefore the target calculation in this thesis is performed by solving the following optimization problem:

$$\begin{aligned} & \min_{x_{ref,\infty}, u_{ref,\infty}} \\ & (y_d - y_{ref,\infty})^T Q (y_d - y_{ref,\infty}) \\ & +(u_d - u_{ref,\infty})^T W (u_d - u_{ref,\infty}) \end{aligned} \tag{3.98}$$

$$s.t \qquad x_{ref,\infty} = Ax_{ref,\infty} + Bu_{ref,\infty} + B_d d_\infty \tag{3.99}$$
$$y_{ref,\infty} = Cx_{ref,\infty} + Du_{ref,\infty} + D_d d_\infty \tag{3.100}$$
$$U_l \leq u_{ref,\infty} \leq U_u \tag{3.101}$$
$$Y_l \leq y_{ref,\infty} \leq Y_u \tag{3.102}$$

Further by substituting (3.100) into the objective function and by setting the desired input $u_d = 0$, the optimization problem becomes

$$\begin{aligned} \min_{x_{ref,\infty}, u_{ref,\infty}} \\ (y_d - Cx_{ref,\infty} - Du_{ref,\infty} - D_d d_\infty)^T Q (y_d - Cx_{ref,\infty} - Du_{ref,\infty} - D_d d_\infty) \\ + u_{ref,\infty}^T W u_{ref,\infty} \end{aligned} \tag{3.103}$$

$$s.t \qquad \begin{bmatrix} I - A & -B \end{bmatrix} \begin{bmatrix} x_{ref,\infty} \\ u_{ref,\infty} \end{bmatrix} = B_d d_\infty \tag{3.104}$$
$$\begin{bmatrix} I \\ -I \end{bmatrix} u_{ref,\infty} \leq \begin{bmatrix} U_u \\ -U_l \end{bmatrix} \tag{3.105}$$

then by structuring

$$\boldsymbol{x} = \begin{bmatrix} x_{ref,\infty} \\ u_{ref,\infty} \end{bmatrix} \tag{3.106}$$

and finally by removing the terms which does not effect the solution, the QP problem can be formulated as

$$\min_{\boldsymbol{x}} \qquad \boldsymbol{x}^t H \boldsymbol{x} + f\boldsymbol{x} \tag{3.107}$$
$$s.t \qquad A_{eq}\boldsymbol{x} = B_{eq} \tag{3.108}$$
$$A_{ineq}\boldsymbol{x} \leq B_{ineq} \tag{3.109}$$

where

$$H = \begin{bmatrix} C & D \end{bmatrix}^T Q \begin{bmatrix} C & D \end{bmatrix} + \begin{bmatrix} 0 & I \end{bmatrix}^T W \begin{bmatrix} 0 & I \end{bmatrix} \tag{3.110}$$
$$f = -2y_d^T Q \begin{bmatrix} C & D \end{bmatrix} + 2d_\infty^T D_d^T Q \begin{bmatrix} C & D \end{bmatrix} \tag{3.111}$$

$$A_{eq} = \begin{bmatrix} I - A & B \end{bmatrix} \qquad B_{eq} = B_d d_\infty \tag{3.112}$$
$$A_{ineq} = \begin{bmatrix} C & D \\ -C & -D \\ 0 & I \\ 0 & -I \end{bmatrix} \qquad B_{ineq} = \begin{bmatrix} Y_u - Ed_\infty \\ -Y_l + Ed_\infty \\ U_u \\ -U_l \end{bmatrix} \tag{3.113}$$

A positive definite R will in general result in offset in the CVs even when the desired values can be achieved. According to K.R. Muske in [Mus97] the matrix R should therefore be chosen positive semi definite. Further, ibidem found that $R = 0$ can be chosen given that Q is positive definite, the state space is a minimal realization of a discrete transfer function matrix with a full rank steady-state gain matrix, no integrating modes, and there is at least as many measurements as inputs. Furthermore, if the matrix Q is positive semi definite, there should be as many weighted inputs as there are degrees of freedom in order to ensure robust control.

3.4.7 Estimator Design

A model update law must be used in order to estimate the behavior of the process. Even in the somewhat ideal case where there are no noise and disturbances affecting the plant, the plant-model by itself is never accurate enough to predict the future behavior in the infinite horizon. The divergence in the physical response compared to the model response, can be a result of rounding errors or simply inaccurate modeling of the plant. Either way, in a control application, the model needs to be continuously updated by using measurements from the plant in order to correct for the model-plant divergence.

The available update laws used in the industry is vast and ranges from simple bias update laws, to more advanced methods as Kalman-filters or adaptive estimators. It is often desirable to be able to account for more general disturbance dynamics than the bias update law can achieve. Some advanced controllers can estimate the input disturbances, predict the disturbance dynamics in the future, and therefore compensate for the disturbances and in some cases even completely suppress the disturbance acting on the plant.

The estimator used in this thesis is constructed in two steps. First the plant model is augmented with additional states which will account for constant disturbances entering the process. Secondly, in order to update the states in the augmented model, a Kalman-filter is used. The estimator will now estimate the states of the augmented model, and by utilizing the measurements from the plant, the estimator will correct for differences between the (augmented) model output and the plant output.

3.4.7.1 Estimator Model

If an unmeasured, constant disturbance enter the process or if a model error is present, the closed-loop system may never reach the desired controlled variable target. This problem is solved by augmenting the process model with new disturbance states. There is in [MB02] suggested three methods for augmenting

the process model to a disturbance model. The process model defined as

$$\begin{aligned} x_{k+1} &= Ax_k + Bu_k + B_d d_k \\ y_k &= Cx_k + Du_k + Ed \end{aligned} \tag{3.114}$$

can be augmented to the following disturbance models.

The constant output disturbance model is constructed using the following state-space model

$$\begin{aligned} \begin{bmatrix} x_{k+1} \\ p_{k+1} \end{bmatrix} &= \begin{bmatrix} A & 0 \\ 0 & I \end{bmatrix} \begin{bmatrix} x_k \\ p_k \end{bmatrix} + \begin{bmatrix} B \\ 0 \end{bmatrix} u_k + \begin{bmatrix} B_d \\ 0 \end{bmatrix} d_k \\ y_k &= \begin{bmatrix} C & I \end{bmatrix} \begin{bmatrix} x_k \\ p_k \end{bmatrix} + Du_k + Ed \end{aligned} \tag{3.115}$$

The output disturbance model is a deadbeat observer for the output disturbances and a open-loop observer for the model states. It is easy to implement but may lead to poor performance when a disturbance enters elsewhere in the loop.

The input/state disturbance model is constructed using the following state-space model

$$\begin{aligned} \begin{bmatrix} x_{k+1} \\ d_{k+1} \end{bmatrix} &= \begin{bmatrix} A & Bd \\ 0 & I \end{bmatrix} \begin{bmatrix} x_k \\ d_k \end{bmatrix} + \begin{bmatrix} B \\ 0 \end{bmatrix} u_k \\ y_k &= \begin{bmatrix} C & E \end{bmatrix} \begin{bmatrix} x_k \\ d_k \end{bmatrix} + Du_k \end{aligned} \tag{3.116}$$

The input/state disturbance model has good performence when the disturbances enters as inputs, but leads to poor performance when subjected to model errors. [MB02] states that the closed-loop controller performance is directly related to how accurately the disturbance model represents the actual disturbances entering a process.

The input/state and output disturbance model is constructed using the following state-space model

$$\begin{aligned} \begin{bmatrix} x_{k+1} \\ d_{k+1} \end{bmatrix} &= \begin{bmatrix} A & Bd & 0 \\ 0 & I & 0 \\ 0 & 0 & I \end{bmatrix} \begin{bmatrix} x_k \\ d_k \\ p_k \end{bmatrix} + \begin{bmatrix} B \\ 0 \\ 0 \end{bmatrix} u_k \\ y_k &= \begin{bmatrix} C & E & I \end{bmatrix} \begin{bmatrix} x_k \\ d_k \\ p_k \end{bmatrix} + Du_k \end{aligned} \tag{3.117}$$

The input/state and output disturbance model has the advantages and disadvantages of both models.

The different disturbance models are now stated as

$$\tilde{x}_{k+1} = \tilde{A}\tilde{x}_k + \tilde{B}u_k \tag{3.118}$$

$$y_k = \tilde{C}\tilde{x}_k + Du_k \tag{3.119}$$

3.4.7.2 The Kalman Filter

In order to use the kalman filter, the model is written on the form:

$$\tilde{x}_{k+1} = \tilde{A}\tilde{x}_k + \tilde{B}u_k + \tilde{B}_w w_k \tag{3.120}$$

$$y_k = \tilde{C}\tilde{x}_k + Du_k + v_k \tag{3.121}$$

where w_k and v_k are random signals satisfying

$$E(w) = E(v) = 0 \qquad E(ww^T) = Q \qquad E(vv^T) = R \tag{3.122}$$

Further, by defining

$$\tilde{B}_w = \begin{bmatrix} 0 \\ I \end{bmatrix} \tag{3.123}$$

the disturbance is approximated as

$$d_{k+1} = d_k + w_k \tag{3.124}$$

The variance of the signal w_k is now the same as d_k and by guessing variances close to the real variances, the Kalman gain L can be calculated in order to give optimal estimates for the disturbances d_k and states x_k. [Hov08] states that if the augmented model is detectable, it is always possible to calculate the Kalman gain. The Kalman filter is now given by

$$\tilde{x}_{k+1} = \tilde{A}\tilde{x}_k + \tilde{B}u_k + L(y_k - \tilde{C}\tilde{x}_k - Du_k) \tag{3.125}$$

$$= (\tilde{A} - L\tilde{C})\tilde{x}_k + (\tilde{B} - LD)u_k + Ly_k \tag{3.126}$$

$$y_k = \tilde{C}\tilde{x}_k + Du_k \tag{3.127}$$

Furthermore, the state $\hat{x}_k$ and disturbance $\hat{d}_k$ estimates are given by

$$\hat{x}_k = \begin{bmatrix} I & 0 \end{bmatrix} \tilde{x}_k \tag{3.128}$$

$$\hat{d}_k = \begin{bmatrix} 0 & I \end{bmatrix} \tilde{x}_k \tag{3.129}$$

For more details about the Kalman filter and the calculation of the Kalman gain L, then [Hwa97] is recommended.

Chapter 4

Model Development

The different applications of a general conveyor-belt dryer model are vast. In this thesis the model is primary intended for prediction in an MPC application. The single-zone model presented in Chapter 4 is later used in Chapter 6, where several zones are combined/interconnected in order to construct a complete dryer model.

Some process models can describe complex dynamics quite accurate, but too complex models are hard to solve and online prediction can therefore be tough. Nonlinear partial difference equations (PDEs) can be approximated by linear ordinary difference equations (ODEs). When approximating PDEs with ODEs, discretization resolution decides the accuracy of the approximation as well as the computational requirements. Further, when approximating a nonlinear model with a linear model some dynamics are always lost and the model will only be accurate in some neighborhood of the linearization point. A trade-off between model accuracy and computational power must be made.

First, a full review of nonlinear modeling for a conveyor-belt dryer zone is presented. The model is constructed using mass- and energy balances and describes the transfer of heat and mass between the product and gas. The model consisting of nonlinear PDEs accounts for variable dew point temperatures and covers the drying in the falling rate period.

Next, the model is discretized spatially while simplifying the PDEs with a finite difference approximation(FDA). The FDA results in nonlinear ODEs. Then, a structure for the discretized model is defined and linearized in order to fit for linear MPC. Finally, a description of how to include linear input dynamics in a dryer model is presented.

4.1 Mathematical Modeling

A mathematical model of a conveyor-belt dryer was first developed in [Sal08a]. This model did not include the falling rate drying period and was therefore extended in [vD09]. In this thesis it will be shown that the extension in [vD09]

was performed with errors. These errors are corrected in this thesis as shown in section 4.1.6.

In section 4.1, nonlinear modeling for a conveyor-belt dryer zone is presented. First, the dryer assumptions/simplifications are discussed. Then, the mass and heat balances are presented. In order to make the section tidy and easy-to-read, the model is summarized and the model nomenclature is posted in its own subsection.

4.1.1 Discussing the Assumptions

The following assumptions/simplifications when modeling the conveyor-belt dryer, has been made:

The product on the conveyor-belt is evenly distributed, and the height is constant throughout each zone. It is common to spread the product evenly on the conveyor-belt, see section 2.2. This is to avoid uneven airflow through the bed of product, which the model does not support. In this thesis, the conveyor belt-dryer zone is spatial discretized with a fixed number of elements in all directions, and all elements in each zone has the same size. The bed height can still vary from zone to zone.

The volume shrinkage is negligible. This is a result from the last assumption. If the bed height is constant through each zone, there can be no shrinking. An implication of this assumption is that even though the product looses moisture it will not decrease in size. This implies that the evaporation area/product volume ratio is constant for all moisture contents.

If the shrinkage was to be included in the model, then the ideal gas law should be used to calculate the decrease of product volume. In addition, the discretized spatial element sizes must be varying.

All mass lost in the product is moisture evaporated to air. This assumption is made in order for the mass balance to be completely balanced. In a physical dryer, there will always be some loss of solid to the drying gas, but this is considered negligible compared to the loss of moisture.

Heat loss of the dryer to the surroundings is negligible. As with the last assumption, this is made in order for the energy balance to be completely balanced. The process is assumed to be adiabatic, with the exception of the product and gas inputs/outputs. In a physical dryer, there will always be some loss of heat to the surroundings, but this is considered negligible compared to the energy lost by moisture evaporation and the product-to-gas heat transfer.

Heat conduction among the particles is negligible. It is assumed that the temperature of the gas, dominate the change of product temperature. This is because the air passing the product particles almost fully covers the particle area, which leaves no room for contact area between the particles.

Pressures is assumed constant. Atmospheric pressure is assumed in the dryer.

Densities, specific heat capacities, evaporation area/product volume radio (ε) and the latent heat of vaporization (λ) are assumed constant. The assumption of constant gas density introduces an inconsistency in the equations because of the fact that the ideal gas law is used in order to derive the dew point temperature stated in (2.7). *Still, the benefit of making this approximation exceeds the error it creates since it significantly reduces the complexity of the model [Sal08a].*

Some constants could be included as variables in the process model. ε and λ can be included as states in the model, resulting in even stronger nonlinearity in the model. Varying densities can be included in the process model by the use of the ideal gas law, see [Sal08b].

The conveyor-belt speed and gas flow are constant The methods of causing changes in the drying rate is by adjusting either the gas temperature, gas moisture, gas flow and belt speed/retention time.

The gas temperature and moisture are available as inputs in the process model. According to [ASM07], the temperature of the air in the dryer is usually the primary variable used to control the drying rate. It is also stated that he humidity level of the air in the conveyor dryer is a critical control variable. But these are often controlled by lower control loops, where the desired values are constant and therefore not process variables.

It is further stated that the airflow through the beds is often set during the design phase and is not a controllable variable. The belt speed/retention time of the product in the dryer, is also a key variable used to control drying. But this is assumed to be constant at each product drying receipt.

Even though it is not normal to use airflow and belt speed as inputs, they can be included in the process model. When including them as inputs in the process model, the nonlinearity of the process model becomes even stronger.

4.1.2 Mass Balance

The mass balances for the dryer mediums are presented here. The mass balance for each volume unit of product $M_p[\mathrm{kg/m^3}]$ and air $M_g[\mathrm{kg/m^3}]$ is given

by

$$\frac{dM_p}{dt} = \delta_M \tag{4.1}$$

$$\frac{dM_g}{dt} = -\delta_M \tag{4.2}$$

where δ_M is the drying rate of the product. It can be seen that the mass lost by the solid in (4.1) is the same as the mass gained by the gas in (4.2). Therefore the mass transfer in the dryer is completely balanced. In both [Lyd85] and [CTK94], the following equation is used to desribe the drying rate:

$$\delta_M = \frac{h\varepsilon}{\lambda_0}(T_{dp}(\gamma) - T_g)\zeta(\alpha) \tag{4.3}$$

$$\tag{4.4}$$

with the exception of the function $\zeta(\alpha)$, given by (2.9). $\zeta(\alpha)$ is the falling rate developed in [vD09], that was added to Salvador's model, which accounts for the different drying rates of the product. Basically, this term is a factor ranging from zero to one. It is one in the constant rate period, and moves toward zero as the humidity of the product moves toward zero. More about the drying rate is found in section 2.3.5. It can be seen that the drying rate is a function of the dew point temperature T_{dp} given by (2.7), gas temperature T_g and the product humidity ratio α.

Because the product travels in the direction of the conveyor-belt (x-direction), there is only product mass transfer in the x-direction. Similar, because the gas is forced through the bed of the product (z-direction), there is only gas mass transfer in the z-direction. The left hand side of (4.1) and (4.2) can now be divided into the partial derivatives

$$\frac{dM_p}{dt} = \frac{\partial M_p}{\partial t} + v_x\frac{\partial M_p}{\partial x} \tag{4.5}$$

$$\frac{dM_g}{dt} = \frac{\partial M_g}{\partial t} + v_z\frac{\partial M_g}{\partial z} \tag{4.6}$$

Then by combining (4.1)-(4.6) the mass transfer equations becomes

$$\frac{\partial M_p}{\partial t} + v_x\frac{\partial M_p}{\partial x} = \delta_M \tag{4.7}$$

$$\frac{\partial M_g}{\partial t} + v_z\frac{\partial M_g}{\partial z} = -\delta_M \tag{4.8}$$

Further by substituting (2.5) and (2.6) into (4.7) and (4.8), the mass transfer equations can be rewritten as the *humidity ratio equations* below

$$\frac{\partial \alpha}{\partial t} + v_x\frac{\partial \alpha}{\partial x} = \frac{\delta_M}{\rho_s} \tag{4.9}$$

$$\frac{\partial \gamma}{\partial t} + v_z\frac{\partial \gamma}{\partial z} = -\frac{\delta_M}{\rho_a} \tag{4.10}$$

4.1.3 Energy Balance

The energy balances for the dryer mediums are presented here. By using (2.14) and (2.23) while considering the energy contained in each volume unit of product $Q_p[J/(m^3 s)]$ and gas $Q_g[J/(m^3 s)]$, the energy can be stated as

$$Q_p = \rho_s h_p \tag{4.11}$$
$$Q_g = \rho_a h_g \tag{4.12}$$

Furthermore the energy transfer equations are given by

$$\frac{dQ_p}{dt} = \delta_M \lambda_0 + \delta_U \tag{4.13}$$
$$\frac{dQ_g}{dt} = -\delta_M \lambda_0 - \delta_U \tag{4.14}$$

where the first term on the right hand side accounts for the energy needed to evaporate water into vapor. δ_U is the heat exchange between the product and the gas passing it and is modeled as

$$\delta_U = h\varepsilon(T_g - T_p) \tag{4.15}$$

It can be seen that the energy lost by the product in (4.13) is the same as the energy gained by the gas in (4.14). Therefore the energy transfer in the dryer is completely balanced. Further the left hand side of (4.13) and (4.14) can be divided into partial derivatives

$$\frac{dQ_p}{dt} = \frac{\partial Q_p}{\partial t} + v_x \frac{\partial Q_p}{\partial x} \tag{4.16}$$
$$\frac{dQ_g}{dt} = \frac{\partial Q_g}{\partial t} + v_z \frac{\partial Q_g}{\partial z} \tag{4.17}$$

Then by combining (4.13) and (4.14) with (4.16) and(4.17), the energy transfer equations becomes

$$\frac{\partial Q_p}{\partial t} + v_x \frac{\partial Q_p}{\partial x} = \delta_M \lambda_0 + \delta_U \tag{4.18}$$
$$\frac{\partial Q_g}{\partial t} + v_z \frac{\partial Q_g}{\partial z} = -\delta_M \lambda_0 - \delta_U \tag{4.19}$$

Finally, by substituting (4.11), (4.12), (2.15) and (2.24) into (4.18) and (4.19) the *heat transfer equations* can be stated as

$$\frac{\delta T_p}{\delta t} + v_x \frac{\delta T_p}{\delta x} = \frac{(\lambda_0 - c_{pw} T_p)\delta_M + \delta_U}{\rho_s (c_{ps} + \alpha c_{pw})} \tag{4.20}$$
$$\frac{\delta T_g}{\delta t} + v_z \frac{\delta T_g}{\delta z} = \frac{c_{pv} T_g \delta_M - \delta_U}{\rho_a (c_{pa} + \gamma c_{pv})} \tag{4.21}$$

A detailed derivation of (4.20) and (4.21) are shown in A.1.

4.1.4 Summarizing the Model

Solid phase:

$$\frac{\partial \alpha}{\partial t} + v_x \frac{\partial \alpha}{\partial x} = \frac{\delta_M}{\rho_s} \tag{4.22}$$

$$\frac{\delta T_p}{\delta t} + v_x \frac{\delta T_p}{\delta x} = \frac{(\lambda_0 - c_{pw} T_p)\delta_M + \delta_U}{\rho_s (c_{ps} + \alpha c_{pw})} \tag{4.23}$$

Gas phase:

$$\frac{\partial \gamma}{\partial t} + v_z \frac{\partial \gamma}{\partial z} = -\frac{\delta_M}{\rho_a} \tag{4.24}$$

$$\frac{\delta T_g}{\delta t} + v_z \frac{\delta T_g}{\delta z} = \frac{c_{pv} T_g \delta_M - \delta_U}{\rho_a (c_{pa} + \gamma c_{pv})} \tag{4.25}$$

where the mass δ_M and heat transfer δ_U is given as

$$\delta_M = \frac{h\varepsilon}{\lambda_0}(T_{dp}(\gamma) - T_g)\zeta(\alpha) \tag{4.26}$$

$$\delta_U = h\varepsilon(T_g - T_p) \tag{4.27}$$

Furthermore the dew point temperature $T_{dp}(\gamma)$ and falling rate $\zeta(\alpha)$ is given as

$$T_{dp}(\gamma) = \left[\frac{1}{T_0} - \frac{R_v}{\lambda_0} ln\left(\frac{P_{atm}\gamma}{p_{s,0}(\beta + \gamma)}\right)\right]^{-1} \tag{4.28}$$

$$\zeta(\alpha)) = p_\theta \alpha^\theta + p_{\theta-1}\alpha^{\theta-1} + \cdots + p_1\alpha + p_0 \tag{4.29}$$

If $\zeta(\alpha)) = 1 \ \forall \ \alpha$, then the model is identical to the model developed in [Sal08a].

4.1.5 Model Nomenclature

T_p = temperature, product [°C]
T_g = temperature, gas mixture [°C]
α = humidity ratio, product [kg/kg]
γ = humidity ratio, air [kg/kg]
δ_M = Drying rate [kg/m^3/s]
δ_U = Heat transfer [J/m^3/s]
T_{dp} = temperature, dew point [°C]
$\zeta(\alpha)$ = falling rate multiplicator of the drying rate [1]
c_{pa} = specific heat capacity, air [J/kg °C]
c_{pv} = specific heat capacity, vapor [J/kg °C]
c_{ps} = specific heat capacity, product [J/kg °C]
c_{pw} = specific heat capacity, water [J/kg °C]
ρ_s = mass density, dry solid [kg/m^3]
ρ_a = mass density, dry air [kg/m^3]
v_x = velocity, conveyor-belt [m/s]
v_z = velocity, air stream [m/s]
h = heat transfer coefficient [J/s m^2 °C]
ε = evaporation area/product volume ratio [1/m]
λ_0 = heat of vaporization, water [J/kg]
M_p = total mass per volume unit, product [kg/m^3]
M_g = total mass per volume unit, gas [kg/m^3]
Q_p = total energy per volume unit, product [J/m^3]
Q_g = total energy per volume unit, gas [J/m^3]
h_p = enthalpy, product [J/kg]
h_g = enthalpy, gas [J/kg]
T_0 = reference temperature, gas [K]
$p_{s,0}$ = partial pressure at reference temperature [hPa]
R_v = specific gas constant [J/kg K]
p_θ = polynomial coefficient in the falling rate
θ = order of the polynomial fit used in the falling rate

4.1.6 Correcting a Modeling Error in [vD09]

In [vD09], the modeling of the falling rate resulted in incorrect equations for the dryer-model. The falling rate $\zeta(\alpha)$ was included into the drying rate δ_M, which was correct. But when the drying rate should have been substituted into the energy equations

$$\frac{\partial Q_p}{\partial t} + v_x \frac{\partial Q_p}{\partial x} = \delta_M \lambda_0 + \delta_U \tag{4.30}$$

$$\frac{\partial Q_g}{\partial t} + v_z \frac{\partial Q_g}{\partial z} = -\delta_M \lambda_0 - \delta_U \tag{4.31}$$

the falling rate $\zeta(\alpha)$, fail to appear, which resulted in the *incorrect* equations

$$\frac{\partial Q_p}{\partial t} + v_x \frac{\partial Q_p}{\partial x} = h\varepsilon(T_{dp}(\gamma) - T_g) + \delta_U \tag{4.32}$$

$$\frac{\partial Q_g}{\partial t} + v_z \frac{\partial Q_g}{\partial z} = -h\varepsilon(T_{dp}(\gamma) - T_g) - \delta_U, \tag{4.33}$$

instead of the *correct* equations

$$\frac{\partial Q_p}{\partial t} + v_x \frac{\partial Q_p}{\partial x} = h\varepsilon(T_{dp}(\gamma) - T_g)\zeta(\alpha) + \delta_U \tag{4.34}$$

$$\frac{\partial Q_g}{\partial t} + v_z \frac{\partial Q_g}{\partial z} = -h\varepsilon(T_{dp}(\gamma) - T_g)\zeta(\alpha) - \delta_U, \tag{4.35}$$

As a consequence of this modeling error, both the nonlinear and linear model was incorrect. Therefore the nonlinear modeling, linearization (hence differentiations) and various comparisons has to be redone and represented in this thesis.

4.2 Approximation by Finite Difference

The primary model given by equations (4.22)-(4.25) consists of partial difference equations (PDEs) and needs to be solved. PDEs are in general hard to solve, and several ways exist for solving them. In this work, as in [Sal08a] and [vD09], the finite difference approximation (FDA) is used in order to simplify the nonlinear model. In order to include the various readers of this thesis, the method is repeated here.

The model for the whole zone is divided into smaller blocks(elements), and if the elements are small enough, we get a close approximation to the PDE model. Figure 4.1 illustrates the control volume approximation, and Figure 4.2 illustrates the element itself. The figures show how the zone is divided into smaller elements depending on the number of spatial intervals. The spatial variables are defined on an interval $n \in [1, N]$ along the x-axis and $m \in [1, M]$ along the z-axis.

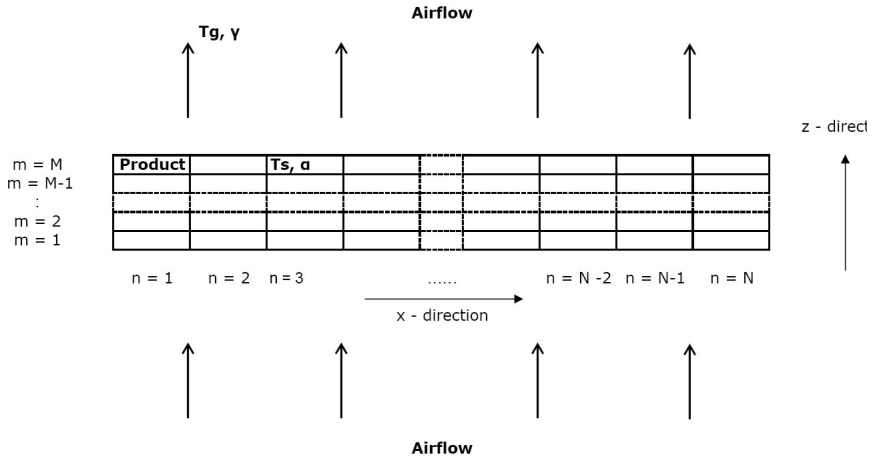

Figure 4.1: Illustration of the PDE finite difference approximation, seen from the side.

The nonlinear model simplified with the FDA results in the differential element, illustrated in Figure 4.2.

The result of this approximation is four ordinary differential equations (ODEs) for each element in each zone. By defining

$$\begin{aligned} x_{1(n,m)} &= \alpha_{(n,m)} \\ x_{2(n,m)} &= T_{s(n,m)} \\ x_{3(n,m)} &= \gamma_{(n,m)} \\ x_{4(n,m)} &= T_{g(n,m)} \end{aligned} \tag{4.36}$$

and by using the explicit Euler method, we can state the ODE's for each element of the current zone as:

$$\dot{x}_{1,(n,m)} = \frac{v_x}{dx}\left[x_{1,(n-1,m)} - x_{1,(n,m)}\right] + r_{1,(n,m)} \tag{4.37}$$

$$\dot{x}_{2,(n,m)} = \frac{v_x}{dx}\left[x_{2,(n-1,m)} - x_{2,(n,m)}\right] + r_{2,(n,m)} \tag{4.38}$$

$$\dot{x}_{3,(n,m)} = \frac{v_z}{dz}\left[x_{3,(n,m-1)} - x_{3,(n,m)}\right] + r_{3,(n,m)} \tag{4.39}$$

$$\dot{x}_{4,(n,m)} = \frac{v_z}{dz}\left[x_{4,(n,m-1)} - x_{4,(n,m)}\right] + r_{4,(n,m)} \tag{4.40}$$

$$m \in [1, M], n \in [1, N]$$

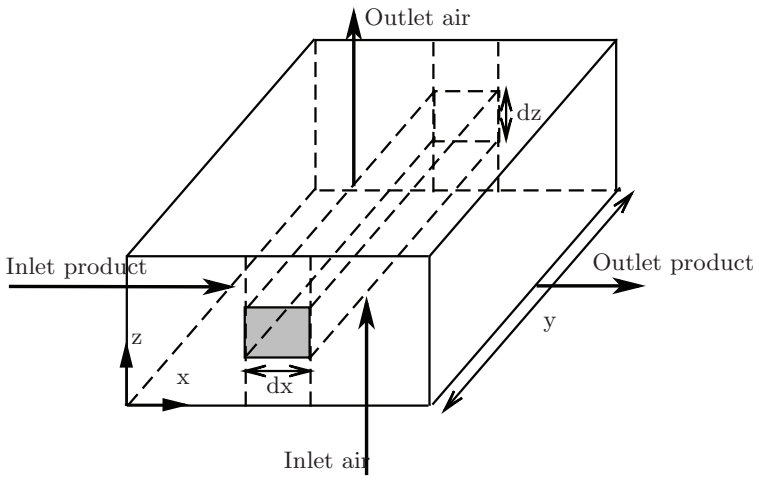

Figure 4.2: Schematic representation of the continuous cross flow belt conveyor dryer differential element

where

$$x_{1,(0,m)} = x_{1,in,(m)} \quad = \text{input humidity of product at m=i [kg/kg]} \tag{4.41}$$

$$x_{2,(0,m)} = x_{2,in,(m)} \quad = \text{input temperature of product m=i [°C]} \tag{4.42}$$

$$i \in [1, M]$$

$$x_{3,(n,0)} = x_{3,in,(n)} \quad = \text{input humidity of air n=i [kg/kg]} \tag{4.43}$$

$$x_{4,(n,0)} = x_{4,in,(n)} \quad = \text{input temperature of air n=i [°C]} \tag{4.44}$$

$$i \in [1, N]$$

where v_z and v_x point in the same directions as the x- and z-axis defined in Figures 4.1 and 4.2, respectively. dz and dx is the length of the sides of each element in the x and y directions, respectively. Furthermore, the nonlinear functions are defined as

$$r_{1,(n,m)} = \frac{\delta_M}{\rho_s} \tag{4.45}$$

$$r_{2,(n,m)} = \frac{(\lambda_0 - c_{pw} x_{2,(n,m)})\delta_M + \delta_U}{\rho_s (c_{ps} + x_{1,(n,m)} c_{pw})} \tag{4.46}$$

$$r_{3,(n,m)} = -\frac{\delta_M}{\rho_a} \tag{4.47}$$

$$r_{4,(n,m)} = \frac{c_{pv} x_{4,(n,m)} \delta_M - \delta_U}{\rho_a (c_{pa} + x_{3,(n,m)} c_{pv})} \tag{4.48}$$

4.3 Model Structuring

In section 4.2 a model with no particular structure was defined. By utilizing the sparse structure of the system, a model which is practical both to implement and to use is created. The structure soon to be stated was also used in [vD09], which is based on the structure developed in [Sal08a]. In order to include the various readers of this thesis, it is repeated here.

The system can be structured as

$$\dot{\boldsymbol{x}}_i = k\boldsymbol{G}_i\boldsymbol{x}_i + \boldsymbol{r}_i(\boldsymbol{x}) + K\boldsymbol{x}_{i,in} \qquad i \in [1,4] \tag{4.49}$$

where

$$K = \begin{cases} \dfrac{v_x}{dx} & i \in 1,2 \\ \dfrac{v_z}{dz} & i \in 3,4 \end{cases} \qquad \boldsymbol{x} = \begin{bmatrix} \boldsymbol{x}_1 \\ \boldsymbol{x}_2 \\ \boldsymbol{x}_3 \\ \boldsymbol{x}_4 \end{bmatrix} \tag{4.50}$$

$$\boldsymbol{x}_i = \begin{bmatrix} x_{i,(1,1)} \\ x_{i,(2,1)} \\ x_{i,(3,1)} \\ \vdots \\ x_{i,(N,1)} \\ x_{i,(1,2)} \\ x_{i,(2,2)} \\ x_{i,(3,2)} \\ \vdots \\ x_{i,(N,2)} \\ x_{i,(1,3)} \\ x_{i,(2,3)} \\ x_{i,(3,3)} \\ \vdots \\ x_{i,(1,M-1)} \\ \vdots \\ x_{i,(N,M)} \end{bmatrix} \qquad \boldsymbol{r}_i = \begin{bmatrix} r_{i,(1,1)} \\ r_{i,(2,1)} \\ r_{i,(3,1)} \\ \vdots \\ r_{i,(N,1)} \\ r_{i,(1,2)} \\ r_{i,(2,2)} \\ r_{i,(3,2)} \\ \vdots \\ r_{i,(N,2)} \\ r_{i,(1,3)} \\ r_{i,(2,3)} \\ r_{i,(3,3)} \\ \vdots \\ r_{i,(1,M-1)} \\ \vdots \\ r_{i,(N,M)} \end{bmatrix} \qquad i \in [1,4] \tag{4.51}$$

Further the transition matrix which describes the interaction between the

elements is defined as:

$$\boldsymbol{G}_i = \begin{bmatrix} \beta & 0 & \cdots & 0 \\ 0 & \beta & \cdots & 0 \\ \vdots & \vdots & \ddots & \vdots \\ 0 & 0 & 0 & \beta \end{bmatrix} \qquad i \in 1,2$$

$$\boldsymbol{G}_i = \begin{bmatrix} -I & 0 & 0 & \cdots & 0 & 0 \\ I & -I & 0 & \cdots & 0 & 0 \\ 0 & I & -I & \cdots & 0 & 0 \\ \vdots & \vdots & \vdots & \ddots & \vdots & \vdots \\ 0 & 0 & 0 & \cdots & I & -I \end{bmatrix} \qquad i \in 3,4$$

where

$$\beta = \begin{bmatrix} -1 & 0 & 0 & \cdots & 0 & 0 \\ 1 & -1 & 0 & \cdots & 0 & 0 \\ 0 & 1 & -1 & \cdots & 0 & 0 \\ \vdots & \vdots & \vdots & \ddots & \vdots & \vdots \\ 0 & 0 & 0 & \cdots & 1 & -1 \end{bmatrix}$$

$$\begin{aligned} dim(\boldsymbol{G}_i) &= (N \cdot M) \times (N \cdot M) \\ dim(\beta) &= N \times N \\ dim(I) &= N \times N \end{aligned}$$

The boundary condition vector(input state vector) for the zone is defined as:

$$\boldsymbol{x}_{i,in} = \begin{bmatrix} x_{i,in(1)} \\ 0 \\ \vdots \\ 0 \\ x_{i,in(2)} \\ \vdots \\ \vdots \\ x_{i,in(M)} \\ 0 \\ \vdots \\ 0 \end{bmatrix} \qquad i \in 1,2 \quad \boldsymbol{x}_{i,in} = \begin{bmatrix} x_{i,in(1)} \\ x_{i,in(2)} \\ x_{i,in(3)} \\ \vdots \\ x_{i,in(N-1)} \\ x_{i,in(N)} \\ 0 \\ \vdots \\ \vdots \\ 0 \end{bmatrix} \qquad i \in 3,4 \quad (4.52)$$

The system for the whole zone can be stated as

$$\boxed{\dot{\boldsymbol{x}} = \boldsymbol{k}\boldsymbol{G}\boldsymbol{x} + \boldsymbol{r}(\boldsymbol{x}) + \boldsymbol{k}\boldsymbol{x}_{in}} \qquad (4.53)$$

where

$$\boldsymbol{G} = \begin{bmatrix} G_1 & 0 & 0 & 0 \\ 0 & G_2 & 0 & 0 \\ 0 & 0 & G_3 & 0 \\ 0 & 0 & 0 & G_4 \end{bmatrix} \qquad \boldsymbol{r}(\boldsymbol{x}) = \begin{bmatrix} \boldsymbol{r}_1(\boldsymbol{x}) \\ \boldsymbol{r}_2(\boldsymbol{x}) \\ \boldsymbol{r}_3(\boldsymbol{x}) \\ \boldsymbol{r}_4(\boldsymbol{x}) \end{bmatrix} \qquad \boldsymbol{x}_{in} = \begin{bmatrix} \boldsymbol{x}_{1,in} \\ \boldsymbol{x}_{2,in} \\ \boldsymbol{x}_{3,in} \\ \boldsymbol{x}_{4,in} \end{bmatrix} \tag{4.54}$$

$$\boldsymbol{k} = \begin{bmatrix} \kappa & 0 & \cdots & 0 \\ 0 & \kappa & \cdots & 0 \\ \vdots & \vdots & \ddots & \vdots \\ 0 & 0 & \cdots & \kappa \end{bmatrix} \qquad \kappa = \begin{cases} \dfrac{v_x}{dx} & \text{for the first } N \cdot M \cdot 2 \text{ rows/columns} \\ \dfrac{v_z}{dz} & \text{for the last } N \cdot M \cdot 2 \text{ rows/columns} \end{cases} \tag{4.55}$$

$$dim(\boldsymbol{G}) = (N \cdot M \cdot 4) \times (N \cdot M \cdot 4)$$
$$dim(\boldsymbol{k}) = (N \cdot M \cdot 4) \times (N \cdot M \cdot 4)$$

4.4 Linearization

To this point, a single zone consisting of nonlinear ODE's (4.53) has been modeled. Even by use of the FDA, the model is still complex and simulation duration is to long for model based control. In order for the model based controller to be able to predict the plant behavior, it must be further simplified. The choice of simplification in this thesis, is linearization, which again, was performed in both [vD09] and [Sal08a]. Later, when constructing the multiple-zone dryer, linear models for the zones of the dryer is created and combined. And in order for the reader to fully understand how to combine these zones, the reader should first have knowledge how the zone-linearization is performed. The linearization structure and matrices are the same as in [vD09].

By condsidering the ODEs in (4.53):

$$\dot{\boldsymbol{x}} = \boldsymbol{k}\boldsymbol{G}\boldsymbol{x} + \boldsymbol{r}(\boldsymbol{x}) + \boldsymbol{k}\boldsymbol{x}_{in}$$

it can be seen that the only nonlinear part of the equation is $\boldsymbol{r}(\boldsymbol{x})$, therefore we only need to linearize this element. The linearization is done by assuming:

$$\boldsymbol{r}(\boldsymbol{x}) \approx J\boldsymbol{x} \tag{4.56}$$

because $\boldsymbol{r}(\boldsymbol{x})$ is independent of $\boldsymbol{x}_{in}$. J is the Jacobian of $\boldsymbol{r}(\boldsymbol{x})$:

$$\boldsymbol{J} \approx \frac{\partial \boldsymbol{r}}{\partial \boldsymbol{x}} = \left[\begin{array}{cccc} \partial \boldsymbol{r}_1/\partial \boldsymbol{x}_1 & \partial \boldsymbol{r}_1/\partial \boldsymbol{x}_2 & \partial \boldsymbol{r}_1/\partial \boldsymbol{x}_3 & \partial \boldsymbol{r}_1/\partial \boldsymbol{x}_4 \\ \partial \boldsymbol{r}_2/\partial \boldsymbol{x}_1 & \partial \boldsymbol{r}_2/\partial \boldsymbol{x}_2 & \partial \boldsymbol{r}_2/\partial \boldsymbol{x}_3 & \partial \boldsymbol{r}_2/\partial \boldsymbol{x}_4 \\ \partial \boldsymbol{r}_3/\partial \boldsymbol{x}_1 & \partial \boldsymbol{r}_3/\partial \boldsymbol{x}_2 & \partial \boldsymbol{r}_3/\partial \boldsymbol{x}_3 & \partial \boldsymbol{r}_3/\partial \boldsymbol{x}_4 \\ \partial \boldsymbol{r}_4/\partial \boldsymbol{x}_1 & \partial \boldsymbol{r}_4/\partial \boldsymbol{x}_2 & \partial \boldsymbol{r}_4/\partial \boldsymbol{x}_3 & \partial \boldsymbol{r}_4/\partial \boldsymbol{x}_4 \end{array} \right] \Bigg|_{\boldsymbol{x}_0} \tag{4.57}$$

where

$$\frac{\partial \boldsymbol{r}_i}{\partial \boldsymbol{x}_j} = \begin{bmatrix} \frac{\partial r_{i(1,1)}}{\partial x_{j(1,1)}} & 0 & \cdots & \cdots & \cdots & 0 & 0 \\ 0 & \frac{\partial r_{i(2,1)}}{\partial x_{j(2,1)}} & \cdots & \cdots & \cdots & 0 & 0 \\ \vdots & \vdots & \ddots & \vdots & \vdots & \vdots & \vdots \\ 0 & \cdots & \cdots & \frac{\partial r_{i,(N,1)}}{\partial x_{j(N,1)}} & \cdots & \cdots & 0 \\ \vdots & \vdots & \cdots & \vdots & \ddots & \vdots & \vdots \\ 0 & 0 & \cdots & 0 & 0 & \frac{\partial r_{i,(N-1,M)}}{\partial x_{j(N-1,M)}} & 0 \\ 0 & 0 & \cdots & 0 & 0 & 0 & \frac{\partial r_{i,(N,M)}}{\partial x_{j(N,M)}} \end{bmatrix} \Bigg|_{\boldsymbol{x}_{j,0}} \tag{4.58}$$

$$[i, j] \in [1, 4]$$

$$\begin{aligned} dim(\boldsymbol{J}) &= (N \cdot M \cdot 4) \times (N \cdot M \cdot 4) \\ dim(\frac{\partial \boldsymbol{r}_i}{\partial \boldsymbol{x}_j}) &= N \times M \\ x_0 &= \text{Linearization point} \end{aligned}$$

Notice that diagonal elements in (4.58) are the same. The only difference between them are the fact that they are linearized around different point in space $x_{j,0(n,m)}$. A detailed differentiation of the different indexes in the Jacobian is shown in (A.2). Furthermore by looking closer at the structure of (4.58), it can be seen that it has a diagonal form. This form is a result of the structure of the state vectors. All the elements with exception of the diagonal are zero, because $r_{i(m,n)}$ is dependent only of the states in the current element. This dependence is easily confirmed by inspecting the equations defining these functions, (4.45)-(4.48).

By approximating (4.56) the linear system describing the dynamics for one zone can be defined as

$$\begin{aligned} \dot{\boldsymbol{x}}_{lin} &= \boldsymbol{kG}\boldsymbol{x}_{lin} + \boldsymbol{J}\boldsymbol{x}_{lin} + \boldsymbol{B}u \\ \dot{\boldsymbol{x}}_{lin} &= (\boldsymbol{kG} + \boldsymbol{J})\boldsymbol{x}_{lin} + \boldsymbol{B}u \end{aligned}$$

$$\boxed{\dot{\boldsymbol{x}}_{lin} = \boldsymbol{A}\boldsymbol{x}_{lin} + \boldsymbol{B}\boldsymbol{u}} \tag{4.59}$$

The system matrices $\boldsymbol{A}$ and $\boldsymbol{B}$ is given by

$$\boldsymbol{A} = \boldsymbol{kG} + \boldsymbol{J} \tag{4.60}$$

$$\boldsymbol{B} = \boldsymbol{k} \tag{4.61}$$

where $\boldsymbol{G}$ and $\boldsymbol{k}$ is given in (4.54) and (4.55), respectively.

$$dim(\boldsymbol{A}) = (N \cdot M \cdot 4) \times (N \cdot M \cdot 4)$$
$$dim(\boldsymbol{B}) = (N \cdot M \cdot 4) \times (N \cdot M \cdot 4)$$

By using the input state vectors defined in (4.52), the input vector for one particular zone of the linear system can now be defined as:

$$\boldsymbol{u} = \begin{bmatrix} \boldsymbol{x}_{1,in} \\ \boldsymbol{x}_{2,in} \\ \boldsymbol{x}_{3,in} \\ \boldsymbol{x}_{4,in} \end{bmatrix} \tag{4.62}$$

Here input product humidity $\boldsymbol{x}_{1,in}$ and input product temperature $\boldsymbol{x}_{2,in}$ are transferred from the previous zone, with the exception of the first zone, in which case the input product humidity and temperature are given by.

$$\boldsymbol{x}_{1,in} = \boldsymbol{\delta} T_{s,in} \qquad \boldsymbol{x}_{2,in} = \boldsymbol{\delta} \alpha_{in} \tag{4.63}$$

where

$$\boldsymbol{\delta} = \begin{bmatrix} 1 \\ \overline{\boldsymbol{0}} \\ 1 \\ \overline{\boldsymbol{0}} \\ \vdots \\ 1 \\ \overline{\boldsymbol{0}} \end{bmatrix} \qquad \overline{\boldsymbol{0}} = \begin{bmatrix} 0 \\ 0 \\ \vdots \\ 0 \end{bmatrix} \tag{4.64}$$

$$dim(\boldsymbol{\delta}) = (N \cdot M) \times 1$$
$$dim(\overline{\boldsymbol{0}}) = (N - 1)) \times 1$$
$$T_{s,in} = \text{input temperature to the zone, product [°C]}$$
$$\alpha_{in} = \text{input humidity ratio to the zone, product [kg/kg]}$$

Input air humidity $\boldsymbol{x}_{3,in}$ and input air temperature $\boldsymbol{x}_{4,in}$ could be output air from another zone, or they could be manipulated variables for the dryer. If the input air to the zone is given as an external input, i.e. not as an output of another zone, then the input air humidity and temperature are given by.

$$\boldsymbol{x}_{3,in} = \boldsymbol{\sigma} T_{g,in} \qquad \boldsymbol{x}_{4,in} = \boldsymbol{\sigma} \gamma_{in} \tag{4.65}$$

where

$$\boldsymbol{\sigma} = \begin{bmatrix} 1 \\ 1 \\ \vdots \\ 1 \\ \underline{\mathbf{0}} \end{bmatrix} \qquad \underline{\mathbf{0}} = \begin{bmatrix} 0 \\ 0 \\ \vdots \\ 0 \end{bmatrix} \tag{4.66}$$

$$\begin{aligned} dim(\boldsymbol{\sigma}) &= (N \cdot M) \times 1 \\ dim(\underline{\mathbf{0}}) &= (N \cdot (M-1)) \times 1 \\ T_{g,in} &= \text{input temperature to the zone, air [°C]} \\ \gamma_{in} &= \text{input humidity ratio to the zone, air [kg/kg]} \end{aligned}$$

4.5 Including Input Dynamics

In the conveyor-belt dryer, the manipulated variables of the dryer are often the input gas temperatures to the various zones. Sometimes these inputs can be very fast relative to the slow dynamics of the conveyor-belt dryer. For example, burners are fast and can often be neglected when modeling the dryer.

On the other hand, if the input gas temperatures to the dryer for example are transferred using slow heat exchangers influenced by the output gas temperatures from the dryer, it is essential to include the input dynamics the process model. In this section it is illustrated how to include linear input dynamics in the process model. Assume the dryer has the linear state-space model

$$\begin{aligned} \dot{x} &= Ax + Bu \\ y &= Cx \end{aligned} \tag{4.67}$$

$$u = \begin{bmatrix} gT_{1,in} \\ \vdots \\ gT_{j,in} \end{bmatrix} \tag{4.68}$$

where $gT_{i,in}$ is the input gas temperature of zone i.

4.5.1 Linear Input Dynamics

The input dynamics are often given by the inner control loops for the burners, heat exchangers and so on. Assuming the dynamics are linear, the input dynamics can be stated in the state space model

$$\begin{aligned} \dot{x}_u &= A_u x_u + B_u u_{ref} + B_y y \\ u &= C_u x_u + D_u u_{ref} \end{aligned} \tag{4.69}$$

where

$$u_{ref} = \begin{bmatrix} gT_{1,in,ref} \\ \vdots \\ gT_{j,in,ref} \end{bmatrix} \qquad y = \begin{bmatrix} gT_{1,out} \\ \vdots \\ gT_{j,out} \end{bmatrix} \tag{4.70}$$

here, $gT_{i,in,ref}$ is the input gas temperature reference of zone i. And $gT_{i,out}$ is the output gas temperature of zone i for the dryer. The term $B_y y$ is included in order to account for the reusage of the exhaust gas of the zones.

Example 4.1. Assume that a dryer consist of only one zone and that the input air temperature of this zone is given by a slow burner which can be approximated with a first order transfer function with time constant T and steady state gain K:

$$gT = \frac{K}{1+Ts} gT_{ref} \tag{4.71}$$

Further this burner can be stated in state space form:

$$\dot{gT} = -\frac{1}{T} gT + \frac{K}{T} gT_{ref} \tag{4.72}$$

which gives A_u, B_u, C_u and D_u in (4.69) as

$$A_u = -\frac{1}{T} \qquad B_u = \frac{K}{T} \qquad C_u = 1 \qquad D_u = 0 \tag{4.73}$$

$B_y = 0$ because the burner is independent of the exhaust gas temperature. □

4.5.2 Augmenting the Process Model

Now by combining the input dynamics (4.69) with the dryer model (4.67) the augmented model becomes

$$\begin{aligned} \dot{\hat{x}} &= \hat{A}\hat{x} + \hat{B}u_{ref} \\ y &= \hat{C}\hat{x} \end{aligned} \tag{4.74}$$

where

$$\hat{A} = \begin{bmatrix} A & BC_u \\ B_y C & A_u \end{bmatrix} \qquad \hat{B} = \begin{bmatrix} BD_u \\ B_u \end{bmatrix} \qquad \hat{C} = \begin{bmatrix} C & 0 \end{bmatrix} \tag{4.75}$$

Equations (4.74) and (4.75) shows how the dynamics of all inputs can be included in a general linear dryer model.

Chapter 5

Model Study

In this chapter some model properties are investigated. The dryer model constructed and used here is only a demonstration, and is not used in the later chapters.

As a consequence of the modeling error in [vD09], both the nonlinear and linear modeling resulted in an incorrect model. Therefore the different comparisons and evaluations is represented in this thesis. Much of section 5.1.1 and 5.2 is repeated from [vD09].

5.1 Single Zone Simulation

In order to verify the correctness of the model, the nonlinear ODEs (4.53) were solved in MATLAB with ode23tb, which is the only solver that could solve the ODEs both fast and accurate without an oscillating response (which is unnatural for a conveyor belt dryer), see [vD09].

By simulating the system we can observe the model dynamics and then compare the model to the laws of physics. Another reason for simulating the nonlinear model is to obtain steady state values of each zone of the dryer, which can be used for

- tuning of the model constants (parameter estimation).
- linearization of the model around certain operating points. More details about the linearization can be found in section 4.4.

To simulate the model we need to determine the model parameters. Some of these are in given tables, while others can only be identified by experimentation on each particular dryer. Since this project is not devoted to a specific dryer, the constants can be chosen arbitrary, within reasonable ranges to obtain a realistic simulation. The majority of the model constants used is obtained from the dryer simulated in [Sal08a]. Table 5.1-5.3 states the parameters used in this simulation.

Variable	Value	Denomination	Description
$T_{s,in}$	65	°C	Input temperature, product
$T_{g,in}$	110	°C	Input temperature, air
α_{in}	0.25	kg/kg	Boundary moisture, product
γ_{in}	0.01	kg/kg	Boundary moisture, air
v_x	0.0043	m/s	Velocity, conveyor-belt
v_z	0.4579	m/s	Velocity, air

Table 5.1: Nominal steady-state operational values, model-study dryer

Variable	Value	Denomination	Description
Δx	1.3	m	Conveyor-belt length
Δy	0.6	m	Conveyor-belt width
Δz	0.055	m	Product stack height

Table 5.2: Approximate control volume dimensions, model-study dryer

Variable	Value	Denomination	Description
α_{crit}	0.14	kg/kg	Critical moisture content
c_{PW}	4220	J/kg K	Specific heat capacity, water (375K)
c_{PS}	2000	J/kg K	Specific heat capacity, product (375K)
c_{PV}	1890	J/kg K	Specific heat capacity, steam (375K)
c_{PA}	1000	J/kg K	Specific heat capacity, Air (375K)
h	25	J/s m^2 K	Heat transfer coefficient
M_g	28.97×10^{-3}	kg/mol	Molar mass, dry air
P_a	101325	Pa	Atmospheric pressure
P_{s0}	6.11	hPa	Partial pressure at reference temperature
R	8.14472	J/K mol	Universal gas constant
R_v	461.5	J/kg K	Specific gas constant, steam
T_0	273.15	K	Reference temperature
β	0.62197	1	Specific mass ratio, steam/dry air
ε	100 - 300	m^2/m^3	Vaporization area per product volume
λ_0	2257000	J/kg	Latent heat of vaporization
ρ_s	600	kg/m^3	Mass density, product
ρ_g	1.009	kg/m^3	Mass density, air

Table 5.3: Model constants, model-study dryer

5.1.1 Distribution and Average Value Plots

We simulate the nonlinear model until steady state is achieved. Some various simulation details:

- The entire conveyor-belt is fully loaded with pellets.
- Initially, the air temperature surrounding the pellets equals the product temperature at $65°C$.
- Initially, the product moisture is 25%, while air moisture is 3%.
- The input product temperature to the zone is $65°C$ and the input product moisture is 25%.
- The input air temperature to the zone is $110°C$ and the input air moisture is 2%.
- N = 40, M = 15, $\varepsilon = 150$

Figure 5.1-5.7 visualizes the moisture and temperature distribution as a function of time. Figure 5.8 shows how the output moisture and temperature average values changes as a function of time.

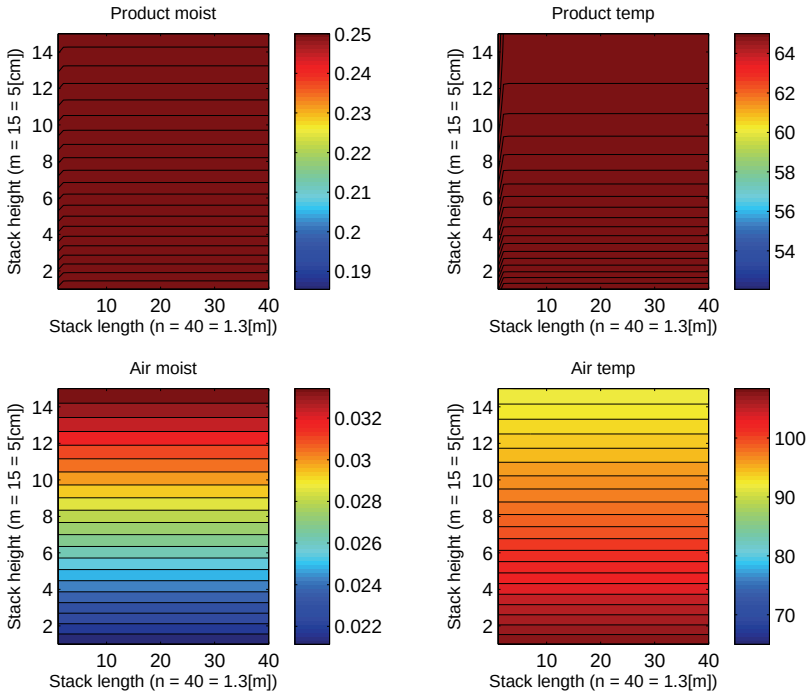

Figure 5.1: Single zone distrubution at t = 0.25 s

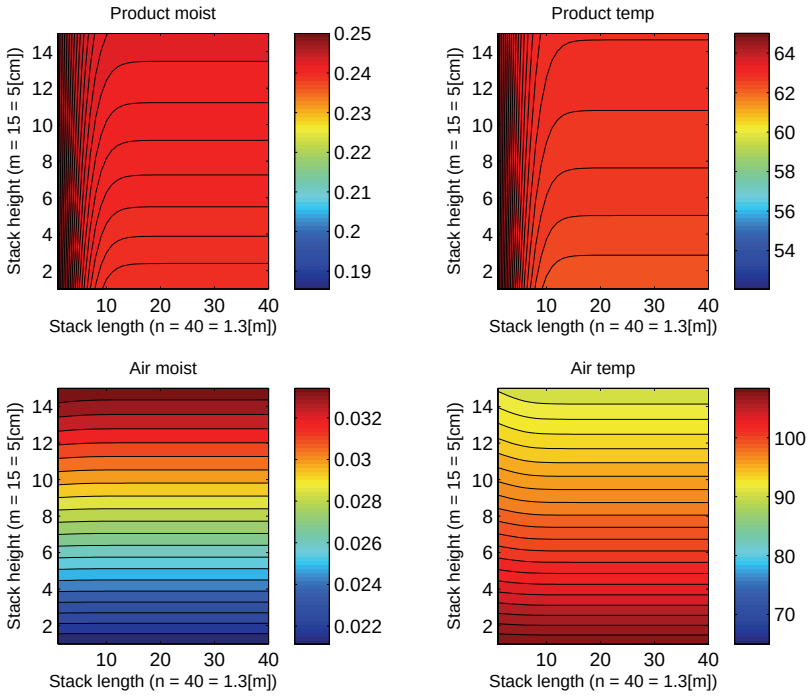

Figure 5.2: Single zone distrubution at t = 50 s

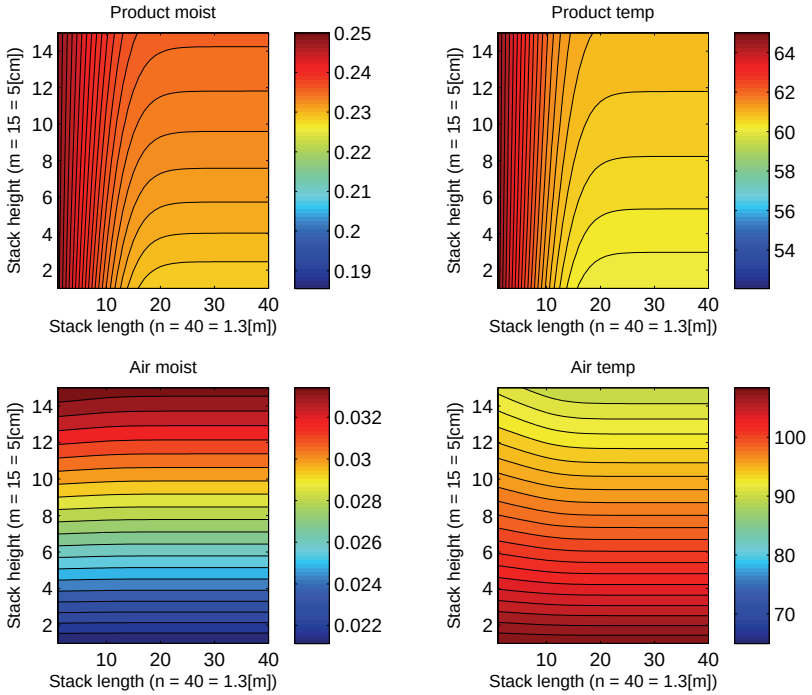

Figure 5.3: Single zone distrubution at t = 100 s

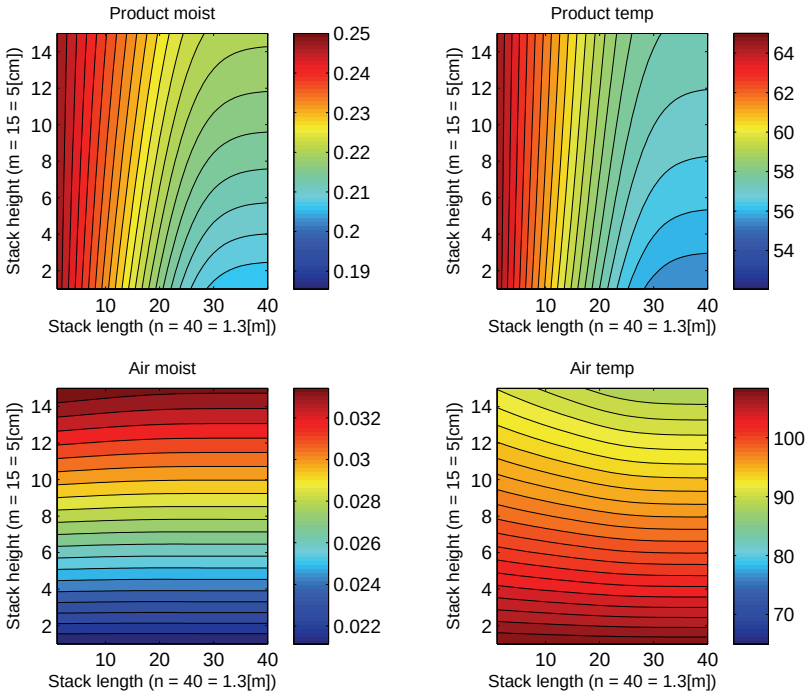

Figure 5.4: Single zone distrubution at t = 200 s

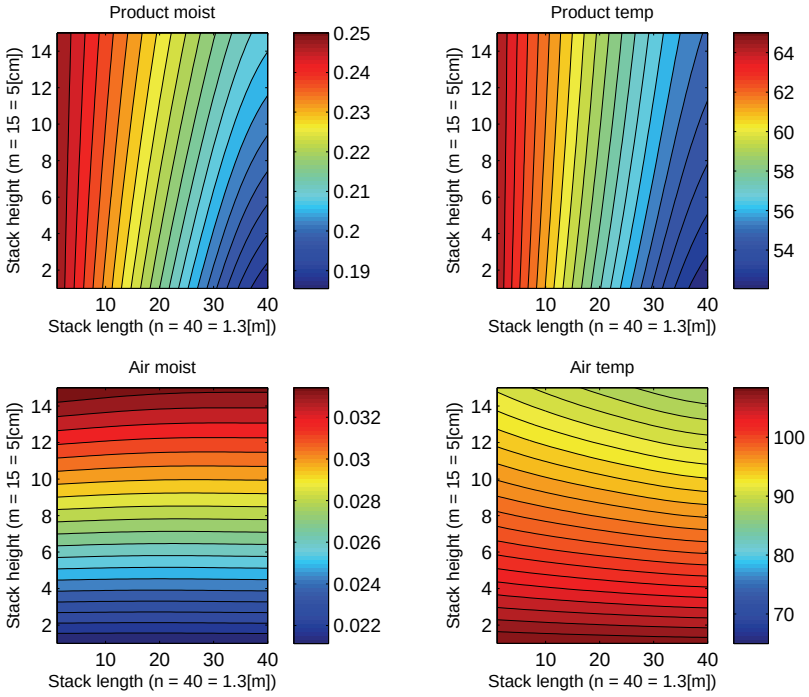

Figure 5.5: Single zone distrubution at t = 300 s

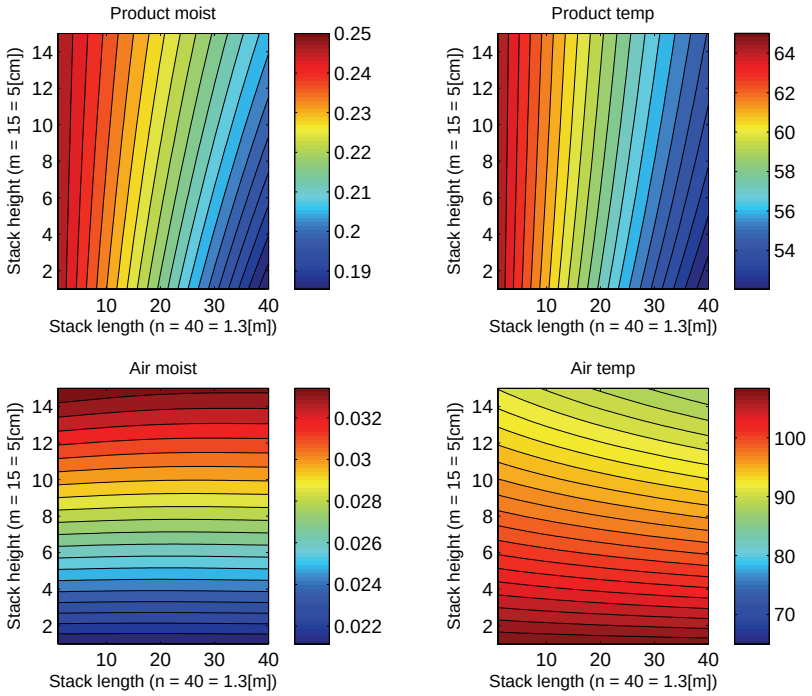

Figure 5.6: Single zone distrubution at t = 400 s

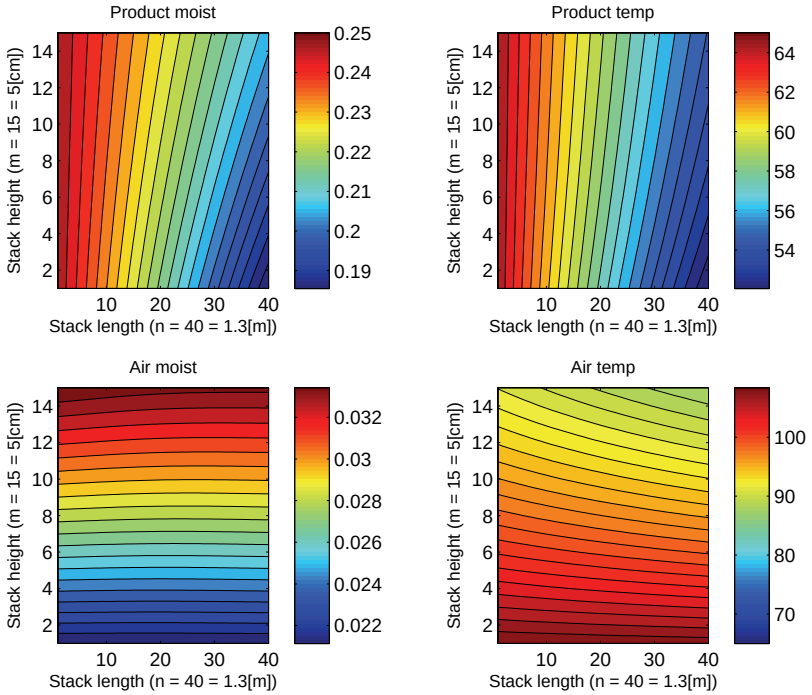

Figure 5.7: Single zone distrubution at t = 500 s

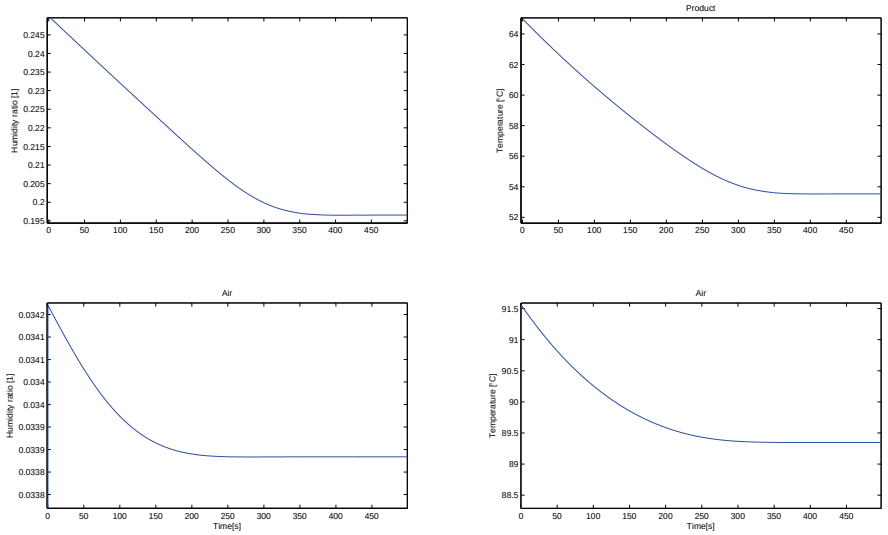

Figure 5.8: Average output values of the zone

5.1.2 Review of the Simulation Results

In the distribution plots it can be observed that the airflow enters from beneath and subsequently cools down when coming in contact with the product. It can also be seen that the air entering the dryer ($m = 1$) have constant temperature and moisture. The same applies for the product entering the dryer ($n = 1$).

Both product and air moisture has follows a natural drying progress. When inspecting the product moisture distribution, it can be seen that the moisture decreases as the product move towards the exit of the zone. The opposite is true for the air moisture, which decreases as the air moves toward the top of the product bed.

The simulation also reveals that the product temperature falls along the conveyor-belt. This is because of heat energy lost as a consequence of moisture evaporation.

In the average output value plot it can be observed how the dryer moves toward steady state. It can be seen that the states converge after 350-400 seconds. This is reasonable when the time the product uses from entry to exit is 300 seconds.

5.1.3 Energy Balance

In order for the preservation of energy to hold, the energy changes in the dryer must be correctly balanced. In [vD09] an energy balance consideration of the system, which erroneously resulted in the energy input-output being

imbalance, was performed. This imbalance is investigated and corrected below.

5.1.3.1 Correcting the Imbalance Found in Previous Work

The reason for the imbalance in [vD09] can be found in the definition of energy change that was used when inspecting the energy balance. The *incorrect* equation used for describing the product energy balance was

$$\frac{dE_p}{dt} = [w_p h_p]_{in} - [w_p h_p]_{out} \tag{5.1}$$

where w_p is the mass flow of product [kg/s] given by

$$w_p = \rho_s(\alpha + 1)v_p A_p, \tag{5.2}$$

resulted into the *incorrect equation*

$$\frac{dE_p}{dt} = [w_p(c_{ps} + \alpha c_{pw})T_p]_{in} - [w_p(c_{ps} + \alpha c_{pw})T_p]_{out} \tag{5.3}$$

instead of the *correct equation* derived in section 2.4.3.1:

$$\frac{dE_p}{dt} = [w_s(c_{ps} + \alpha c_{pw})T_p]_{in} - [w_s(c_{ps} + \alpha c_{pw})T_p]_{out} \tag{5.4}$$

where w_s is the mass flow of solid [kg/s] and is given by

$$w_s = \rho_s v_p A_p \tag{5.5}$$

The same mistake was done when inspecting the gas mixture energy balance which resulted in the *incorrect* equation:

$$\frac{dE_g}{dt} = [w_g h_g]_{in} - [w_g h_g]_{out} \tag{5.6}$$

instead of the *correct equation* derived in section 2.4.3.2:

$$\frac{dE_g}{dt} = [w_a h_g]_{in} - [w_a h_g]_{out} \tag{5.7}$$

where w_a is the mass flux of air [kg/s] and is given by

$$w_a = \rho_a v_g A_g \tag{5.8}$$

5.1.3.2 Energy Balance of the Zone

By doing an energy balance consideration of the system, it can be determined if the model is balanced or not. At steady state the energy going into a zone is equal to the energy leaving the zone. The energy balance for a zone at steady state is described by

$$\dot{E} = \dot{E}_{in} - \dot{E}_{out} = 0 \tag{5.9}$$

The energy input and output is the sum of the solid and gas energies

$$\dot{E}_{in} = \dot{E}_{p,in} + \dot{E}_{g,in} \tag{5.10}$$

$$\dot{E}_{out} = \dot{E}_{p,out} + \dot{E}_{g,out} \tag{5.11}$$

where the energy input and output of the product are given by

$$\dot{E}_{p,in} = w_s h_{p,in} \tag{5.12}$$

$$\dot{E}_{p,out} = w_s h_{p,out} \tag{5.13}$$

and the energy input and output of the gas are given by

$$\dot{E}_{g,in} = w_a h_{g,in} \tag{5.14}$$

$$\dot{E}_{g,out} = w_a h_{g,out} \tag{5.15}$$

5.1.3.3 Energy Balance for the Finite Difference Approximated model

Because the system where split in to elements when simplifying the model with the finite difference approximation, the element energies must be summarized. In Figure 5.9 there is a illustration of the energy balance of the zone.

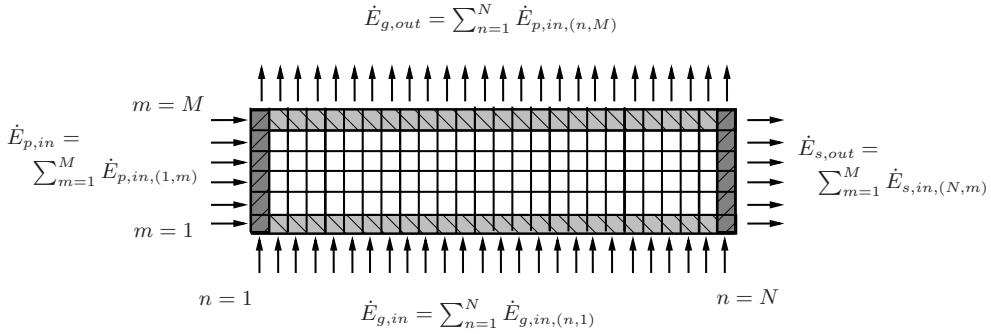

Figure 5.9: Illustration of the energy input and output of the zone simplified with FDA

By defining the energy input and output for each element as

$$\dot{E}_{p,in,(n,m)}$$

$$\dot{E}_{g,in,(n,m)}$$

$$\dot{E}_{p,out,(n,m)}$$

$$\dot{E}_{g,out,(n,m)}$$

The energy balance of both the product and the gas for the whole zone is given by the equations:

$$\dot{E}_{p,in} = \sum_{m=1}^{M} \dot{E}_{p,in,(1,m)} \tag{5.16}$$

$$\dot{E}_{p,out} = \sum_{m=1}^{M} \dot{E}_{p,in,(N,m)} \tag{5.17}$$

$$\dot{E}_{g,in} = \sum_{n=1}^{N} \dot{E}_{g,in,(n,1)} \tag{5.18}$$

$$\dot{E}_{g,out} = \sum_{n=1}^{N} \dot{E}_{g,in,(n,M)} \tag{5.19}$$

5.1.3.4 Illstrating the Energy Balance

While simulating the dryer towards steady state in section 5.1.1 the energy input and output of the system should converge towards each other. The modeling in section 4.1.2 and 4.1.3 ensure that the mass and energy balances hold. This is also illustrated in Figure 5.10 where (5.16) and (5.19) are numerically calculated for the zone. It can be seen that the energy going into the dryer is equal the energy exiting the dryer.

5.2 Linear Versus the Nonlinear Model

By simplification of the nonlinear model, a linear model was obtained. The linearizing of a nonlinear model is only accurate in the local area around the linearization point, and in some cases this area could be very small. Therefore, before using the linear model, the differences between the nonlinear and linear model is investigated in the area around the linearization point. The linear model must meet some requirements before it can substitute the nonlinear model. First, the steady state gain of the reduced model should match the non-reduced model. Secondly, in order to predict the correct behavior of the dryer, the dynamics should be as similar as possible. By comparing the step responses of the linear and the nonlinear model, the differences in dynamics as well as steady state gain can be inspected.

A dryer consisting of two identical zones is modeled. Figure 5.11 illustrates this dryer, it can be seen that both zones have independent inputs. By using two zones, a step in the input air of zone 1 will provide a response in the product output of zone 1, which will change the product input for the next zone. This way, several zone inputs are excited by doing one step.

Figure 5.12 and 5.13, shows comparisons between the models when applying a -10 degree step in input gas temperature in zone 1. The first figure com-

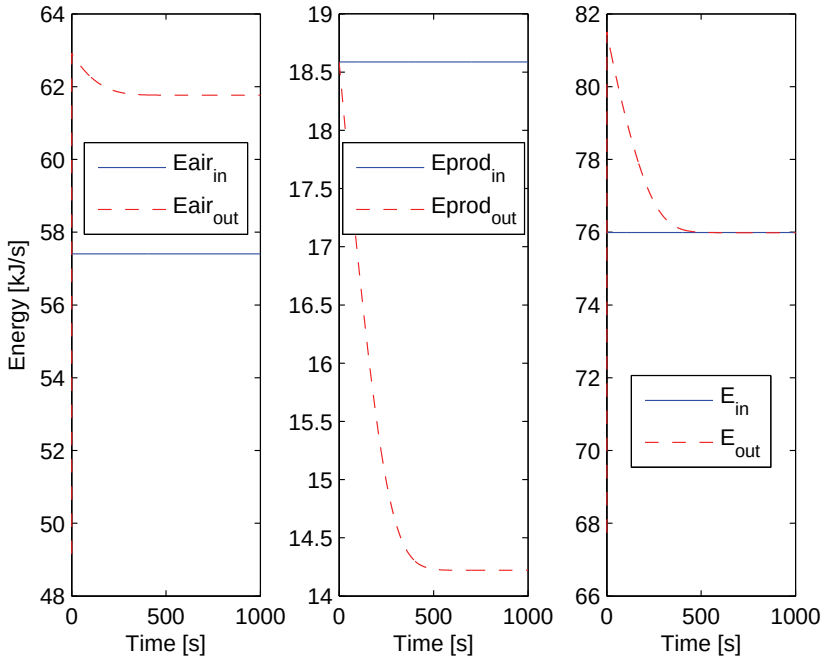

Figure 5.10: Energy balance of the single zone simulation

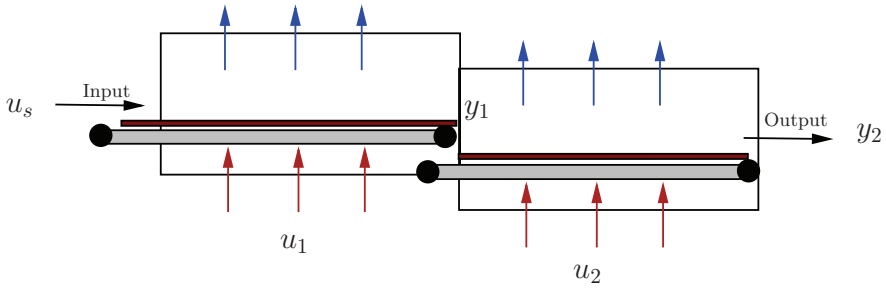

Figure 5.11: The multiple-zone dryer used in the linear vs nonlinear model comparison

pares the models while exciting the input gas temperature, while the second figure compares the models when there are changes in the product temperature and moisture input of the zone.

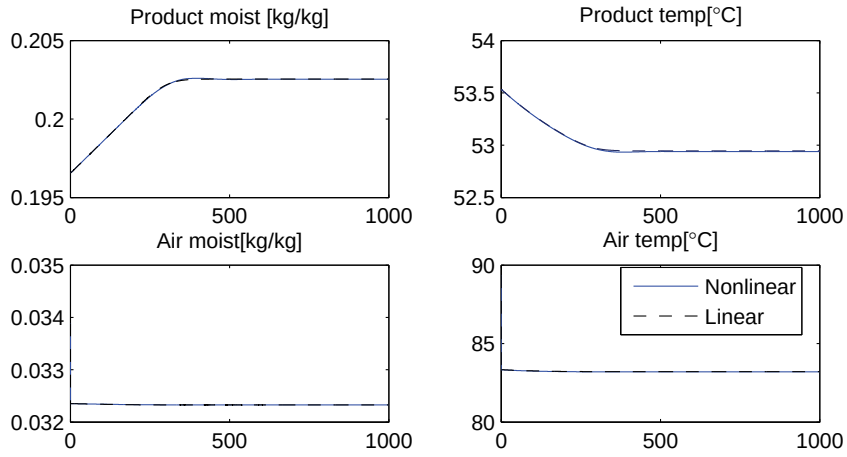

Figure 5.12: Linear vs nonlinear response, zone 1

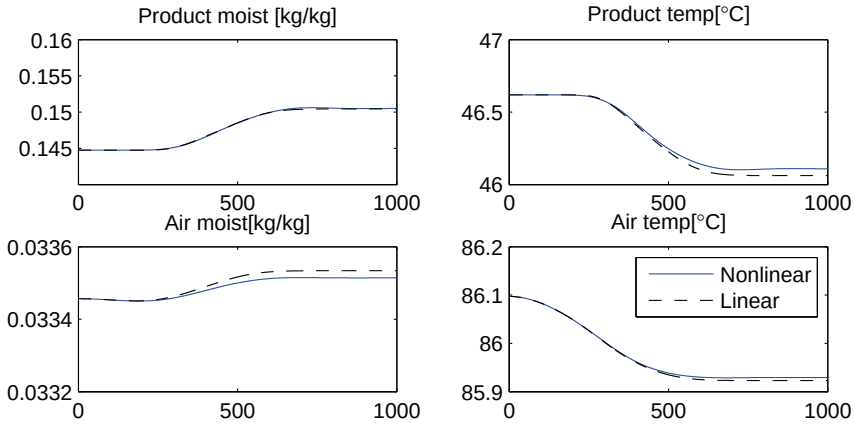

Figure 5.13: Linear vs nonlinear response, zone 2

As it can be seen in Figure 5.12, the linear response is very similar to the nonlinear. When comparing the dynamics of the models, the nonlinear model has over- and undershoots in the product moisture and temperature, respectively, which the linear model has not. The air moisture and temperature is observed close to constant. This is because of the fast gas dynamics, which stabilizes within the the first second of the simulation (see Figure 5.1).

When inspecting the response in zone 2 in Figure 5.13, it can be observed a small offset between the steady state gains. This offset is expected when

keeping in mind the effect the falling rate has on the dryer model. As it were explained in section 2.3.5, the falling rate is highly non linear. And to further illustrate the influence of the falling rate, the falling rate is removed (e.g $\zeta(\alpha) = 1$) and the simulation results are shown in Figure 5.14 and 5.15. Here the steady state offset is approximately gone, which confirms that the falling rate has a strong effect on the model.

Because the linear model is to be used in a MPC, the offset in steady state gain, will be compensated by integrators in the controller (estimator). The small loss of dynamics in the linear model is acceptable, unless the dryer is to be controlled much faster than needed. Therefore it can be concluded that the linear model could substitute the nonlinear model in a control application intended for normal control of the dryer.

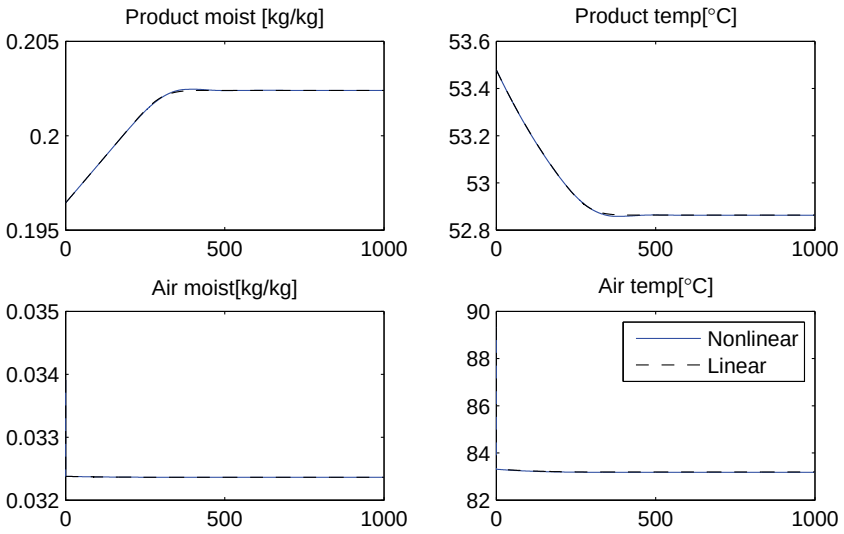

Figure 5.14: Linear vs nonlinear respons, zone 1, without including the nonlinear falling rate in the model (i.e. $\zeta(\alpha) = 1$).

5.3 Evaluating the Falling Rate

The effect of the falling rate is easily seen when observing the product as it moves along the conveyor-belt while the product crosses the critical moisture content. Figure 5.16 shows how the moisture content of the product decreases as the product is transported through the multiple-zone dryer. The multiple-zone dryer used, is the case-study dryer. More configuration or simulation details is found in chapter 6.

In [ASM07] it is stated that when the product moisture drops below the critical moisture content, dry spots on the surface of the product appears

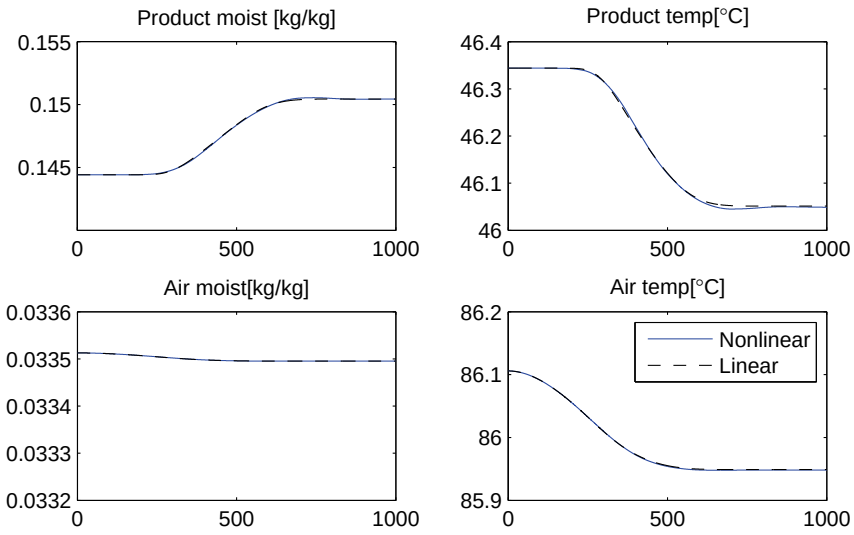

Figure 5.15: Linear vs nonlinear respons, zone 2, without including the nonlinear falling rate in the model (i.e. $\zeta(\alpha) = 1$).

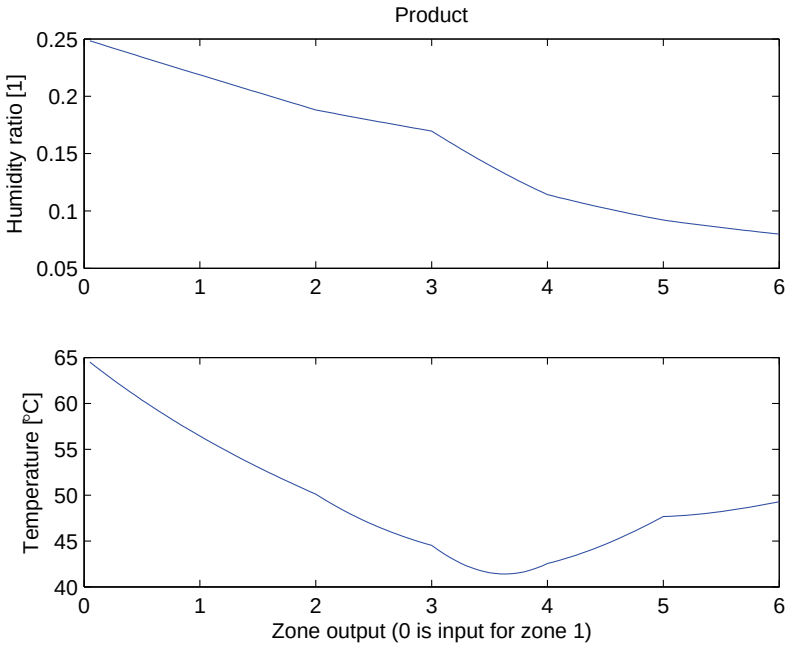

Figure 5.16: Plot of the average product states as the product is transported through the different zones. The x-axis integers indicate the zone exits

and the temperature of the solid approaches the dry bulb temperature of the drying medium. When inspecting the product temperature in Figure 5.16 this increase of temperature is found. The product reaches the critical moisture content at 0.14[kg/kg] and the product temperature increases. Further, when the critical moisture content is reached, the drying rate diminishes, which can be seen when observing the second derivative of the product moisture, which is positive. The simulation therefore reveal that the behavior of the falling rate resemble the behavior it should have due to the physics of drying theory.

Remark: An observation that may seem odd is that the temperature decreases -20°C before reaching the critical moisture content. It could be argued that the falling rate should have been reached earlier by defining the critical moisture content higher than 0.14[kg/kg]. As mentioned in section 2.3.5, the falling rate is product specific, and it could be that the chosen drying rate causes an unnatural drying progress.

Chapter 6

Case study - Control of a Six-Zone Multiple-Pass Dryer

This chapter links the theory presented in the previous chapters to a more practical setting where a specific dryer is to be modeled and controlled.

The conveyor belt dryer used in this case study is a hypothetical one, but its configuration is based on realistic assumptions according to the literature in section 2.2. The conveyor-belt dryer consist of six zones where one zone uses the exhaust air from another zone, hence the term "multiple-pass".

A mathematical model describing the dryer is constructed. The model is initially highly nonlinear and consists of PDEs which are discretized in the spatial dimension, resulting in nonlinear ODEs. Various nonlinear simulations are made in order to fit the model to the dryer configuration. Here the vaporization constant ϵ and drying rate curve $\zeta(\alpha)$ are fitted. Steady state operational points are also found, which are used later in the linearization. The model is further simplified through linearization and model reduction, resulting in a linear model small enough to be used in MPC applications.

Next, a model predictive controller (MPC) is designed for the conveyor-belt dryer, based on the control theory presented in Chapter 3. The functionality of the controller is presented and justified.

Finally, several simulations are done. The simulations ranges from input constrained MPC, to input and output constrained MPC under the influence of noise and disturbances. In addition, PI control of the dryer is configured and tuned, and the PI control is compared with MPC control.

6.1 Conveyor-Belt Dryer Description

Here a conveyor-belt dryer is defined, configured and described.

6.1.1 Choosing Which Dryer to Model

Initially, modeling an existing conveyor belt dryer, currently operating at a fish feed production line was planned. It was later decided that the modeling of this dryer, could not be successfully accomplished with the basis in the modeling framework developed in [vD09] and [Sal08a].

Secondly, a search was made for existing dryers that would fit the modeling framework. The dryer used in [Sal08a], would fit the framework, but the configuration of this dryer was considered too simple and would not demonstrate the full potential of the model and controller developed in this thesis. Later, an applicable dryer was found. However, because of the timeframe this company required in order to supply the dryer documentation needed to configure the model properly, this dryer was also discarded.

Finally, it was decided that in order to complete the modeling of a conveyor-belt dryer in the remaining timeframe given to Master students at NTNU, a hypothetical dryer had to be modeled. Further, when deciding which dryer configuration to use, it was decided that a realistic dryer for the research

- is a dryer consisting of several zones
- has a multiple-pass configuration
- has clear zone boundaries
- has a clear airstream pattern
- has known gas temperatures and flows entering the zones.
- has constant belt speed and air flows
- is a dryer where the product is evenly distributed along the conveyor-belt.

6.1.2 Conveyor-Belt Dryer Functionality

An illustration of the dryer configuration is shown in Figure 6.1. The conveyor-belt dryer consists of a six zones, and has a multiple-pass function. It has 5 external air inputs (MV's), and the product input is given by the production processes prior to the drying. All zones with the exception of zone 3 are single pass zones, and the air flowing through the product bed in zone 3 is exhaust air from zone 4. As the sizing indicates on the figure, the dimensions of zone 1,2,5 and 6 are equal. The dimensions of zone 3 and 4 are equal and the lengths are double the lengths of the zones 1,2,5 and 6. Further, in order to construct a more realistic dryer, the product bed heights in the bottom zones are higher than in the top zones. This is a normal configuration because of the fact that semi-dried products can usually be stacked higher than wet products without clumping or airstream blockage. This increase of product bed height enables

longer retention time in the bottom bed than the top bed. The bed thickness, zone dimensions and various zone parameters are listed in Table 6.2-6.4.

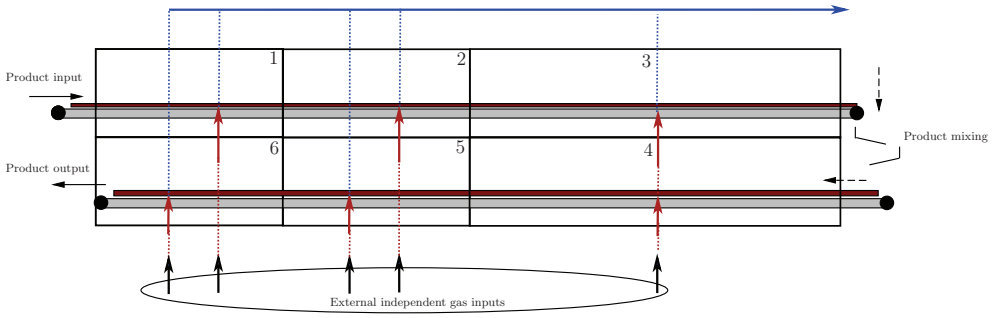

Figure 6.1: Illustration of the case-study dryer configuration

It is assumed that the input has a direct effect on the dryer, which means that the input dynamics are neglected. Input dynamics are the lower control loops controlling the input gas temperatures for the different zones. This is a reasonable assumption if the time constants of the lower control loops are much faster than the sampling time in the MPC. Burners, for example, have often fast dynamics and can therefore often be neglected when modeling the conveyor-belt dryer. Details of how to include linear input dynamics in the dryer model, can be found in section 4.5.

Remark : Sometimes, including input dynamics in the dryer model will have little or no effect at all. For example: Given that the input dynamics consisted of PIDs controlling fast burners with time constants $T_b \leq 1s$, and the sampling time for the discrete conveyor-belt dryer model was $T_s = 60s$. Then, after the model reduction technique (balanced residualization), a reduced model where the input dynamics was originally included, would be approximately the same as a reduced model where the input dynamics was neglected.

6.1.3 Defining Measurements, MVs and Disturbances

When considering what measurements typically available in conveyor-belt dryers, several issues comes into consideration. First, the temperature of the gas exhaust can be measured by simple gas temperature sensors, which can be relatively cheap, compared to moisture sensors. A moisture sensor is often slow as well as expensive. In many dryer installations, there are no moisture sensors at all. This means that the product moisture is estimated/measured by manually extruding some of the product. And then by using methods such as spectroscopy or estimating the moisture by measuring the temperature and weighing the product. Further, it is not common to have product moisture measurements inside the dryer, mainly because of the high moisture content

of the gas used for drying. In addition, it is hard to measure product bulk-moisture while still on a conveyor-belt. This can lead to a single moisture measurement at the end of the dryer, which imposes a long time delay from inlet to outlet.

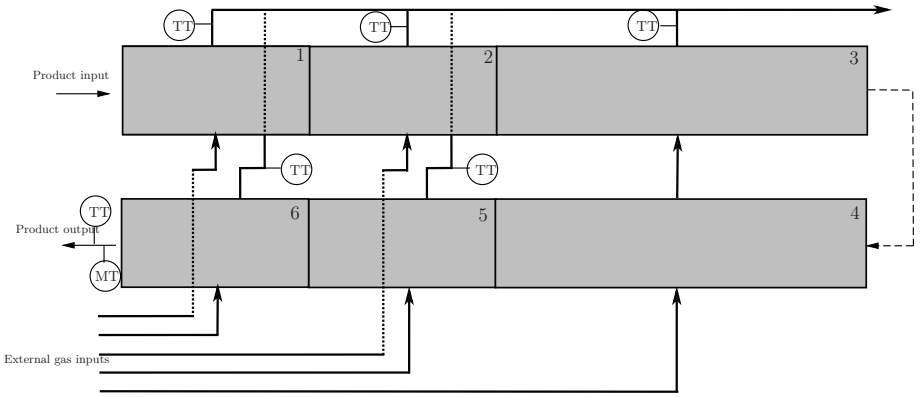

Figure 6.2: P&ID[1] illustrating the available measurements. TT=temperature transmitter, MT=moisture transmitter.

For the case study dryer, measurements are defined on the gas exhausts from each of the zones, except of zone 4, because of the multiple-pass configuration. Further, measurements are defined on the product moisture and temperature at the end of zone 6. The product temperature measurement is needed in the MPC in order to maintain the product temperature constraints during the drying. Figure 6.2 illustrates the available measurements in the dryer.

The inputs to the dryer are the product input and five gas inputs. The mass flow of each input is assumed constant, and each input is described by two variables; temperature and moisture. A realistic assumption is that the gas temperatures are the manipulated variables. The gas moisture is assumed to be slowly varying and acts as a disturbance for the dryer. Furthermore, the moisture and temperature of the product entering the dryer are given by the upstream sections of the production process, and are also considered disturbances. Table 6.1 summarizes all measurements, inputs and disturbances.

Remark: When modeling a genuine dryer, defining which disturbances a process is subjected to is not a straightforward task. In MPC for example, we want to estimate those disturbances affecting the dryer most. Even if the disturbances listed in Table 6.1 can be estimated with high accuracy, it does

Variable	**Type**	**Description**
$gT_{1,out}$	Measurement	Output gas temperature, zone 1
$gT_{2,out}$	Measurement	Output gas temperature, zone 2
$gT_{3,out}$	Measurement	Output gas temperature, zone 3
$gT_{5,out}$	Measurement	Output gas temperature, zone 5
$gT_{6,out}$	Measurement	Output gas temperature, zone 6
$pT_{6,out}$	Measurement	Output product temperature, zone 6
$\alpha_{6,out}$	Measurement	Output product moisture, zone 6
$gT_{1,in}$	CV	Input gas temperature, zone 1
$gT_{2,in}$	CV	Input gas temperature, zone 2
$gT_{4,in}$	CV	Input gas temperature, zone 4
$gT_{5,in}$	CV	Input gas temperature, zone 5
$gT_{6,in}$	CV	Input gas temperature, zone 6
$pT_{1,in}$	Disturbance	Input product moisture, zone 1
$\alpha_{1,in}$	Disturbance	Input product temperature, zone 1
$\gamma_{1,in}$	Disturbance	Input gas moisture, zone 1
$\gamma_{2,in}$	Disturbance	Input gas moisture, zone 2
$\gamma_{4,in}$	Disturbance	Input gas moisture, zone 4
$\gamma_{5,in}$	Disturbance	Input gas moisture, zone 5
$\gamma_{6,in}$	Disturbance	Input gas moisture, zone 6

Table 6.1: Dryer measurements, controlled variables(CVs) and input disturbances.

not imply robust and efficient control of the dryer, the disturbances defined can for example be negligible factors relative to other unknown disturbances. Furthermore, when defining disturbances, it should also be considered which disturbances could compensate for model errors most effectively. Increase of performance has also been observed when including the estimated disturbances as load disturbances in the manipulated variables. More about estimators and disturbance models is found in section 3.4.7.

6.1.4 Dryer and Medium Parameters

The product to be dried is fish feed pellets. Some of the medium parameters used can be found in given tables, while others can only be identified by experimentation on each particular dryer. Because this thesis is not devoted to a genuine dryer, in order to obtain a realistic simulation, the majority of the model constants are found in the dryer and product simulated in [Sal08a]. Table 6.2-6.4 lists the paramaters used.

Further, it is assumed that the product to be dried should not exceed a temperature of 60 °C[2] during the drying. Temperatures above this will lower the nutrition quality of the product. In addition, in order to avoid high temperature gradients within the product, the product temperature rate should not exceed 0.005°C/s[3]. Rates above this may lead to shrinking and therefore structural changes within the product itself.

[2]It can be argued that the 60°C constraint is somewhat low, especially when the product input temperature is at 65°C. The constraint is chosen this low in order for the constraint to be active in the MPC later. In other words, to demonstrate the constraint capabilities of the MPC.

[3]The temperature rate constraint at 0.005°C/s is chosen this low for the the same reason as the temperature constraint is chosen[2].

Variable	Value	Denomination	Description
α_{crit}	0.14	kg/kg	Critical moisture content
c_{PW}	4220	J/kg K	Specific heat capacity, water (375K)
c_{PS}	2000	J/kg K	Specific heat capacity, product (375K)
c_{PV}	1890	J/kg K	Specific heat capacity, steam (375K)
c_{PA}	1000	J/kg K	Specific heat capacity, Air (375K)
h	25	J/s m^2 K	Heat transfer coefficient
M_g	28.97×10^{-3}	kg/mol	Molar mass, dry air
P_a	101325	Pa	Atmospheric pressure
T_0	273.15	K	Reference temperature
P_{s0}	6.11	hPa	Partial pressure at T_0
R	8.14472	J/K mol	Universal gas constant
R_v	461.5	J/kg K	Specific gas constant, steam
β	0.62197	1	Specific mass ratio, steam/dry air
ε	100	m^2/m^3	Vaporization area per product volume
λ_0	2257000	J/kg	Latent heat of vaporization
ρ_s	600	kg/m^3	Mass density, product
ρ_g	1.009	kg/m^3	Mass density, air

Table 6.2: Model constants, case-study dryer

Variable	Value	Denomination	Description
Δx_1	2	m	Conveyor-belt length, zone 1
Δx_2	2	m	Conveyor-belt length, zone 2
Δx_3	4	m	Conveyor-belt length, zone 3
Δx_4	4	m	Conveyor-belt length, zone 4
Δx_5	2	m	Conveyor-belt length, zone 5
Δx_6	2	m	Conveyor-belt length, zone 6
Δz_1	0.05	m	Product stack height, zone 1
Δz_2	0.05	m	Product stack height, zone 2
Δz_3	0.05	m	Product stack height, zone 3
Δz_4	0.075	m	Product stack height, zone 4
Δz_5	0.075	m	Product stack height, zone 5
Δz_6	0.075	m	Product stack height, zone 6
Δy	0.6	m	Conveyor-belt width, zone 1-6

Table 6.3: Control volume dimensions, case-study dryer

Variable	**Value**	**Denomination**	**Description**
Δt_1	5	[minutes]	retention time, zone 1
Δt_2	5	[minutes]	retention time, zone 2
Δt_3	10	[minutes]	retention time, zone 3
Δt_4	15	[minutes]	retention time, zone 4
Δt_5	7.5	[minutes]	retention time, zone 5
Δt_6	7.5	[minutes]	retention time, zone 6
$v_{x,t}$	0.0067	[m/s]	velocity, top belt
$v_{x,b}$	0.0044	[m/s]	velocity, bottom belt
$v_{z,1}$	0.2315	[m/s]	velocity, air, zone 1
$v_{z,2}$	0.2315	[m/s]	velocity, air, zone 2
$v_{z,3}$	0.1819	[m/s]	velocity, air, zone 3
$v_{z,4}$	0.1819	[m/s]	velocity, air, zone 4
$v_{z,5}$	0.2315	[m/s]	velocity, air, zone 5
$v_{z,6}$	0.2315	[m/s]	velocity, air, zone 6

Table 6.4: Nominal steady-state operational values, case-study dryer

6.2 Building the Model

After an applicable conveyor-belt dryer has been found and the configuration has been identified, the next step is to build the model.

First, a nonlinear model for the dryer is build. Then, various nonlinear simulations are done in order to fit the model to the actual plant. Here the vaporization constant ϵ and drying rate curve $\zeta(\alpha)$ is identified. Operational points are are also found, which are used in the linearization later. Next, by linearizing each zone around the steady state values obtained by the nonlinear simulation, a linear model (4.59) for each zone is obtained:

$$\dot{x}_j = A_j x_j + B_j u_j \tag{6.1}$$

Here j is the zone number. u_j is the input of product and air to the zone, which can either be transfered from another zone, or it could be an external input for the dryer. For more details of the zone structure, see section 4.3. For some examples of u_j see appendix A.3.

6.2.1 Structuring the Conveyor-Belt Model

By using the structure developed in [vD09], which is reposted in appendix A.3, the linear model for the conveyor-belt dryer becomes:

$$\begin{aligned} \dot{x} &= Ax + B'u' \\ z &= Cx \end{aligned} \tag{6.2}$$

where

$$A = \begin{bmatrix} A_1 & 0 & 0 & 0 & 0 & 0 \\ B_2\Phi_s & A_2 & 0 & 0 & 0 & 0 \\ 0 & B_3\Phi_s & A_3 & B_3\Phi_g & 0 & 0 \\ 0 & 0 & B_4\Phi_{\bar{s}} & A_4 & 0 & 0 \\ 0 & 0 & 0 & B_5\Phi_s & A_5 & 0 \\ 0 & 0 & 0 & 0 & B_6\Phi_s & A_6 \end{bmatrix} \tag{6.3}$$

$$B' = \begin{bmatrix} B_1B_s & B_1B_g & 0 & 0 & 0 & 0 \\ 0 & 0 & B_2B_g & 0 & 0 & 0 \\ 0 & 0 & 0 & 0 & 0 & 0 \\ 0 & 0 & 0 & B_4B_g & 0 & 0 \\ 0 & 0 & 0 & 0 & B_5B_g & 0 \\ 0 & 0 & 0 & 0 & 0 & B_6B_g \end{bmatrix} \tag{6.4}$$

$$C = \begin{bmatrix} C_1 & C_2 & C_3 & C_4 & C_5 & C_6 \end{bmatrix} \tag{6.5}$$

where C_j is the ouput extraction matrix of zone j, and is in this case defined by the following matrices:

$$C_1 = \begin{bmatrix} 0 & 0 & 0 & 0 \\ 0 & 0 & 0 & 0 \\ 0 & 0 & 0 & C_g \\ 0 & 0 & 0 & 0 \\ 0 & 0 & 0 & 0 \\ 0 & 0 & 0 & 0 \\ 0 & 0 & 0 & 0 \\ 0 & C_s & 0 & 0 \\ 0 & 0 & 0 & 0 \\ 0 & 0 & 0 & 0 \\ 0 & 0 & 0 & 0 \\ 0 & 0 & 0 & 0 \end{bmatrix} \quad C_2 = \begin{bmatrix} 0 & 0 & 0 & 0 \\ 0 & 0 & 0 & 0 \\ 0 & 0 & 0 & 0 \\ 0 & 0 & 0 & C_g \\ 0 & 0 & 0 & 0 \\ 0 & 0 & 0 & 0 \\ 0 & 0 & 0 & 0 \\ 0 & C_s & 0 & 0 \\ 0 & 0 & 0 & 0 \\ 0 & 0 & 0 & 0 \\ 0 & 0 & 0 & 0 \\ 0 & 0 & 0 & 0 \end{bmatrix} \quad C_3 = \begin{bmatrix} 0 & 0 & 0 & 0 \\ 0 & 0 & 0 & 0 \\ 0 & 0 & 0 & 0 \\ 0 & 0 & 0 & 0 \\ 0 & 0 & 0 & C_g \\ 0 & 0 & 0 & 0 \\ 0 & 0 & 0 & 0 \\ 0 & 0 & 0 & 0 \\ 0 & 0 & 0 & 0 \\ 0 & C_s & 0 & 0 \\ 0 & 0 & 0 & 0 \\ 0 & 0 & 0 & 0 \end{bmatrix} \tag{6.6}$$

$$C_4 = \begin{bmatrix} 0 & 0 & 0 & 0 \\ 0 & 0 & 0 & 0 \\ 0 & 0 & 0 & 0 \\ 0 & 0 & 0 & 0 \\ 0 & 0 & 0 & 0 \\ 0 & 0 & 0 & 0 \\ 0 & 0 & 0 & 0 \\ 0 & 0 & 0 & 0 \\ 0 & 0 & 0 & 0 \\ 0 & 0 & 0 & 0 \\ 0 & C_s & 0 & 0 \\ 0 & 0 & 0 & 0 \end{bmatrix} \quad C_5 = \begin{bmatrix} 0 & 0 & 0 & 0 \\ 0 & 0 & 0 & 0 \\ 0 & 0 & 0 & 0 \\ 0 & 0 & 0 & 0 \\ 0 & 0 & 0 & C_g \\ 0 & 0 & 0 & 0 \\ 0 & 0 & 0 & 0 \\ 0 & 0 & 0 & 0 \\ 0 & 0 & 0 & 0 \\ 0 & 0 & 0 & 0 \\ 0 & C_s & 0 & 0 \end{bmatrix} \quad C_6 = \begin{bmatrix} C_s & 0 & 0 & 0 \\ 0 & C_s & 0 & 0 \\ 0 & 0 & 0 & 0 \\ 0 & 0 & 0 & 0 \\ 0 & 0 & 0 & 0 \\ 0 & 0 & 0 & 0 \\ 0 & 0 & 0 & C_g \\ 0 & 0 & 0 & 0 \\ 0 & 0 & 0 & 0 \\ 0 & 0 & 0 & 0 \\ 0 & 0 & 0 & 0 \\ 0 & 0 & 0 & 0 \end{bmatrix} \tag{6.7}$$

where the matrices $\boldsymbol{A}_j, \boldsymbol{B}_j, \boldsymbol{B}_s, \boldsymbol{B}_g, \boldsymbol{\Phi}_s, \boldsymbol{\Phi}_{\overline{s}}$ and $\boldsymbol{\Phi}_g$ are defined in (4.60), (4.61), (A.62), (A.64), (A.59), (A.60) and (A.66) respecively. The output matrices $\boldsymbol{C}_s$ and $\boldsymbol{C}_g$ are defined in (A.82).

The dryer model (6.2) is a simple form, where both inputs and disturbances

have been stacked in the input vector u':

$$u' = \begin{bmatrix} \alpha_{1,in} \\ pT_{1,in} \\ \gamma_{1,in} \\ gT_{1,in} \\ \gamma_{2,in} \\ gT_{2,in} \\ \gamma_{4,in} \\ gT_{4,in} \\ \gamma_{5,in} \\ gT_{5,in} \\ \gamma_{6,in} \\ gT_{6,in} \end{bmatrix} \tag{6.8}$$

Further, the output vector z is given by

$$z = \begin{bmatrix} y \\ y_e \end{bmatrix} \tag{6.9}$$

where the elements in y are the measured outputs of the model. The elements in y_e are the outputs of the model which is not measured, but will be estimated by the Kalman filter in the MPC. Later, constraints are placed on the elements in y_e in order to keep the temperature of the product below some level. y and y_e is structured as

$$y = \begin{bmatrix} \alpha_6, out \\ pT_{6,out} \\ gT_{1,out} \\ gT_{2,out} \\ gT_{3,out} \\ gT_{5,out} \\ gT_{6,out} \end{bmatrix} \qquad y_e = \begin{bmatrix} pT_{1,out} \\ pT_{2,out} \\ pT_{3,out} \\ pT_{4,out} \\ pT_{5,out} \end{bmatrix} \tag{6.10}$$

6.2.2 Choosing the Spatial Discretization Resolution

When simplifying the system with the FDA, a discretization resolution is used. Ideally this resolution is infinite, but because of hardware limitations the resolution is limited. The total number of states in the system has a strong correlation with the simulation duration and memory usage of the hardware. The simulations performed in this thesis was limited by the available memory in the hardware[4]. The model was simulated using *ode23tb* in MATLAB[5] running Microsoft Windows 7 Enterprise 64-bit. The total number of states which were

[4]Intel core 2 Duo CPU P8700 @ 2.53GHz 2.54GHz, 4GB DDR2 ram

[5]MATLAB R2009b, 7.9.0.529. Software package used: Control System Toolbox V8.4

possible to simulate without virtual memory swapping, was approximately $25 \times 25 \times 4 \times 6(N \times M \times STATES\_PER\_ZONE \times ZONES) = 15000$. If virtual memory swapping occurred the simulation duration increased severely, therefore virtual memory swapping must be avoided. After simulating the dryer with different resolutions, it was found that the total number of spatial elements, should not exceed $M \times N \leq 600$ because of the harware limitations. Increasing the total number of spatial elements above this level caused virtual memory swapping.

In Figure 6.3 the same nonlinear dryer simulation is performed using several different discretization resolutions. (Input configuration has been chosen arbitrarily, and is not used further in this thesis). Here several things can be observed:

- When N approaches 20, convergence is close, with regard to the product temperature.
- M should be higher than 20, for convergence with regard to product temperature.
- When M approaches 20, convergence is close, with regard to the product moisture.
- N should be higher than 20, for convergence with regard to product moisture,

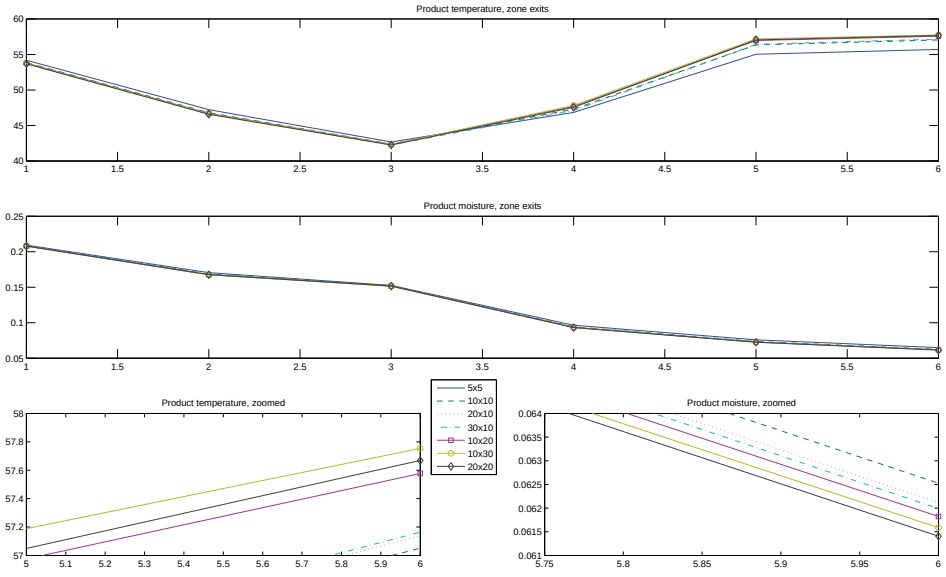

Figure 6.3: Dryer steady-states, simulated with different discretization resolutions($N \times M$).

Because increasing N above 20 does not significantly affect the product temperature, and because increasing M above 20 does not significantly affect the product moisture, both N and M should be the same size, at least for the control volume dimensions (Table 6.3) used in this case-study. Further for a fast simulation duration and model reduction duration $N = 20$ and $M = 20$ is used, even though it is possible to simulate the system with the resolution 25×25.

Remark: It could be argued that zones of different sizes should have different discretization resolutions. But for implementation ease, all zones are spatially discretized with the same resolution.

6.2.3 Simplifying the Model

Because the model is to be used in an MPC application, the computational requirements should be realistic for a real implementation. Because each zone of the dryer has 1600 states, the conveyor-belt dryer model (6.2) has a total of $1600 \times 6 = 9600$ states.

In order to use the model in an MPC application, the linear model (6.2) was discretized and then simplified(reduced) by *balanced residualization*. The discretization, which takes place before the model reduction technique, is the first step toward model reduction. This is because model dynamics with time constants much lower than the sampling time are lost during the discretization, and therefore, the total states of the reduced discretized model will be lower than it would be without discretizing before the model reduction. The dryer model (6.2), is discretized by the method *c2d* in MATLAB. A zero order hold exact approximation was used. This means that the control inputs are assumed piecewise constant over the sampling time ($60s$). The term 'exact' means that the time responses of the continuous and discretized models would match exactly for a staircase input. More detail about (exact) discretization can be found in [Che99]. The discrete model can now stated be as

$$\begin{aligned} x_{k+1} &= A_d x_k + B'_d u'_k \\ z_k &= C_d x_k \end{aligned} \tag{6.11}$$

Before defining a disturbance model, the discrete model (6.11) is reduced by *balanced residualization*. It can be seen in equation (3.13), that even though the D matrix obtained by modeling is a zero-matrix, the reduction method supplies a non-zero reduced D_r matrix. The reduced discrete model is now given by

$$\begin{aligned} x_{r,k+1} &= A_r x_{r,k} + B'_r u'_k \\ z_{r,k} &= C_r x_{r,k} + D'_r u'_k \end{aligned} \tag{6.12}$$

The reduced model obtained by balanced residualization, is a model where the states having little effect on the input/output behavior are removed. The

number of states which can be removed is dependent of the configuration of the dryer. With the configuration used in the case study dryer, the model were reduced from 9600 states to 121 states. The tolerance for the Hankel singular values is 10^{-7}. More about balanced residualization, can be found in section 3.3 or [SP05].

Remark: Since the balanced residualization and the zero order hold discretization both were time consuming with similar durations, the model was actually reduced two times by balanced residualization. By reducing before discretizing the system, the discretization duration was negligible compared to the unreduced discretization duration. The final balanced residualization duration of the discrete system was also negligible compared to the first.

6.2.4 Defining the Disturbance Model

The dryer model (6.12) is now restructured in order to separate the disturbances from the manipulated variables. The dryer is now given by

$$\begin{aligned} \dot{x}_{r,k} &= A_r x_{r,k} + B_r u_k + B_r d_k \\ z_k &= C_r x_{r,k} + D_r u_k + E_r d_k \end{aligned} \tag{6.13}$$

where the input u and disturbance d vector are defined as

$$u = \begin{bmatrix} gT_{1,in} \\ gT_{2,in} \\ gT_{4,in} \\ gT_{5,in} \\ gT_{6,in} \end{bmatrix} \qquad d = \begin{bmatrix} \alpha_{1,in} \\ pT_{1,in} \\ \gamma_{1,in} \\ \gamma_{2,in} \\ \gamma_{4,in} \\ \gamma_{5,in} \\ \gamma_{6,in} \end{bmatrix} \tag{6.14}$$

Here, the B and B_d matrices is obtained by simple splitting and reordering of the column in B'. In the same way, D_r and E_r are obtained by simple splitting and reordering of the columns in D_r'.

6.2.5 Dryer Steady-State

Here the nonlinear model is simulated toward steady-state. Several simulations are performed in order to fit the model to a realistic operational point, but only the final steady-state is shown. The steady-state is also used when linearizing the system.

6.2.5.1 Simulation Details

The model is simulated using *ode23tb*[6] in MATLAB[7] on a laptop[8] running Microsoft Windows 7 Enterprise 64-bit. Ode23tb was found in [vD09] to be the most efficient, stable and non-oscillating solver. Further, by optimalizing the solver code/algorithm[9] developed in [vD09], a further increase of effiency was achieved. Furthermore, by supplying the solver with the system Jacobian, the efficiency of the solver increased significantly. In Table 6.5 the decrease of simulation duration is observed.

Solution algorithm	**Simulation duration**
Code/algorithm used in [vD09] & [Sal08a]	4 hours, 52 minutes
Optimized code/algorithm	3 hours, 25 minutes
Suppling solver with Jacobian & new structure	12 minutes

Table 6.5: Simulation durations when solving the nonlinear model with different algorithms. The system solved has a discretization resolution of 20x20, which results in a system with $20 \times 20 \times 4 \times 6 = 9600$ states. The stiff solver *ode23tb* were used in all simulations.

6.2.5.2 Input Values

Before simulating toward steady state, a reasonable operational area must be found. It is assumed that the product exiting the dryer has a moisture content around 8%, which the dryer studied in [Sal08a] had. A reasonable assumption for the product entering the dryer is a moisture content and temperature of 25% and 65°C respectively.

It is common to use higher temperatures early in conveyor-belt dryers. Reasons for this are among others that the very wet product has much higher resistance to cracking and overheating than the dried product. Now by tuning/adapting the input gas temperatures, the configuration of which the product leaving the dryer has a moisture content of 8% can be identified. By using the input configuration listed in Table 6.6, reasonable steady-state is achieved.

[6] Ode23tb is a stiff implicit Runge-Kutta solver, which uses the trapezoidal rule to solve the system. More about the trapezoidal rule can be found in [EG03].

[7] MATLAB R2009b, 7.9.0.529

[8] Intel core 2 Duo CPU P8700 @ 2.53GHz 2.54GHz, 4GB DDR2 ram

[9] The code/algorithm was originally developed in [Sal08a], and later modified in [vD09].

Variable	Value	Denomination	Description
$gT_{1,in}$	100	°C	Gas temperature, zone 1
$gT_{2,in}$	100	°C	Gas temperature, zone 2
$gT_{4,in}$	90	°C	Gas temperature, zone 4
$gT_{5,in}$	90	°C	Gas temperature, zone 5
$gT_{6,in}$	70	°C	Gas temperature, zone 6
γ_{in}	0.02	kg/kg	Gas moisture, zone 1,2,4,5,6
$pT_{1,in}$	65	°C	Product temperature
$\alpha_{1,in}$	0.25	kg/kg	Product moisture

Table 6.6: Input configuration obtaining the operational area.

6.2.5.3 Average Value Review

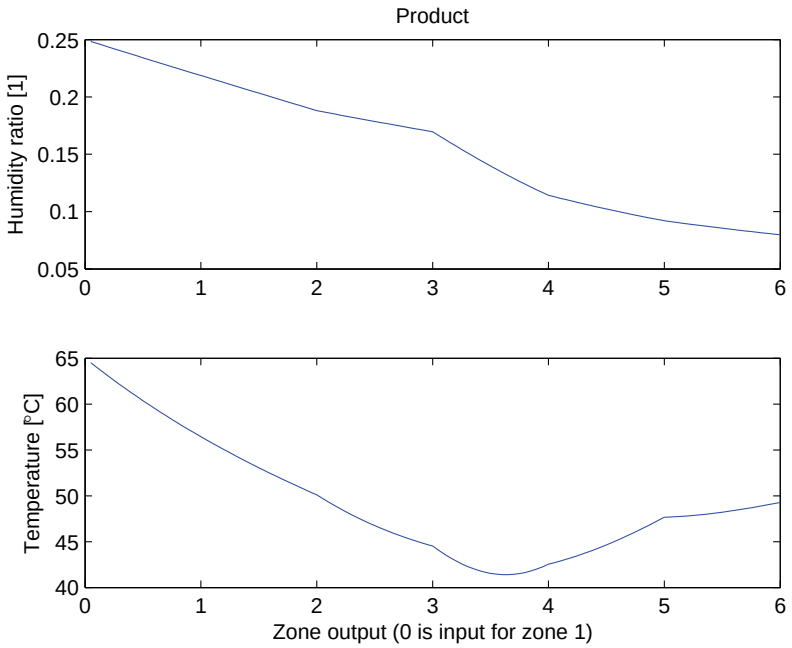

Figure 6.4: Plot of the average product states as the product is transported through the different zones. The x-axis integers indicate the zone exits. Keep in mind that zone 3 and 4 have twice the length of the other zones, but are spatially discretized with the same resolution as the other zones

Figure 6.4 shows the average product states as the product is transported through the different zones. Several things can be observed about the drying rate:

- The drying rate in zone 1 and 2 is approximately equal. This is because

these zones have identical parameters as well as input gas temperatures. In addition, the falling rate has not been reached yet, which means that the drying rate is primarily governed by the gas temperature.

- Because zone 3 uses the exhaust air from zone 4 it can be seen that the drying rate is lower than the previous zones, even though the zone has a retention time of 10 minutes.
- Zone 4 has a higher drying rate than the other zones, primarily because of the retention time of 15 minutes.
- Zone 5 and 6 has similar drying rates as zone 1 and 2 resulting from lower gas temperatures, higher retention time and the fact that the critical moisture content[10] was reached in zone 3.

Further, when inspecting the product temperature it can be seen that the temperature decreases until zone 3. Here the critical moisture content is reached and the temperature increases. The effect of the falling rate in this simulation is more thoroughly explained in section 5.3. Furthermore, the temperature gradient in zone 5 is higher than in zone 6 because of a higher gas temperature and moisture content.

6.2.5.4 Product and Gas Distrubution Review

In Figures 6.5-6.8 the product and gas distributions for the dryer is shown. The zones are aligned as the dryer is configured, with the product entering at the top left, being mixed between zone 3 and 4, and exiting at the bottom left. The x-axis integers indicate the zone exits. Each zone is discretized with resolution 20x20, resulting in a total of 20 X 20 X 6 elements in each figure.

Figure 6.5 and 6.6 shows the product distrubution through the dryer. It can be seen that the product entering zone 4, has an evenly distributed moisture and temperature as a result of the product mixing. Further, the product states seem to have a realistic distribution with the moisture content being lower near the bottom of the bed. And the temperature being lower near the bottom of the bed before the critical moisture content, and as the critical moisture content is reached, the temperature near the bottom of the bed increases.

Figure 6.7 and 6.8 shows the gas distribution through the dryer. It can be seen that the gas entering zone 3, has an evenly distributed moisture and temperature near the bottom of the bed, as a result of using the exhaust gas[11] from zone 4. Another outcome of the multiple-pass configuration can be seen

[10] The critical moisture content is at 0.14[kg/kg]. After this point the falling rate begins, and the drying rate decreases. More about the critical moisture content is found in section 2.3.5.

[11] The exhaust air from zone 4 is mixed before entering zone 4, see Appendix A.3.1.3

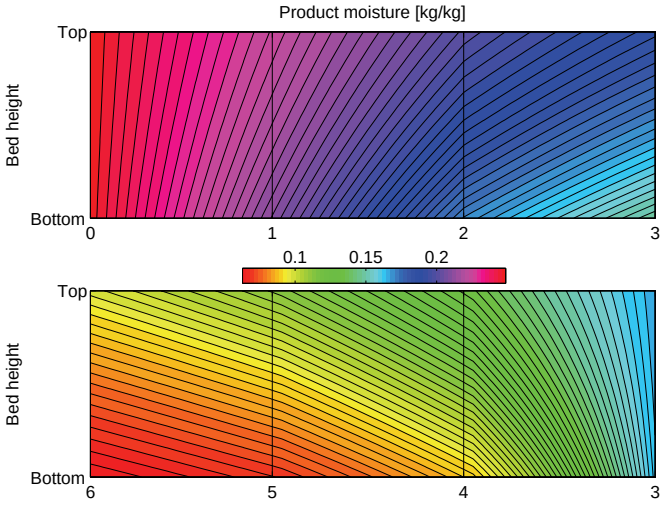

Figure 6.5: Product moisture distrubution at steadystate

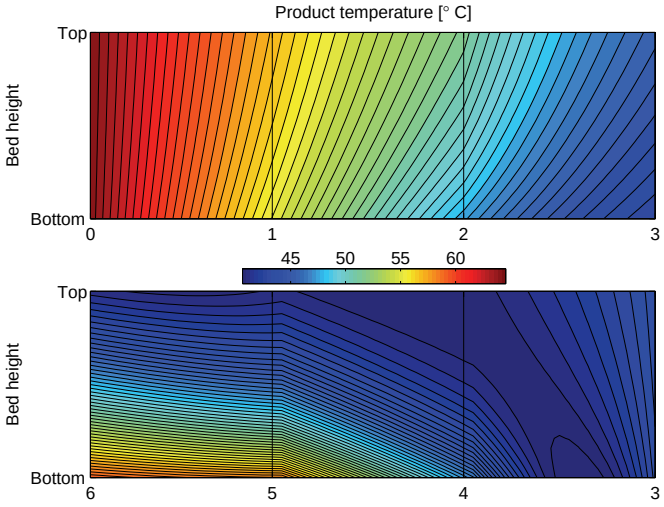

Figure 6.6: Product temperature distrubution at steadystate

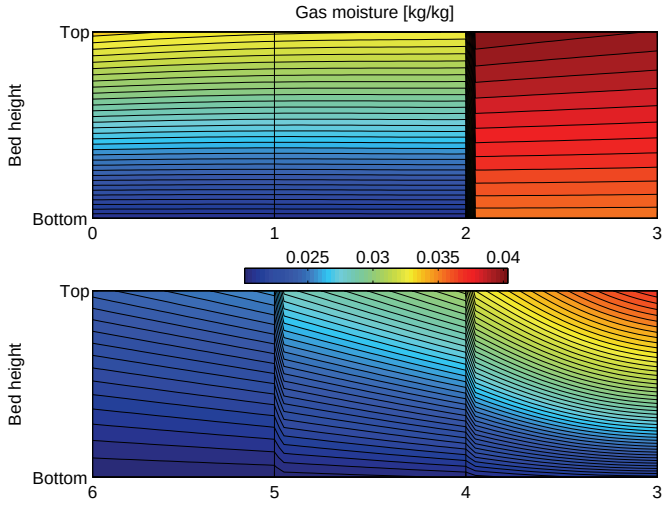

Figure 6.7: Gas moisture distrubution at steadystate

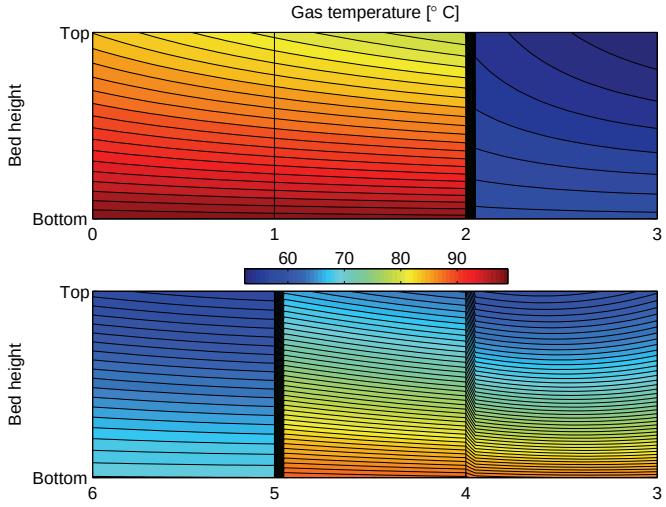

Figure 6.8: Gas temperature distrubution at steadystate

in zone 3, where the gas temperature is lower and the moisture content higher that the other zones.

Further, the gas states, just as the product states, seems to have a realistic distribution with the moisture content being lower near the bottom of the bed, while absorbing the product moisture towards the top. And the temperature is higher near the bottom of the bed, while decreasing as the heat energy is used to evaporate the product moisture.

6.3 MPC Functionality

The model predictive controller is an advanced controller that accounts for constraints in the input, output and process states. These constraints are met while simultaneously either maximizing the throughput, minimizing the input or a combination of these. This can only be practically achieved by implementing algorithms that are robust, as well as efficient. In section 3.4 the theory behind the model predictive controller were presented. In this section the theory is set in context with the case-study. Also, the controller objectives and functionality for the case study is presented.

6.3.1 Controller Objectives

The objective of the controller is to control the moisture content of the product exiting the dryer. At the same time, the product temperature should be below 60°C in order to maintain a high product nutrition quality. Furthermore, the product should not have high temperature rates during the drying process, which means that there are constraints imposed on the change of product temperature from one time step to the next.

6.3.2 Functionality Arguments

The model predictive controller can be divided into three parts (illustrated in Figure 3.1), a target calculation routine, an estimator and a main optimization routine. The controlled variables are the product moisture content at the zone exits, while the manipulated variables are the input air temperatures.

6.3.2.1 Target Calculation Routine

The target calculation routine, supplies the main optimization routine with a trajectory to follow along the prediction horizon. Because there are constraints both on the inputs and outputs, the main optimization routine must be provided with a feasible target. This feasible target provided by the target calculation routine, must account for the current state of the dryer, as well as disturbances and reference trajectory.

A poor target calculation routine may provide the main optimization routine with a non-feasible target, which may lead to a poor solution or a non-feasible problem. Because it is not given that the conveyor-belt dryer has equal amount of outputs as inputs, it is not always possible to invert the system matrices in order to find a feasible solution, and a pseudo inverse, may lead to poor solutions diverging from the reference trajectories.

A target calculation routine which is an optimization prior to the main optimization routine is therefore chosen. This optimization accounts for the estimated/measured disturbances, as well as reference trajectory. In addition, the target will always be optimal and respect the constraints.

6.3.2.2 Estimator

The estimator is used for estimating the states and disturbances, which is supplied to the target calculation routine and main optimization routine, see Figure 3.1. The Kalman filter is the estimator used in this thesis.

First it was attempted to use a Leuenberg observer as estimator, but the attempt failed. There are two reasons for why the Leuenberg observer failed. First, the linear model was not observable, even after the balanced residualization. This implied that the poles of the observer could not be arbitrarily chosen. Secondly, the reduced model had no particular structure in the system matrix, which made it difficult to choose which poles to move.

The choice of estimator therefore fell upon the Kalman filter, which only demands that the system is detectable, see. section 3.4.7.2. Furthermore, by using the Kalman filter as an estimator, the estimator poles are calculated using tuning matrices, which is more straightforward, than placing the poles directly.

6.3.2.3 Main Optimization Routine

The main optimization routine of the MPC consist of several features, where each feature contributes to either

- Stability
- Optimalization feasibility
- Control optimality
- Algorithm efficiency

In order to induce stability in the controller, an infinite horizon criterion is used. The infinite horizon criterion is solved by choosing an input horizon, where a linear quadratic regulator (LQR) is used after the input horizon. The use of the LQR is based on the assumption that the system is within the constraints by the end of input horizon. The infinite horizon criteria is implemented by penalizing the distance between the target and the moisture content at time step $k = H_u$. If the predicted distance between the product moisture content and the target at $k = H_u$ is high, then the controller will use more input in order to ensure convergence toward the target for the product moisture content.

If the conveyor-belt dryer is to operate close to the constraints and a disturbance push some constrained output outside the feasible region, then the controller should still be able to find a solution and control the dryer in to the feasible region again. To ensure that a feasible solution always exist for the MPC, soft constraints in the form of slack variables are introduced. There is no

weighting on the slack constraints, which means that all constraint violations will have the same cost in the optimization criteria.

By using future inputs as optimization variables, the QP-solver drastically decreases the number of variables to calculate. This is not always efficient, and depends on the nature of the optimization problem. In this case, by calculating the matrices in (3.76), the result is an efficient algorithm relative to the optimization problem where the optimization variables are both future states and inputs.

6.3.3 Controller Parameters

6.3.3.1 Prediction Timeframe

In order for the MPC to achieve an optimal input sequence, the controller must predict the future dynamics of the process. The future prediction timeframe should be chosen so that it would capture the main dynamics given a step in the slowest input of the dryer. As it is known, the total retention time of the product is 50 minutes. This means that if the controller predict the process at least 50 minutes ahead in time, all model dynamics are captured and an optimal input sequence can be calculated.

Further, when choosing the prediction timeframe, a control horizon H_u and sampling time T_s must be chosen. First, the sampling time T_s should be chosen as small as possible in order to ensure efficient control and stability of the dryer. Secondly the control horizon H_u should be chosen long enough such that $H_u T_s \geq 50$ minutes. Finally, the controller should be able to calculate the optimal input sequence in an acceptable timeframe. The controller calculation delay is a result of hardware limitation, algorithm efficiency and choice of controller horizon H_u. The first two points cannot be changed (easily), which means that H_u should be chosen small enough in order for the controller to supply the input within a reasonable amount of time.

By choosing

$$T_s = 60 \text{ seconds} \tag{6.15}$$

$$H_u = 60 \text{ time steps} \tag{6.16}$$

the prediction horizon results 60 minutes.

6.3.3.2 MPC Tuning Matrices

The objective is to control only one of the 12 measured/estimated outputs. The priority tuning matrix Q is therefore chosen as

$$Q = \begin{bmatrix} 10^7 & 0 & \cdots & 0 \\ 0 & 0 & \cdots & 0 \\ \vdots & \vdots & \ddots & \vdots \\ 0 & 0 & \cdots & 0 \end{bmatrix} \qquad dim(Q) = 12 \times 12 \tag{6.17}$$

Further, the input cost matrix R must be chosen. In order to ensure a convex optimization problem, R should be positive definite. Furthermore, to ensure a robust controller there should be weight on as many outputs as there are degrees of freedom in the controller. In theory, only one input is needed to control the moisture of the product, given no constraints and reasonable steady state values on the remaining inputs. Then, if all inputs are given equal weights, then the controller could rapidly switch between the inputs, resulting in an oscillating or even an unstable controller. R is therefore chosen as

$$R = \begin{bmatrix} 1.03 & 0 & 0 & 0 & 0 \\ 0 & 1.02 & 0 & 0 & 0 \\ 0 & 0 & 0.98 & 0 & 0 \\ 0 & 0 & 0 & 1.01 & 0 \\ 0 & 0 & 0 & 0 & 1 \end{bmatrix} \tag{6.18}$$

where the cost is lowest on the input affecting the multiple-pass zones 4-3, because this input is assumed to be more energy efficient than the other inputs. Further, for faster control of the dryer, the inputs near the end of the dryer have lower cost.

The slack variable ρ used in the main optimalization routine in order to always obtain a feasible solution, is chosen as

$$\rho = 10^{11} \tag{6.19}$$

which is high enough to provide a response close to exact[12] without giving a violent response when active.

6.3.3.3 Controller Constraints

In addition to the physical constraints imposed by actuator limitations, constraints are applied on both product temperatures and product temperature rates in each zone. These constraints are implemented by constraining the output product temperatures from each zone. The constraints are chosen so that they can be easily identified in the simulation plots later in the thesis.

The product temperature constraints can be stated as

$$\begin{aligned} pT_{1,out,k} &\leq 60 \ [^\circ\text{C}] \\ pT_{2,out,k} &\leq 60 \ [^\circ\text{C}] \\ pT_{3,out,k} &\leq 60 \ [^\circ\text{C}] \\ pT_{4,out,k} &\leq 60 \ [^\circ\text{C}] \\ pT_{5,out,k} &\leq 60 \ [^\circ\text{C}] \\ pT_{6,out,k} &\leq 60 \ [^\circ\text{C}] \end{aligned} \qquad \text{for } 1 \leq k \leq H_u - 1 \tag{6.20}$$

[12] As it is stated in [Mac02]: It can be shown that, choosing ρ large enough, gives an 'exact penalty' method, which means that constraint violations will not occur unless there is no feasible solution to the original 'hard' problem.

The product temperature rate constraints can be stated as

$$\begin{aligned}
&|pT_{1,out,k} - pT_{1,out,k-1}| \leq 0.3\ [^\circ\mathrm{C}/T_s] \\
&|pT_{2,out,k} - pT_{2,out,k-1}| \leq 0.3\ [^\circ\mathrm{C}/T_s] \\
&|pT_{3,out,k} - pT_{3,out,k-1}| \leq 0.3\ [^\circ\mathrm{C}/T_s] \\
&|pT_{4,out,k} - pT_{4,out,k-1}| \leq 0.3\ [^\circ\mathrm{C}/T_s] \\
&|pT_{5,out,k} - pT_{5,out,k-1}| \leq 0.3\ [^\circ\mathrm{C}/T_s] \\
&|pT_{6,out,k} - pT_{6,out,k-1}| \leq 0.3\ [^\circ\mathrm{C}/T_s]
\end{aligned} \qquad \text{for } 0 \leq k \leq H_u - 1 \tag{6.21}$$

The constraints in temperature is given from $k = 1$ because it is not possible to control the temperature of the product at $k = 0$. On the other hand, the constraints in the temperature rates starts from $k = 0$ because it is possible to limit the change from $k = 0$ to $k = 1$.

Then, similar to (3.82)-(3.84), all constraints are structured and summarized as

$$Z_l \leq z_k \leq Z_u \qquad 1 \leq k \leq H_u - 1 \tag{6.22}$$

$$U_l \leq u_k \leq U_u \qquad 0 \leq k \leq H_u - 1 \tag{6.23}$$

$$-\Delta y_e \leq |y_{e,k+1} - y_{e,k}| \leq \Delta y \qquad 0 \leq k \leq H_u - 1 \tag{6.24}$$

where y and y_e were given by (6.10), and u by (6.14):

$$z = \begin{bmatrix} y \\ y_e \end{bmatrix} \qquad y = \begin{bmatrix} \alpha_{6,out} \\ pT_{6,out} \\ gT_{1,out} \\ gT_{2,out} \\ gT_{3,out} \\ gT_{5,out} \\ gT_{6,out} \end{bmatrix} \qquad y_e = \begin{bmatrix} pT_{1,out} \\ pT_{2,out} \\ pT_{3,out} \\ pT_{4,out} \\ pT_{5,out} \end{bmatrix} \qquad u = \begin{bmatrix} gT_{1,in} \\ gT_{2,in} \\ gT_{4,in} \\ gT_{5,in} \\ gT_{6,in} \end{bmatrix} \tag{6.25}$$

$$Z_l = \begin{bmatrix} -\infty \\ -\infty \\ -\infty \\ -\infty \\ -\infty \\ -\infty \\ -\infty \\ -\infty \\ -\infty \\ -\infty \\ -\infty \\ -\infty \end{bmatrix} \qquad Z_u = \begin{bmatrix} \infty \\ 60 \\ \infty \\ \infty \\ \infty \\ \infty \\ \infty \\ 60 \\ 60 \\ 60 \\ 60 \\ 60 \end{bmatrix} \qquad \Delta y_e = \begin{bmatrix} 0.3 \\ 0.3 \\ 0.3 \\ 0.3 \\ 0.3 \\ 0.3 \end{bmatrix} \tag{6.26}$$

$$U_l = \begin{bmatrix} 25 \\ 25 \\ 25 \\ 25 \\ 25 \\ 25 \end{bmatrix} \qquad U_u = \begin{bmatrix} 110 \\ 110 \\ 110 \\ 110 \\ 110 \\ 110 \end{bmatrix} \tag{6.27}$$

Further, by using the theory presented in section 3.4.4, the constraints are stated as

$$\Omega v \leq \omega \tag{6.28}$$

where Ω and ω is given by

$$\Omega = \begin{bmatrix} \hat{C}I_x\Theta + \hat{D}I_u \\ -\hat{C}I_x\Theta - \hat{D}I_u \\ \Lambda\left[\hat{C}_eI_x\Theta + \hat{D}_eI_u\right] \\ I \\ -I \end{bmatrix} \tag{6.29}$$

$$\omega = \begin{bmatrix} \hat{Z}_u - \hat{C}I_x\Psi x_0 - [\hat{C}I_x\Theta + \hat{D}I_u]\tilde{t} - [\hat{C}I_x\Xi + \hat{E}I_d]d \\ -\hat{Z}_l + \hat{C}I_x\Psi x_0 + [\hat{C}I_x\Theta + \hat{D}I_u]\tilde{t} + [\hat{C}I_x\Xi + \hat{E}I_d]d \\ \Delta Y_e - \Lambda\left[\hat{C}_eI_x\Psi x_0 + [\hat{C}_eI_x\Theta + \hat{D}_eI_u]\tilde{t} + [\hat{C}_eI_x\Xi + \hat{E}_eI_d]d\right] \\ \hat{U}_u - \tilde{t} \\ -\hat{U}_l + \tilde{t} \end{bmatrix} \tag{6.30}$$

6.3.3.4 Kalman Filter Parameters

The Kalman Filter is discretized with the same time step as the model used in the main optimization routine. The discrete model used in the main optimization is a model which is reduced after the discretization in order to obtain the smallest possible optimization problem. Therefore, in order for the Kalman filter to obtain the same states, it must use the reduced discretized model and therefore the same time step.

By using a Kalman filter, the measurement noise is rejected by assuming white noise characteristics, and by guessing the variance of the white noise. Because the product temperatures are 10^4 higher than the product and gas moistures, the variance for product temperature should be at least 10^4 higher than the moisture for both product and gas. The covariance matrix for the

process disturbances after tuning[13] the estimator is configured as:

$$Q_{kal} = \begin{bmatrix} 1 & 0 & 0 & 0 & 0 & 0 & 0 \\ 0 & 10^5 & 0 & 0 & 0 & 0 & 0 \\ 0 & 0 & 0.1 & 0 & 0 & 0 & 0 \\ 0 & 0 & 0 & 0.1 & 0 & 0 & 0 \\ 0 & 0 & 0 & 0 & 0.1 & 0 & 0 \\ 0 & 0 & 0 & 0 & 0 & 0.1 & 0 \\ 0 & 0 & 0 & 0 & 0 & 0 & 0.1 \end{bmatrix} \tag{6.31}$$

where each diagonal element $Q(i,i)$ correspond to the element at row i in d. Further, it is assumed that the measurement noise of the moisture control is ten times lower than the product and gas temperature noise, therefore the covariance matrix for the measurement noise is configured as

$$R_{kal} = \begin{bmatrix} 0.1 & 0 & 0 & 0 & 0 & 0 & 0 \\ 0 & 1 & 0 & 0 & 0 & 0 & 0 \\ 0 & 0 & 1 & 0 & 0 & 0 & 0 \\ 0 & 0 & 0 & 1 & 0 & 0 & 0 \\ 0 & 0 & 0 & 0 & 1 & 0 & 0 \\ 0 & 0 & 0 & 0 & 0 & 1 & 0 \\ 0 & 0 & 0 & 0 & 0 & 0 & 1 \end{bmatrix} \tag{6.32}$$

where each diagonal element $R(i,i)$ correspond to the element at row i in y.

[13] The tuning was based on rejecting the disturbances given by Table 6.7, and measurement noise with the variance 10^{-7} for the product moisture and 10^{-6} for the product and gas temperatures.

6.4 Controller Response

Here several simulations are performed. As it was explained earlier, the MPC uses a reduced model to predict the future behavior of the dryer. The dryer model simulated is an unreduced version of the model. By successfully controlling the unreduced model, it can be proven that the quality of the reduced model is good enough for MPC.

First, the dryer is simulated without measurement noise and input disturbances. In this simulation there are only constraints on the inputs. Then the dryer is simulated with measurement noise and input disturbances. Still, there are only constraints on the inputs. Next, the dryer is simulated with constraints on the inputs, outputs and the product temperature rate. Constraint softening is also inspected. Finally, PI control of the dryer is configured. The behavior of the dryer with PI control is compared to the behavior with MPC, which has constraints on the inputs, outputs and on the product temperature rate.

The MPC in the following simulations do not use soft constraints, unless stated in advance. The reason for this is that MPC input calulation duration doubles when using soft constraints. However, in section 6.4.3.2 it will be shown how the controller reacts with soft constraints included.

The figures in this section have a special structure. As it can be seen in Figure 6.1, the conveyor-belt dryer has its first zone in the upper left and the last zone in the bottom left. Therefore the graph describing a zone, is placed in the figure where the zone is located . A graph describing something in zone 4 for example, will be placed in the bottom right of the figure, which is the location of zone 4 in Figure 6.1.

6.4.1 Step in Reference Signal

To illustrate the fast response an MPC can provide, the dryer is simulated without noise and disturbances and there are only constraints in the manipulated variables. Figure 6.9 shows the results when the controller is provided with the reference trajectory beforehand, and it can be observed that the controller acts before the step in reference take place. This early response is desired and is a result of the tuning given by the Q and R matrices in (6.17) and (6.17), respectively.

The output gas temperatures from the zones are shown in Figure 6.10. As expected, there is a strong correlation between the input gas temperatures illustrated in Figure 6.9 and the exhaust gas from the zones. Because the discretization time step is much higher than the time constant of the air dynamics, the exhaust gas stabelizes within one time step with respect to input gas temperature. It can also be observed in the figure that the exhaust gas from zone three has significantly lower temperature than the other zones. This is because the gas exiting zone three has been traveling through both

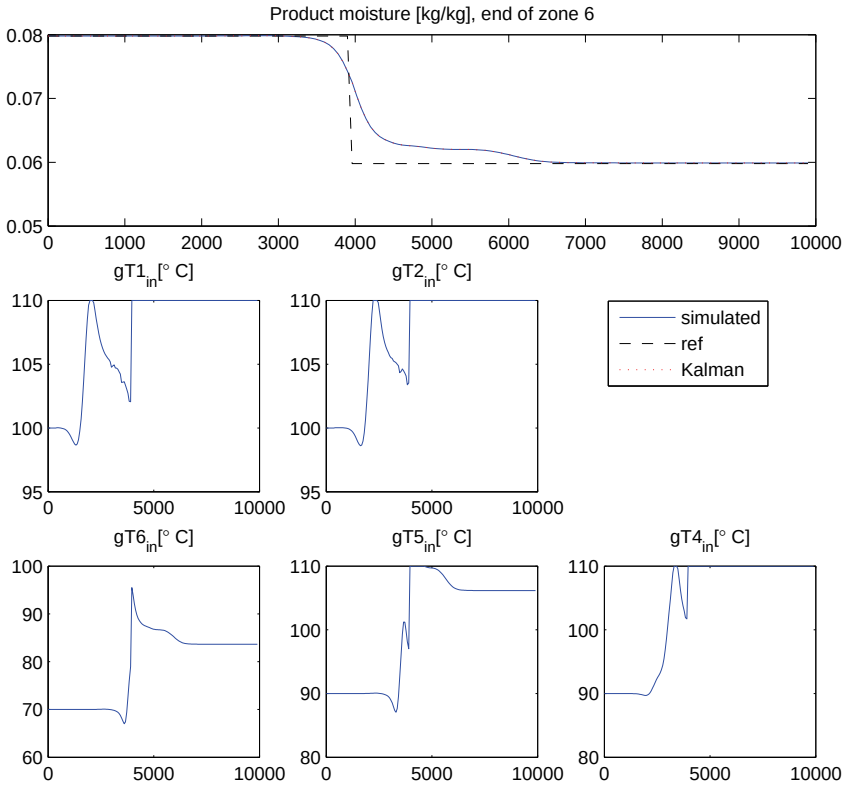

Figure 6.9: Moisture tracking without measurement noise and input disturbances. The top plot display the product moisture content exiting zone 6, and the remaining plots displays the input sequence given by the controller. All inputs are constrained between $[25, 110]°\mathrm{C}$. The Y-axes ranges from 0-10000 seconds.

zone three and four.

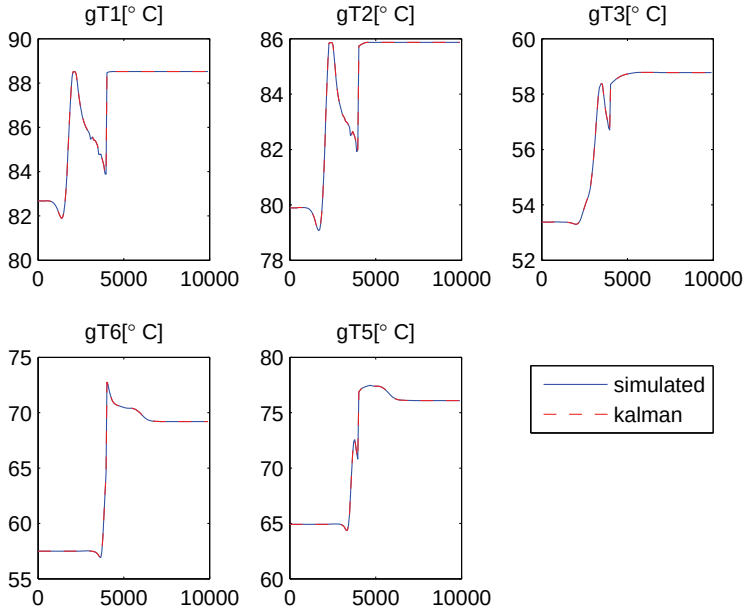

Figure 6.10: Exit gas temperatures of the different zones

6.4.2 Noise and Disturbance Rejection

By including measurement noise and input disturbances, it can be observed how efficient the MPC reject these. The timing and magnitude of the input disturbances are shown in Table 6.7. The measurement noise variances are 10^{-7} for the product moisture and 10^{-6} for the product and gas temperatures.

Disturbance	**Time[s]**	**Magnitude**
Input product moisture	180	0.03 [kg/kg]
Input product temperature	2940	5 [°C]
Input gas moisture, zone 4	5940	0.02 [kg/kg]

Table 6.7: Timing and magnitude of the input disturbances affecting the dryer.

In Figure 6.11 the MPC response is shown. In order to show the magnitude of the disturbance steps, the *free response*[14] is also plotted. It can be observed that the controller has significant supression of the disturbances. The duration of which the product uses to travel through the dryer is 3000 seconds. And by inspecting the product moisture content at t=3180s, where the product being affected by the product moisture disturbance has just reached the dryer-output, it can be observed that the disturbance already has been significantly suppressed.

The fast estimation of disturbances ensures good suppression of disturbances. Figure 6.12 and 6.13 shows the estimates provided by the Kalman filter. When inspecting the product moisture disturbance estimate, it can be observed that the estimates converges even before the product has reached the zone output ($t = 3180$). This means that the controller begin to suppress the disturbances before they are noticed in the product moisture measurement. When inspecting the product temperature disturbance estimation, it can be observed that this disturbance is estimated even faster than the product moisture disturbance, which gives even more time to the MPC for disturbance suppression. When inspecting the gas moisture disturbance estimates, the disturbance is estimated within one time step (60s). The result of this is easily observed in Figure 6.11, where the MPC at $t = 6000s$ instantly compensate for the increase of gas moisture in zone 4.

[14] The *free response* of a plant, is the response that would be obtained if the future input trajectory remained at the latest value.

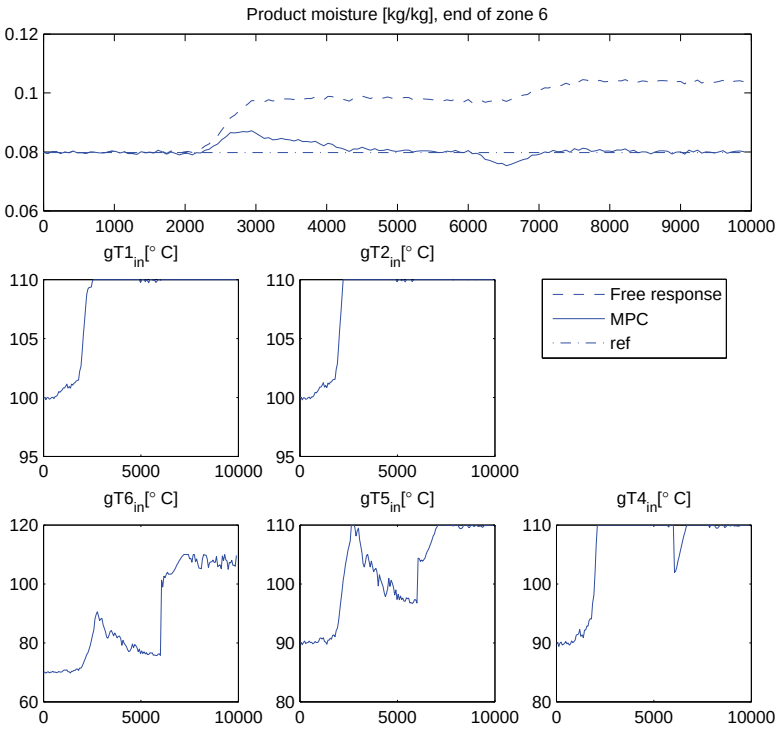

Figure 6.11: Moisture tracking with measurement noise and input disturbances. In order to show the magnitude of the disturbances, the *free response* is also plotted. All inputs are constrained between $[25, 110]^\circ$C.

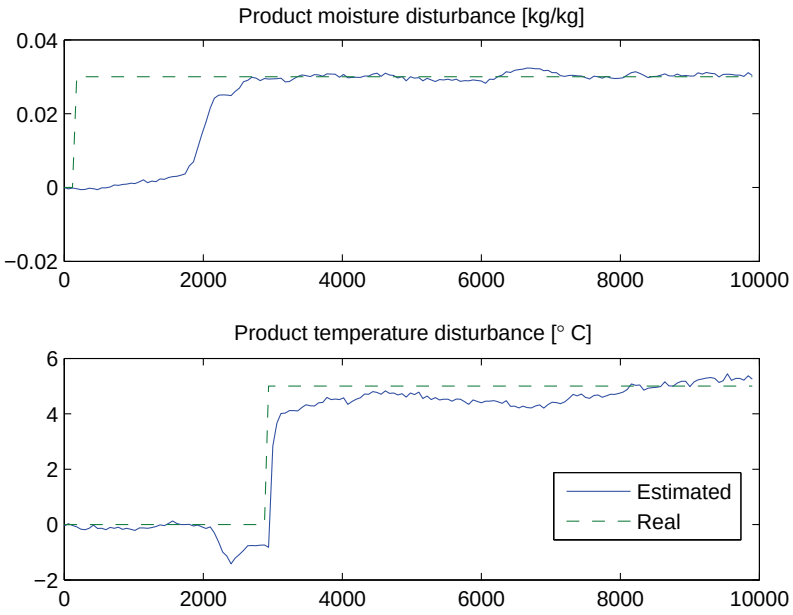

Figure 6.12: Estimated input disturbances, product moisture in the top plot and product temperature in the bottom plot.

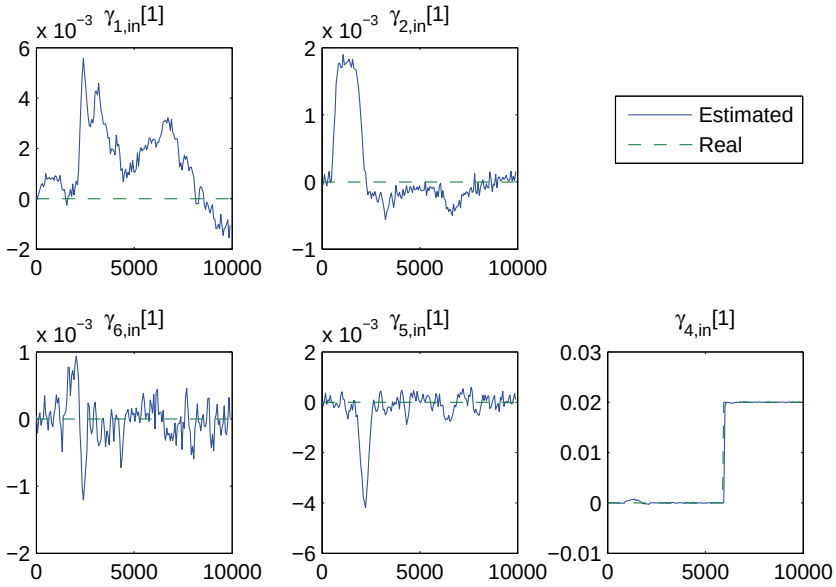

Figure 6.13: Estimated input disturbances, gas moisture

6.4.3 Constraint Handling

Here the dryer is simulated with constraints on the inputs, product temperatures and product temperature rates. Because the product temperature through the zones are not measured, they are estimated as explained in section 6.2. Therefore the product temperatures, as well as product temperature rates at the zone exits can be constrained.

6.4.3.1 Constraints on Product Temperatures and Product Gradient Temperatures

Variables	**Range**
Input gas temperatures	$25 \leq gT_{in} \leq 110$ [°C]
Product temperatures at zone exits	$pT_{out} \leq 60$ [°C]
Product temperature rates at zone exits	$\lvert pT_{k,out} - pT_{k-1,out} \rvert$ ≤ 0.3[°C/time step]

Table 6.8: Constraint values. The product temperatures are not to change more than 0.3°C between each time step. This results in $\frac{0.3°C}{60s} = 0.005$[°C/s]

The constraints used in the following simulation are listed in Table 6.8. Figure 6.14 shows the response of a reference step with disturbances included. The input disturbances acting on the dryer are almost the same as in Table 6.7, here decreased by a factor of 0.1. It can be observed on the figure that the constraints limit the system to reach the desired target. When inspecting Figure 6.15, it can be seen that the product temperature constraint in zone 6 is active. The only input which is not at its constraint is the input gas temperature to zone 6, but because of the active product temperature constraint, it is not possible to raise the input in zone 6 without constraint violation. Therefore the system cannot reach the desired target.

Active temperature rate constraints can be observed in Figure 6.15. Here, the product temperature rate constraints are characterized by the straight parts of the pT_5 and pT_6 graphs with $\frac{d}{dt}(pT) \neq 0$. In Figure 6.16, the numerical differences are calculated, and it can be seen that the temperature rate constraint at ± 0.3 is respected for all time steps.

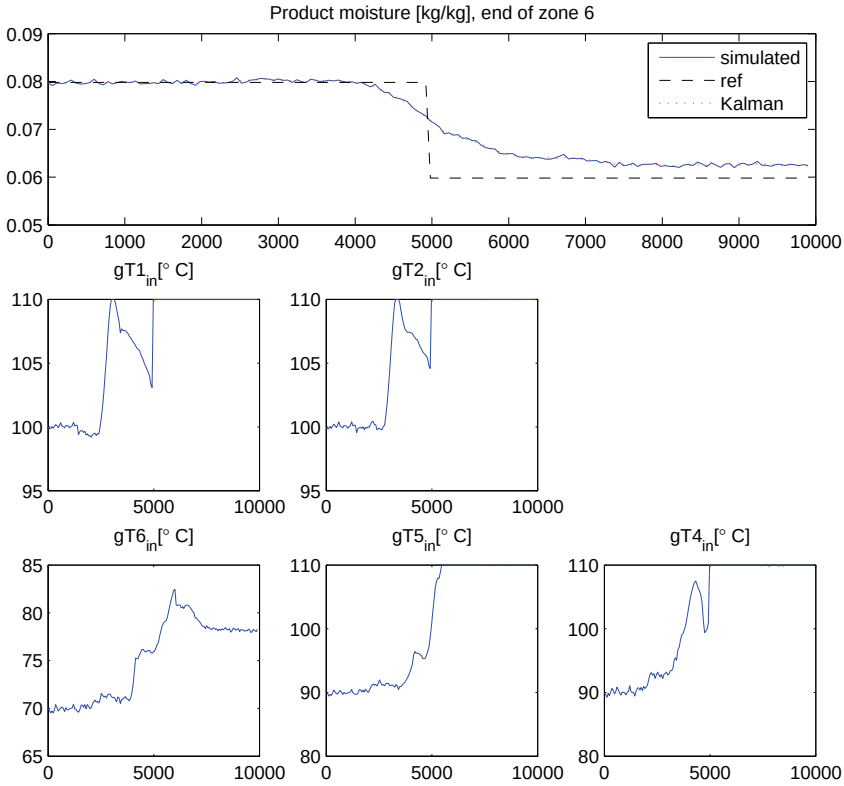

Figure 6.14: Moisture tracking with measurement noise and input disturbances. Constraints are on the inputs, the product temperatures and the product temperature rates. It can be observed that the constraints limits the system to reach the desired target

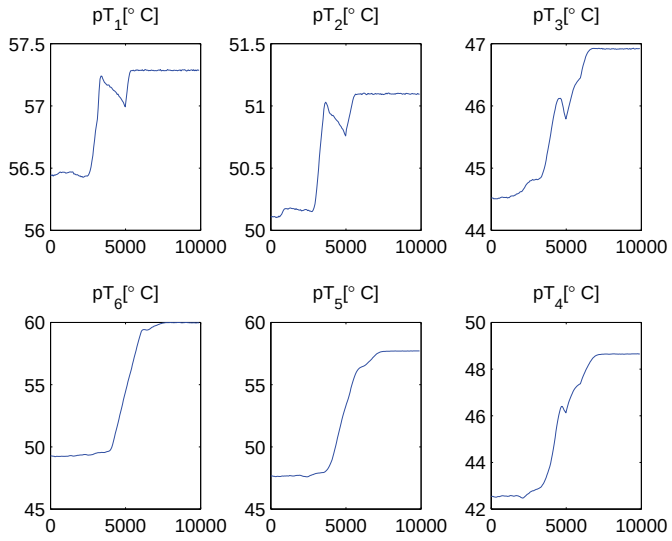

Figure 6.15: Exit product temperatures of the different zones. It can be observed that the product temperature constraint at 60°C in zone 6 is active by the end of the simulation. Active product temperature rate constraints can also be observed, these are characterized by the straight parts of the pT_5 and pT_6 graphs with $\frac{d}{dt}(pT) \neq 0$.

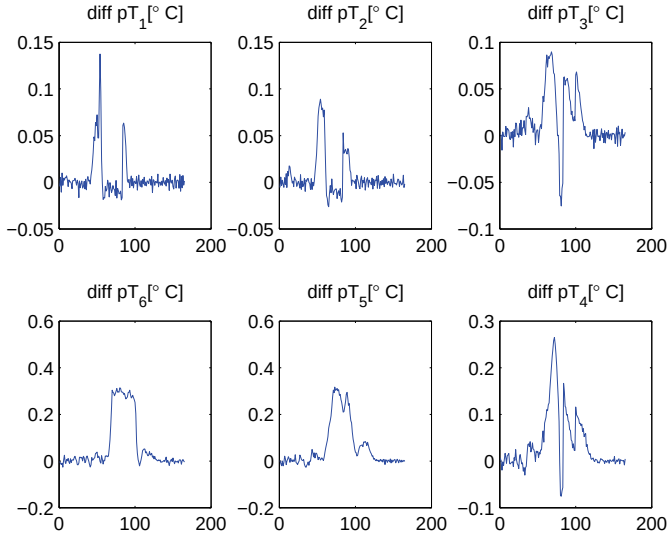

Figure 6.16: Product temperature rates. The values on the y-axes are calculated by $pT(k) - pT(k-1)$. The temperature rate constraint at ± 0.3 is respected for all time steps.

6.4.3.2 Constraint Softening

If disturbances push the states of the system outside the feasible region, then without constraint softening, the optimization routine would not be able to provide a feasible solution to the optimization problem.

By applying a +10°C step in the product temperature disturbance, it is not possible for the MPC to respect the temperature constraint. Figure 6.17 shows the response of the disturbance step. As with the simulation done in section 6.4.3.1, it can be observed that the constraints limits the system to reach the desired setpoint. To soften the constraints one slack variable is introduced, which is plotted in Figure 6.18.

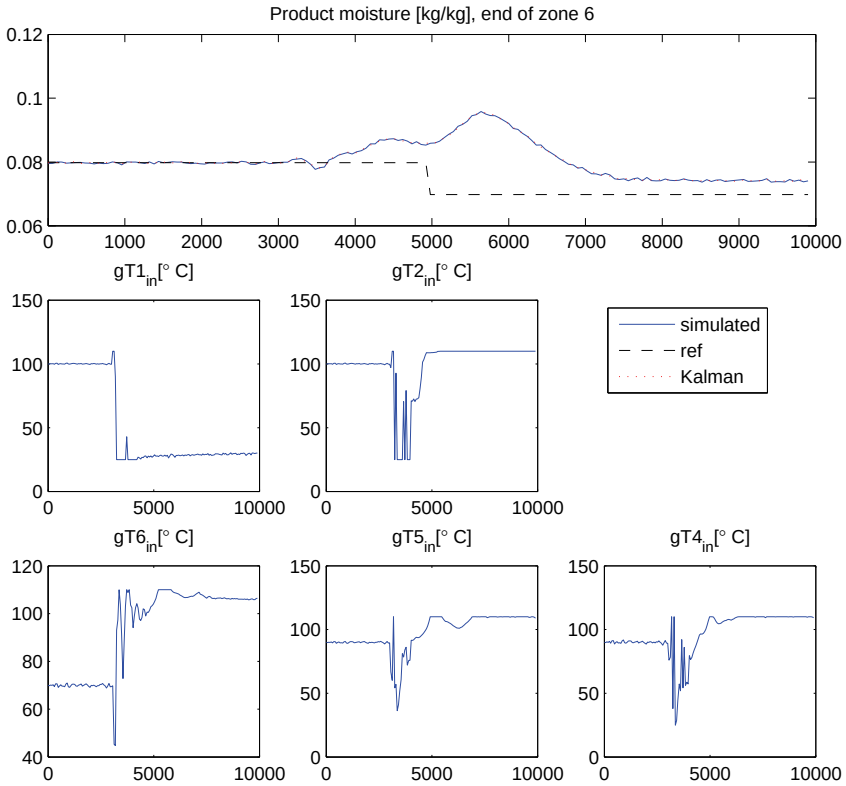

Figure 6.17: Moisture tracking with constraint softening included. There are constraints on the inputs, the product temperatures and the product temperature rates. The dryer is subjected to input disturbances

Some oscillations are observed in the inputs when the slack variable is active. This could be a result of the optimization predicting when the slack variable is active. This can result in the states not being where they are

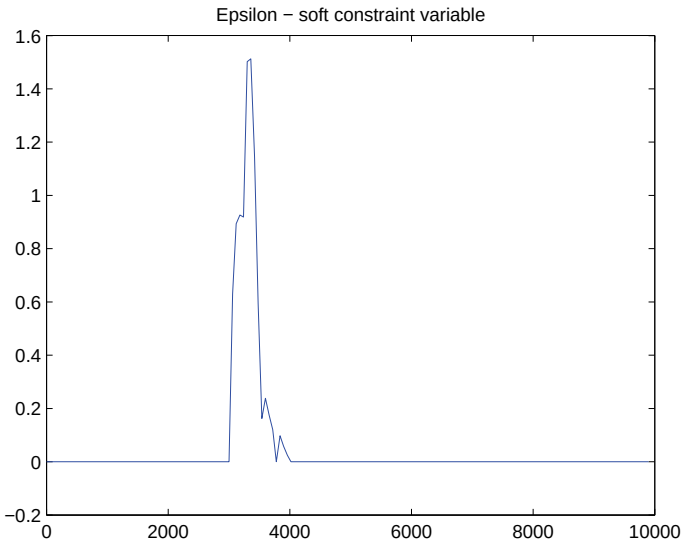

Figure 6.18: Soft constraint variable, defined in (3.88). It can be observed that the variable is active from $t = 3000$ to $t \approx 4000$.

supposed at the next time step, because the slack variable have changed from the last time step. [SR99] and [RR98] suggests that better performance can be achieved by using different slack variables in the future predictions.

The result of the constraint softening can be seen in Figure 6.19. In zone 1, there are two clear indications of the constraint softening. First there is a peak in the product temperature, exceeding the 60°C constraint. Secondly, the product temperature is exceeding the constraint toward the end of the simulation, even though it could be respected by lowering the gas temperature.

The first indication is more easely explained than the second. This is a result of the MPC not being able to suppress the large disturbance fast enough, which is because the disturbance is not estimated fast enough.

The second indication is a result of the penalty function not being *exact*. This means that the penality when violating the product temperature constraint, contributes less to the cost function (3.88), than the decrease in cost would do by either decreasing the distance between the CV and CV-trajectory or by the use of input. The MPC will therefore try to place the CV closer to the setpoint, rather than respecting the constraint. For more about *exact penality functions*, see [Mac02].

In Figure 6.20 the product temperature rates are shown. It can be seen that the rates are mostly within the ± 0.3 constraint. There are peaks exceeding the constraints, some are only exceeded for one time step, while some are exceeded for several time steps. Some of the peaks which are exceeded for several time steps, might be results of the slack variable being activated beforehand.

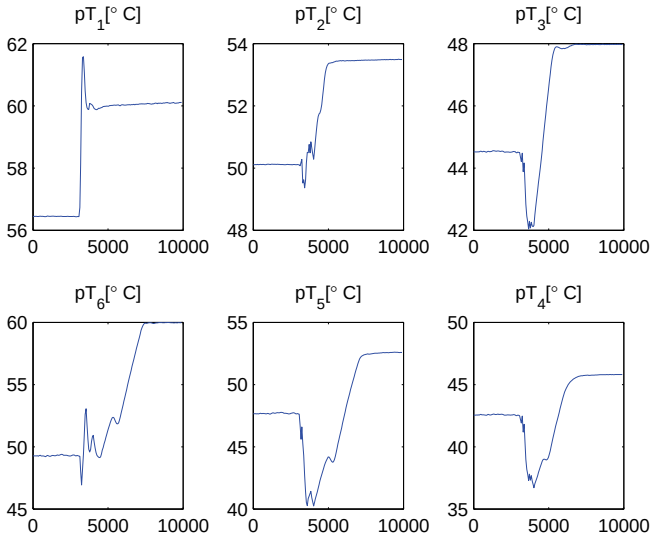

Figure 6.19: Exit product temperatures, as constraint softening is included. It can be observed that the product temperature at zone 6 is limited by the 60°C constraint.

The slack variable can for example be activated by a product temperature constraint violation, and then all constraints using this slack variable will have their regions extended. The rest of the peaks exceeding the constraints for several time steps are simply unavoidable and would cause an infeasible optimization problem without constraint softening.

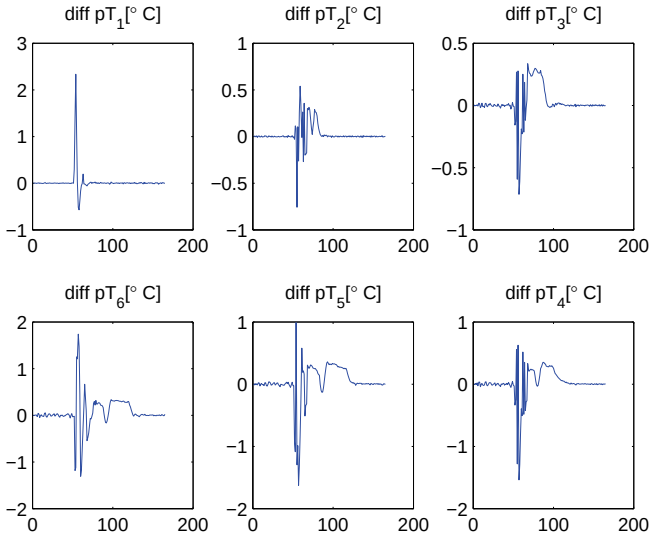

Figure 6.20: Product temperature rates, as constraint softening is included. The values on the y-axes are calculated by $pT(k) - pT(k-1)$.

6.4.4 MPC vs PI Control

By comparing MPC with PI control, one can investigate advantages/disadvantages with the controller schemes. In this section, the MPC with the constraints listed Table 6.8, is compared with simple PI moisture control of the dryer. As with the MPC, the PI controller outputs are temperature targets for lower control loops. The lower loops are fast and therefore negligible, which means that output changes from the PI controllers provide instant changes of the input gas temperatures for the dryer.

6.4.4.1 Controller Configuration

Because there are five inputs and only one output to control, a PID configuration must be defined. There are many ways to configure these, ranging from one PID supplying all inputs to five PIDs supplying one input each. It was decided that a configuration consisting of two PI controllers controlling two and three inputs each would give satisfying control if configured correctly. This configuration would also keep the PID tuning work relative small.

Figure 6.21 illustrates the PI-configuration. Here the moisture controllers are parallel configurated PID controllers (see Figure 6.22), configured with the parameters listed in Table 6.9. The figure illustrates how moisture controller 1 controls the input gas temperature to zone 1,2 and 4, while the input gas temperatures to zone 5 and 6 are controlled by moisture controller 2. In the figure there are illustrated two burners/heaters, as explained in section 6.2 the burners/heaters and their belonging inner loop dynamics are neglected. If the inner loop dynamics were significant, they could be included by using the technique from section 4.5.

Controller	**Proportional**	**Integral**	**Derivate**
Moisture controller 1	500	0.5 [sec]	0 [sec]
Moisture controller 2	1000	0.75 [sec]	0 [sec]

Table 6.9: PID controller gains

6.4.4.2 Reference Step

The MPC controller with the constraints listed in Table 6.8 is here compared with PI control of the dryer. Figure 6.23 shows the response of the two control schemes. It can be observed that the MPC has a response about 1000 seconds faster than the PI-control. In Figure 6.24 the product temperature for both control schemes is shown. Here, it is observed that the product temperature constraint is respected for the MPC, but not for the PI control in zone 6.

Further, when inspecting Figure 6.24 and 6.25, it can be observed that the product temperature rate constraint is respected for the MPC, but not for the

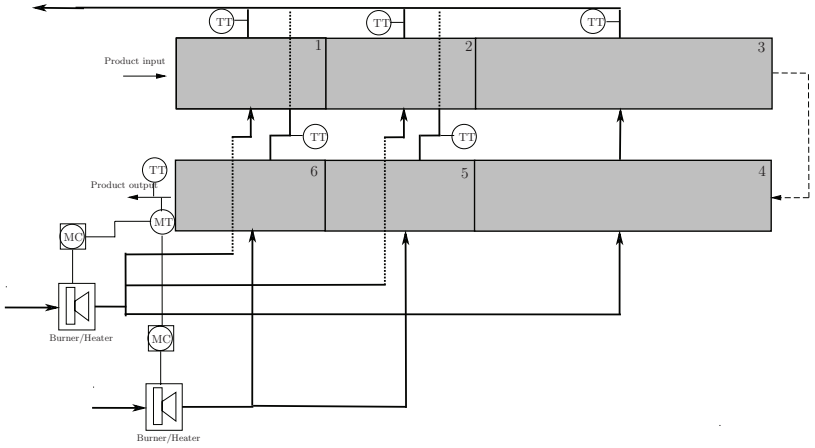

Figure 6.21: P&ID of the PI control configuration. TT=temperature transmitter, MT=moisture transmitter (PI control), MC=moisture controller, TC=temperature controller. Both MCs are PI-controllers. The burner/heater dynamics are excluded and independent of the gas leaving the dryer, in other words, when the MCs provide set point changes for the burners/heaters, the set points are instantly reached

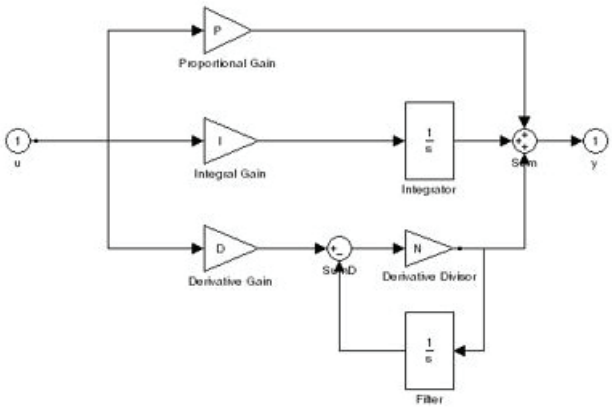

Figure 6.22: PID block diagram (parallel configuration)

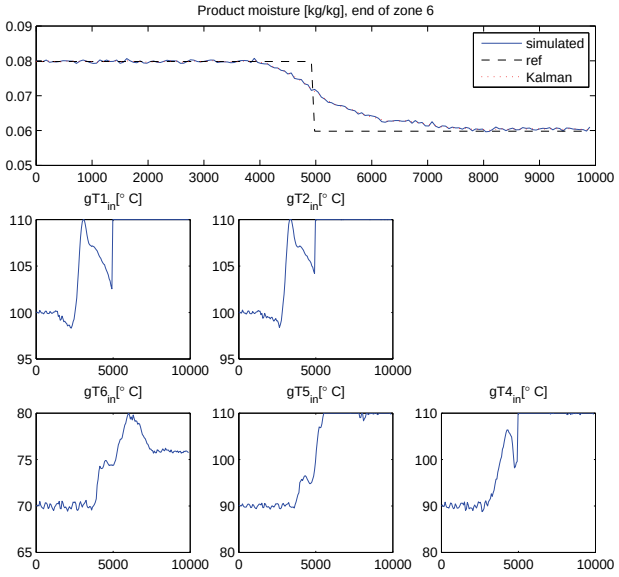

(a)

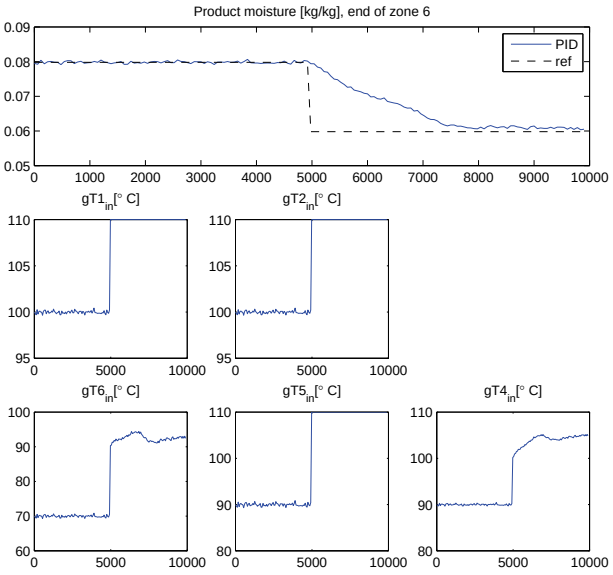

(b)

Figure 6.23: Moisture tracking comparison between the control schemes. (a) MPC response, and (b) PI control response. The top plot in both (a) and (b) displays the product moisture content leaving zone 6, and the remaining plots displays the input sequence of the two controllers.

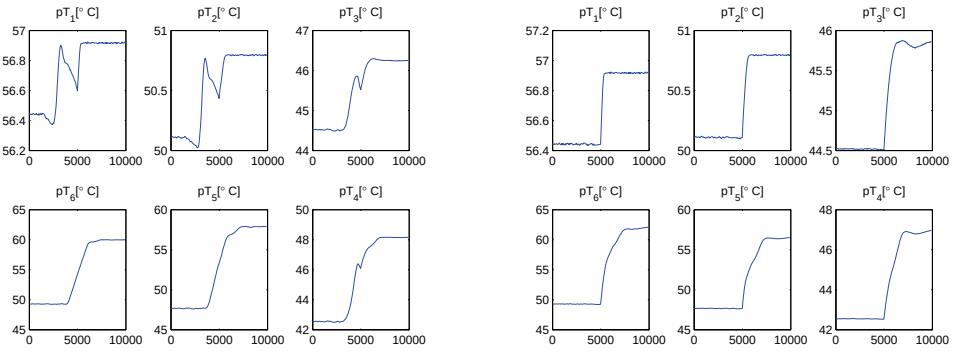

(a) (b)

Figure 6.24: Exit product temperatures. (a) MPC response, and (b) PI control response.

PI control (which obviously cannot respect state constraints).

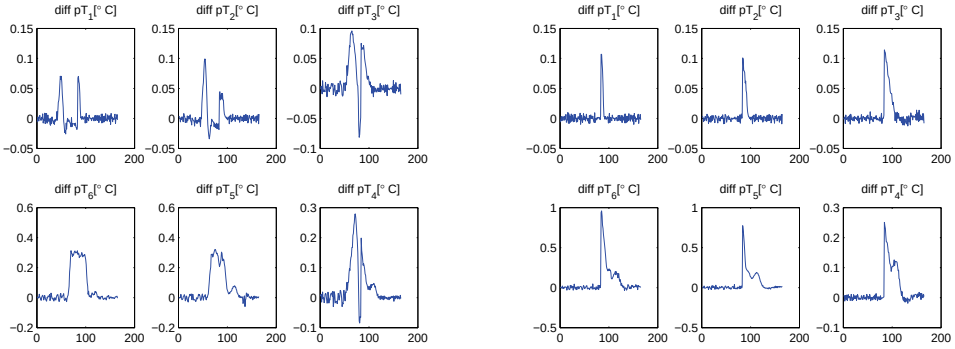

(a) (b)

Figure 6.25: Exit product temperature rates. (a) MPC response, and (b) PI control response. The values on the y-axes are calculated by $pT(k) - pT(k-1)$.

When comparing the reference step responses of the MPC with the PI control, it is clear that the MPC delivers best results. The MPC provides a faster response, while also respecting the constraints placed on both product temperature and product temperature rate.

6.4.4.3 Rejection of Input Disturbances

Here the responses of the two control schemes are compared when disturbances affect the dryer. Figure 6.26 shows the moisture tracking of both schemes. It can be seen that the MPC outperform the PI controllers, where the disturbances are supressed almost twice as much by the MPC. Further, when inspecting the input sequences, it can be observed that the MPC is more aggressive than the PI controllers. This aggressiveness is a results of the tuning of the MPC, in combination with the temperature constraint handeling and the fact that the changes of input is not included in the optimization criteria.

Figure 6.27 shows the input disturbances and the estimates made by the MPC. The estimation dynamics are very similar to those in Figure 6.11, and are therefore not further commented.

In Figure 6.28 the product temperatures are shown. In this simulation, the temperature does not exceed the 60°C constraint in any of the zones or control schemes.

When inspecting the product temperature rate of the different zones, Figure 6.29 shows that the PI control exceeds the product temperature rate constraints in all zones. The MPC, by the other hand, is within the constraint for almost all time steps and zones. The constraints are sometimes exceeded for one time step, but and respected for the next. This is especially seen in zone 4, where the temperature exceeds its constraint for one time step, but at the following time steps it is within its constraint, then gradually converging toward zero rate. This is because the measurement noise and disturbances are unknown and therefore the MPC cannot *guarantee*[15] that they will be within the constraints for the current time step, but only for the following time steps.

[15] The MPC can only guarantee that the constraints are respected at the next time step, if the measurement noise and input disturbance are unchanged. Keep in mind two things, first, the product temperatures are estimated, and estimates are affected by measurement noise. Second, measurement noise affects the output directly, and it cannot be compensated by the input before the next time step.

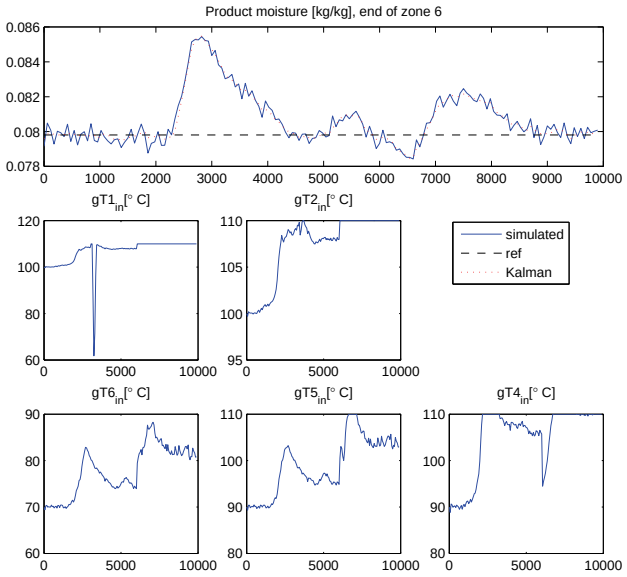

(a)

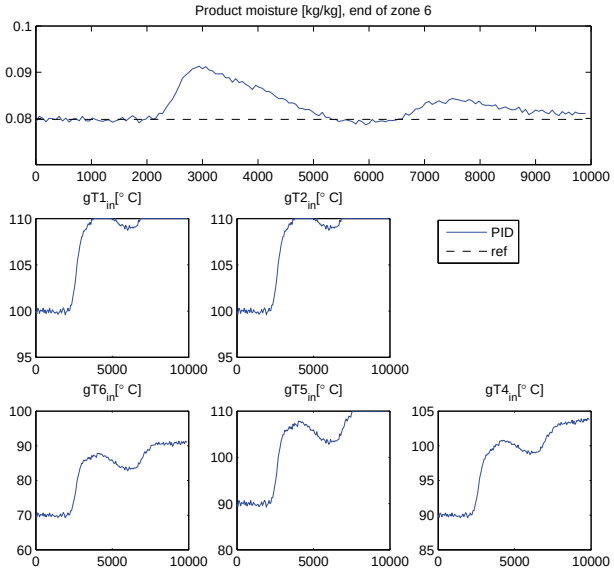

(b)

Figure 6.26: Moisture tracking comparison between the control schemes, subjected to input disturbances. (a) MPC response, and (b) PI control response. The top plot in both (a) and (b) displays the product moisture content leaving zone 6, and the remaining plots displays the input sequence of the two controllers.

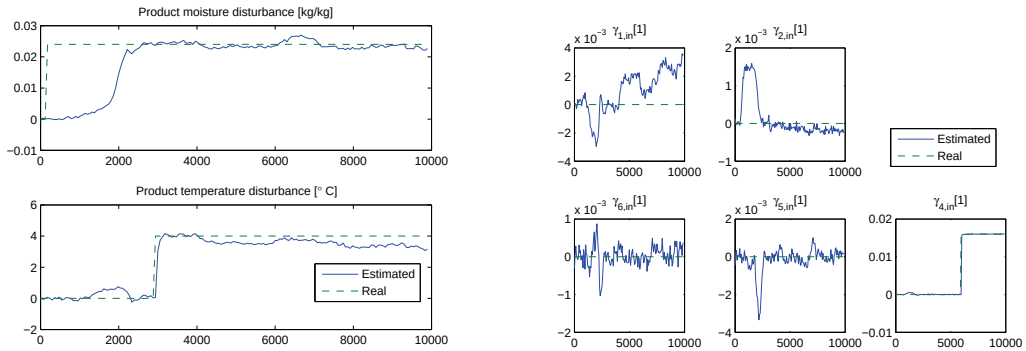

(a) (b)

Figure 6.27: Disturbances and estimated disturbances. (a) Input product moisture and temperature disturbances. (b) Input gas temperature disturbances.

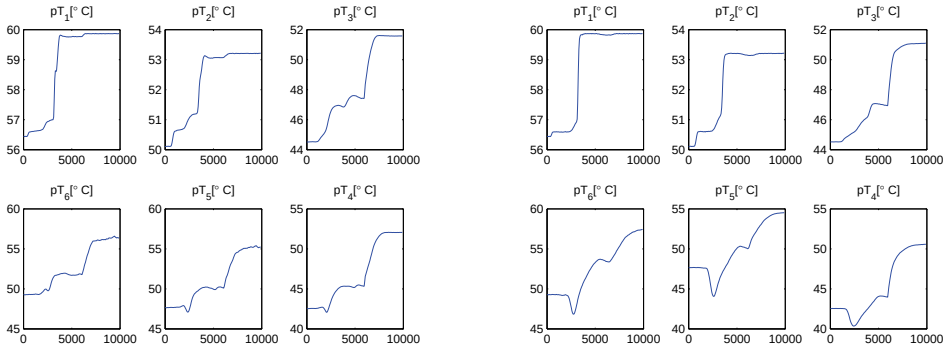

(a) (b)

Figure 6.28: Product temperatures, as input disturbances influences the system. (a) MPC response, and (b) PI control response.

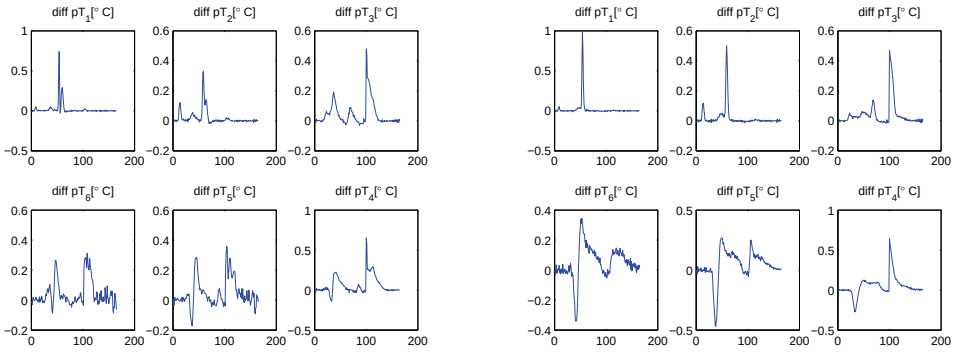

Figure 6.29: Product temperature rates, as input disturbances affect the system. (a) MPC response, and (b) PID response. The values on the y-axes are calculated by $pT(k) - pT(k-1)$.

6.4.5 Rejection of Model/Parameter Errors

By introducing a model error into the dryer model, it can be observed if the control schemes are able to control the dryer under the influence of model uncertainty. Introducing model errors can be done by many techniques, here the error is introduced by changing a model constant.

The model to be controlled is obtained by the same procedure as in section 6.2, but now the vaporization area per product volume constant ε is changed from 100 to 130.

6.4.5.1 Choosing the Disturbance Model

In section 3.4.7.1, different disturbance models were defined. In section 6.4.2, the input/state disturbance model (3.116) was used to estimate the input disturbances. The input disturbance model was here a clear choice, because the closed-loop controller performance with the *input disturbance model* is directly related to how accurately the disturbance model represents the actual disturbances entering a process [MB02].

First, the input disturbance model was attempted for estimating the error model, but the Kalman filter was not able to converge towards the error model, and diverged toward infinity even though several attempts tuning the Kalman filter as well as several combinations of input disturbances were tried. Because it is known that there exist a model error, a different disturbance model should be used. The estimator should estimate those disturbances that could compensate for the model error most efficiently.

Then the input/state and output disturbance model estimator (3.117) was used, with several combinations of input/output disturbances, but neither did this model converge towards the error model. The error in the model is believed to be too severe in order to use the input model in the disturbance model.

Finally it was decided that the output disturbance model (3.115) was to be used for estimating the error model. This approach is not as model dependent as the other two, but is not very effective when estimating input disturbances. [Shi94] points out that when using the output disturbance model, a PID controller can outperform the typical industrial MPC implementation when a disturbance enters the input of a process upstream of a dominant lag.

The new parameters for the Kalman filter are

$$Q_{kal} = \begin{bmatrix} 0.1 & 0 & 0 & 0 & 0 & 0 & 0 \\ 0 & 1 & 0 & 0 & 0 & 0 & 0 \\ 0 & 0 & 1 & 0 & 0 & 0 & 0 \\ 0 & 0 & 0 & 1 & 0 & 0 & 0 \\ 0 & 0 & 0 & 0 & 1 & 0 & 0 \\ 0 & 0 & 0 & 0 & 0 & 1 & 0 \\ 0 & 0 & 0 & 0 & 0 & 0 & 1 \end{bmatrix} \quad R_{kal} = \begin{bmatrix} 0.1 & 0 & 0 & 0 & 0 & 0 & 0 \\ 0 & 1 & 0 & 0 & 0 & 0 & 0 \\ 0 & 0 & 1 & 0 & 0 & 0 & 0 \\ 0 & 0 & 0 & 1 & 0 & 0 & 0 \\ 0 & 0 & 0 & 0 & 1 & 0 & 0 \\ 0 & 0 & 0 & 0 & 0 & 1 & 0 \\ 0 & 0 & 0 & 0 & 0 & 0 & 1 \end{bmatrix} \tag{6.33}$$

6.4.5.2 Reference Step

The MPC controller with the constraints listed in Table 6.8 is here compared with PI control of the dryer. It can be seen that the reference step response when including the modeling error, is very similar to the previous simulations without modeling error. As before, the MPC outperforms the PI control with a response about 1000 seconds faster, even while respecting the constraints. Further, in Figure 6.31 and 6.32, it can be seen that the constraints are respected. In the latter figure, the measurement noise and model error provides noise on the product temperature rate estimates which sometimes exceed the constraints, but as before is respected the following time step.

Figure 6.33 shows the estimation of output disturbances, which makes the estimator model converge towards the error model.

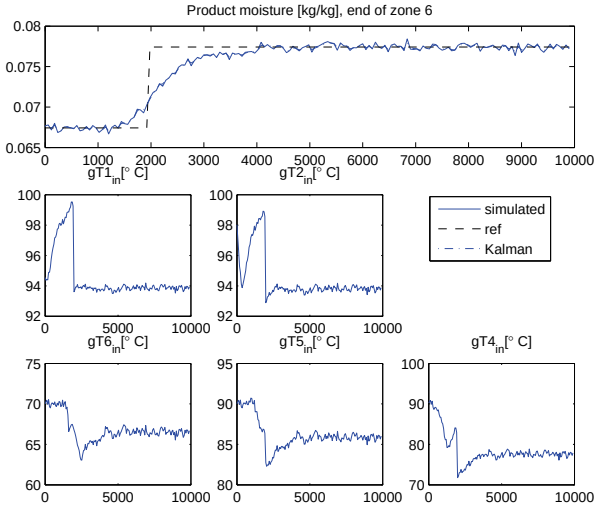

(a)

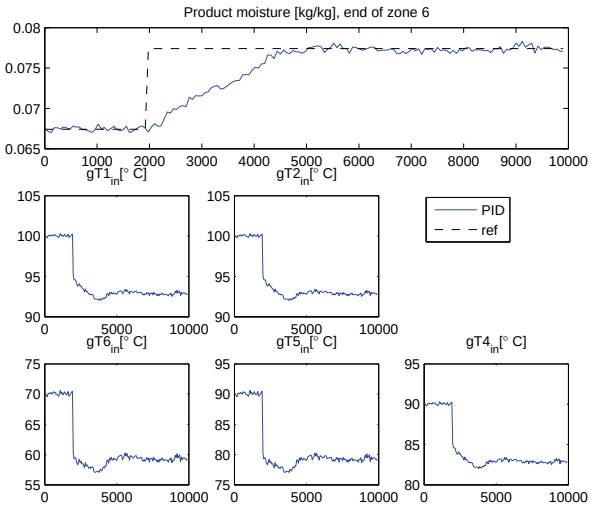

(b)

Figure 6.30: Product moisture tracking at a reference step. (a) MPC response, and (b) PI control response. The top plot in both (a) and (b) displays the product moisture content leaving zone 6, and the remaining plots displays the input sequence of the two controllers.

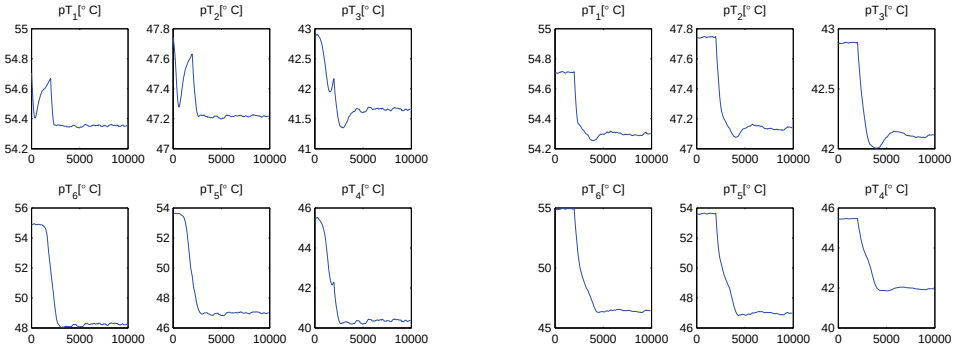

(a) (b)

Figure 6.31: Product temperatures, reference step, controlling the error model. (a) MPC, (b) PI control

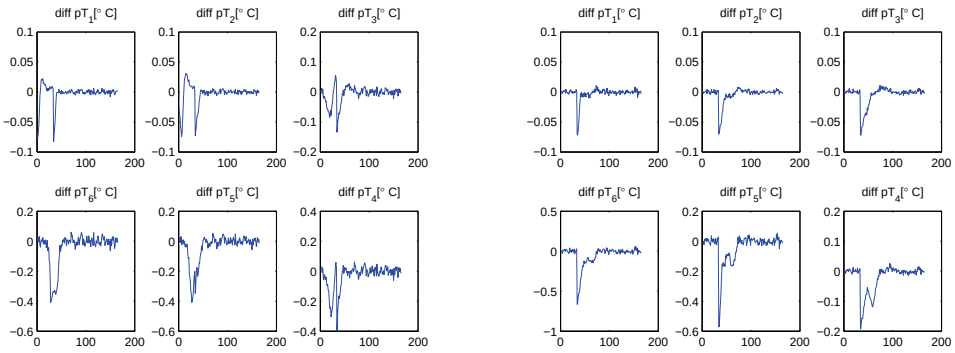

(a) (b)

Figure 6.32: Product temperature rates, at a reference step when controlling the error model. (a) MPC, (b) PI control. The values on the y-axes are calculated by $pT(k) - pT(k-1)$.

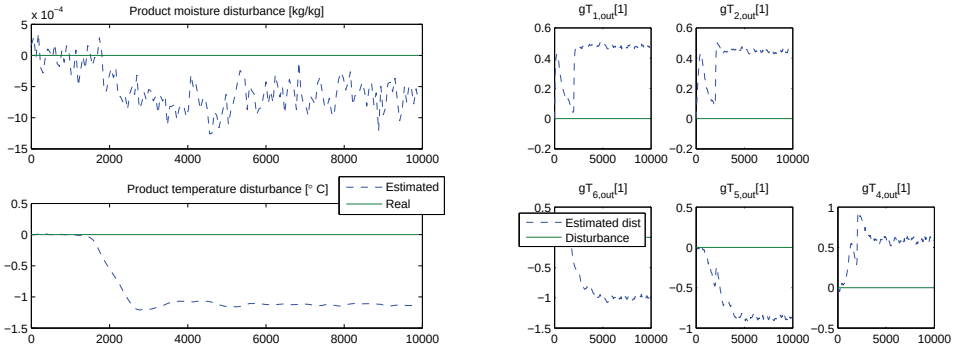

(a) (b)

Figure 6.33: Estimated disturbances, controlling the error model. (a) displays ouput product moisture and temperature disturbances. (b) displays output gas temperature disturbances.

6.4.5.3 Rejection of Input Disturbances

The closed loop responses of the two control schemes are compared when subjected to the input disturbances listed in Table 6.7. Figure 6.34 shows the moisture tracking of both schemes. Unlike before, the controllers suppress the disturbances with almost the same efficiency. Again it is referred to [Shi94], which points out that when using the output disturbance model, a PID controller can outperform the typical industrial MPC implementation when a disturbance enters the input of a process upstream of a dominant lag.

Figure 6.33 shows the estimation of the *output* disturbances used in the MPC to compensate for the *input* disturbances. The simulation shows that with the model error, the MPC is able to respect the constraints. Figure 6.36 shows how the temperature constraints are respected for the MPC. The temperature rate constraints are mostly respected, but are exceeded more frequently than in the non-error model simulations.

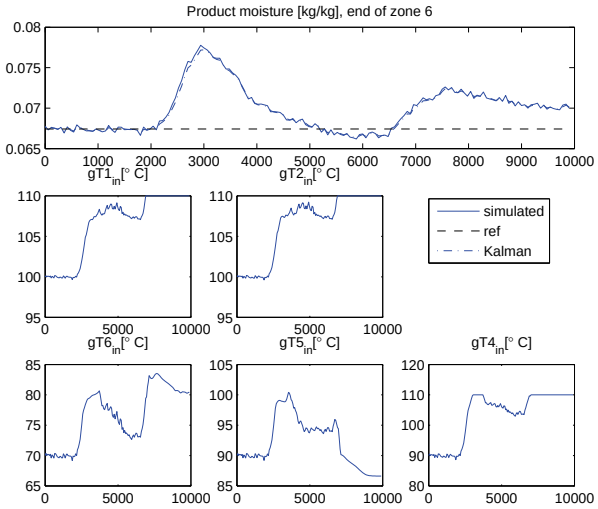

(a)

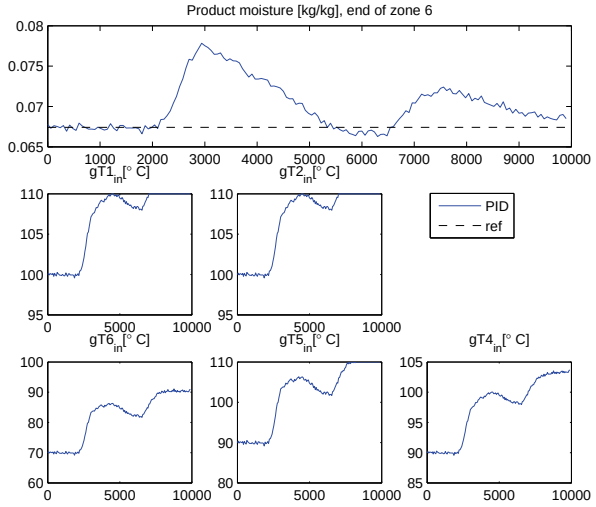

(b)

Figure 6.34: Product moisture tracking as the dryer is subjected to input disturbances while controlling the error model. (a) displays the MPC response and (b) displays the PI control response. The top plot in both (a) and (b) displays the product moisture content leaving zone 6, and the remaining plots display the input sequence of the two controllers.

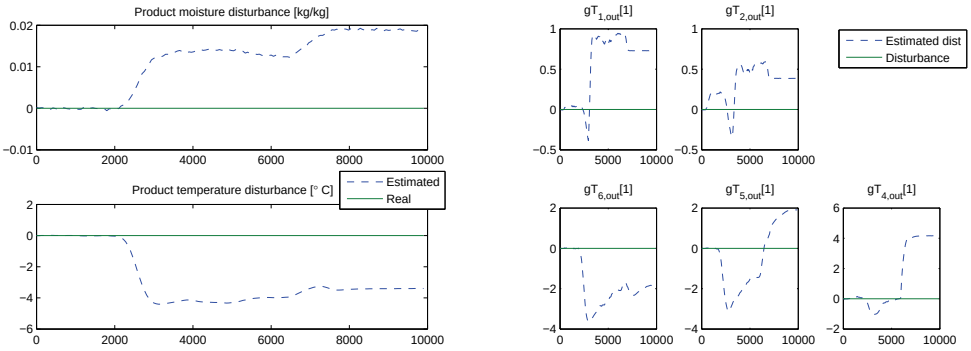

(a) (b)

Figure 6.35: Estimated output disturbances, as the dryer is subjected to input disturbances while controlling the error model. (a) displays input product moisture and temperature disturbances. (b) displays input gas temperature disturbances.

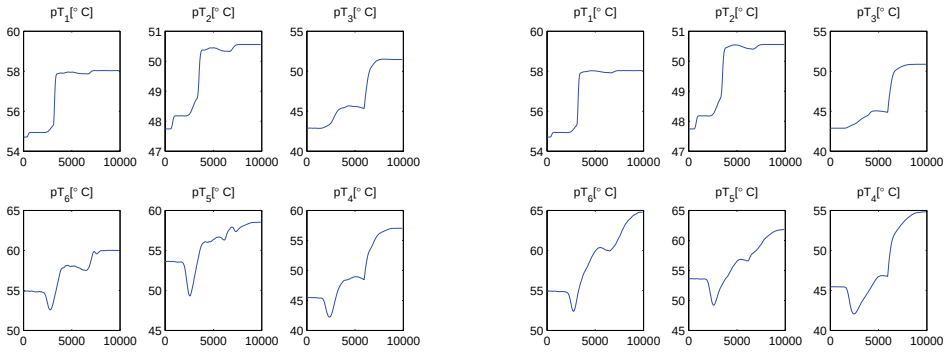

(a) (b)

Figure 6.36: Product temperatures as the dryer is subjected to input disturbances while controlling the error model. (a) displays the MPC response and (b) displays the PI control response

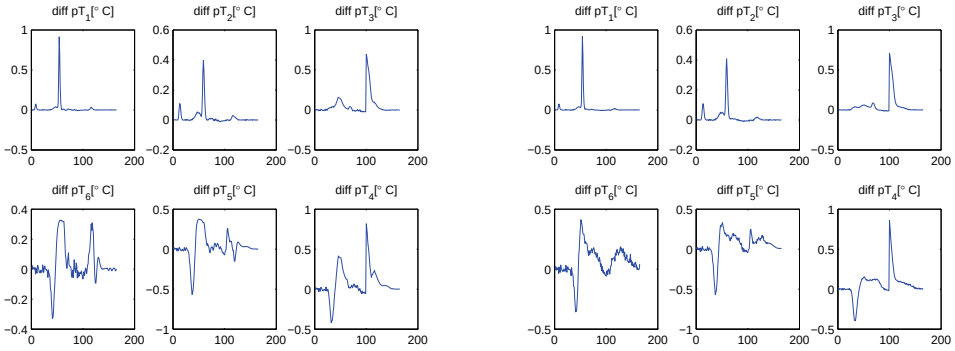

(a) (b)

Figure 6.37: Product temperatures as the dryer is subjected to input disturbances while controlling the error model. (a) displays the MPC response and (b) displays the PI control response. The values on the y-axes are calculated by $pT(k) - pT(k-1)$.

6.4.6 Response Summary

The MPC has controlled the dryer with constraints on the inputs, product temperature and product temperature rates. When applying a reference step the controller acts before the step takes place, and a closed loop response time of approximately 2000 seconds is obtained. This response is fast, compared to the time it takes the product to travel through the entire dryer, which is 3000 seconds.

When the dryer is subject to input disturbances, the MPC efficiently suppress the disturbances. The estimator using the input disturbance model (see section 3.4.7.1), is provided with the reduced version of the simulated model. The reduced model is such a close approximation to the simulated model that the disturbance estimates converge fast to the real values. This makes the MPC able to quickly react and suppress the disturbances.

It was shown on the simulations that by estimating the product temperatures at the zone exits, the MPC was able to constrain the temperatures and temperature rates of the product. Because of the long time delay from product entry to exit, the response times of steps in reference or disturbances only slightly increased when including these constraints.

When including soft constraints in the controller, it was shown that the controller could handle large disturbances pushing the states of the system outside the feasible region. Some oscillations is observed in the inputs when the slack variable is active. This could be a result of the optimization predicting when the slack variable is active, which can result in the states not being where they are supposed be at the next time step, because the slack variable has changed from the last time step. [SR99] and [RR98] suggests that by using different slack variables in future predictions, better performance can be achieved.

Table 6.10 shows the MPC input calculation duration given by the current hardware and software packages. It can be seen that by including the slack variable in the optimization criteria, the duration of the input calculation increases severely. It should also be noticed that the duration of 9.5 seconds was obtained during both reference and disturbance steps, resulting in several active constraints and therefore a very complex optimization problem. The calculations were done in MATLAB[16] on a laptop[17] running Windows 7 Enterprise 64-bit, using the QP solver *quadprog*.

When comparing the reference step responses of the MPC with the PI-control, it is clear that the MPC delivers best results. The MPC provides a faster response while respecting the constraints placed on both product temperature and product temperature rate. The same is true when comparing the resistance to disturbances. Here the MPC outperform the PI control, where

[16] MATLAB R2009b, 7.9.0.529

[17] Intel core 2 Duo CPU P8700 @ 2.53GHz 2.54GHz, 4GB DDR2 ram

Function	**Calculation duration**
Target calulation routine	0.1 second
Main optimization routine	4.5 seconds
Main optimization routine w/soft constraints	9.5 seconds

Table 6.10: Average durations of the MPC input calulation. All simulations were done with a prediction horizon of 60 timesteps.

the disturbances are almost twice as much suppressed by the MPC. It can be argued that the PI-controllers were not properly tuned, or that the configuration could be better, but the same could also be said about the MPC. Furthermore, when the MPC use exactly the same model as the process to be controlled, it is expected that the performance of a MPC is better than PI control.

When introducing a model error in the dryer model, the MPC was not able to control the process with the same configuration as previously used. An output disturbance model had to replace the input disturbance model in the Kalman filter. The new configuration of the MPC was able to control the error model with a similar *reference step* response time as the previous simulation without the modeling error. But the response of a *disturbance step* was degraded. The disturbance suppression of the MPC was now similar to the PI control. This is of course expected because the dynamics of the input disturbances are not accounted for in the output disturbance model.

The PI control was not affected (seemingly) by the modeling error / model parameter change. This was somewhat expected because PI controllers are not model dependent, which MPC is.

Chapter 7

Concluding Remarks

7.1 Conclusion

The main purpose of this thesis was to develop a model and MPC for a conveyor-belt dryer. The resulting nonlinear model describes a six-zone multiple-pass dryer accounting for the drying in the falling rate period, input disturbances, conveyor-belts with different belt speeds and product bed heights. Furthermore, a description of how to include linear input dynamics in the model, has been made.

The modeling has been thoroughly documented and inspected through simulations of a single zone as well as multiple zones. The simulations showed a realistic behavior compared to the laws of physics as well as dryer configuration. A comparison between the linear and nonlinear model, concluded in the linear model being a good approximation able to substitute the nonlinear model in a model based control application. Further, by balanced residualization the linear model was reduced from 9600 to 121 states, making the model fit for MPC.

The MPC design ensures stability and feasibility through the use of an infinite horizon objective function, a target calculation optimization routine, and soft constraints. To make the algorithm computationally efficient, only future inputs is used as optimization variables.

Closed loop simulations using the MPC showed smooth control of the dryer. Even with input disturbances affecting the dryer, constraints on the inputs, product temperature and product temperature rate was respected (if possible). Further, by applying large disturbances the states of the system were pushed outside the feasible region, and the controller was still able to provide a feasible solution to the optimization problem, due to soft constraints.

Finally, the MPC was compared to PI control of the dryer. Here the MPC outperformed the PI control while simultaneously respecting the constraints. Further, a model error was introduced, which the PI control was seemingly unaffected by. The MPC on the other hand, was unstable resulting from the

estimator not being able to converge toward the error model. This was solved by replacing the input disturbance model with an output disturbance model, which resulted in similar disturbance suppression of the control schemes. By using the output disturbance model to estimate the error model, the MPC closed loop response time to reference steps, was approximately equal to the simulation with the input disturbance model applied on the non-error model.

The MPC rejection to model/parameter errors is not good enough at this point. By using an output disturbance model, the disturbance rejection is similar to that of PI-control. There will always be modeling errors when modeling a physical process. Therefore with regard to disturbance rejection, a more robust MPC is recommended when applied to control an uncertain process.

7.2 Future Work

Even though the model extended with the falling rate provides a realistic response, it should be verified through comparison with a physical dryer. Further, in the case for model improvements, suggested future work is:

- Include airflow and belt speed as inputs in the process model. The nonlinearity of the process model will become even stronger with this extension.

- Include the vaporization constant ε as a state in the process model. Estimating ε will probably result in the MPC being more resistant to modeling errors.

- Create a model where the physical size of the zones determine the spatial discretization resolutions. A model with different zone resolutions will be more accurate and could also result in a smaller model.

Furthermore, suggested future work for improving the MPC is:

- The MPC should be more robust to modeling errors. A starting point for this could be to use the input/state and output disturbance model defined in (3.117) as the estimator model. A study to find the optimal configuration of this model must then be done. More about disturbance modeling is found in [MB02].

- Implement a less agressive controller, due to for example wear of actuators. A less aggressive controller can also suppress the oscillations caused by the soft constraint, see Figure 6.18. Solutions like including the change of input in the cost function of the optimization criteria, or by simply constraining the change of input, can be implemented

- The oscillations resulting from the slack variable should be further investigated. [SR99] and [RR98] suggests that better performance can be achieved by using different slack variables in the future predictions.
- In order to decrease the average MPC input calculation, design/study of an optimization algorithm specialized for MPC.

Appendix A

Appendix

A.1 Derivations

Similar derivations were done in [Sal08a], but the derivations here include the extention covering the drying in the falling rate.

A.1.1 Solid Phase Heat Transfer Equation

Q_s is the solid phase volumetric heat energy. The expression becomes:

$$\frac{\delta}{\delta t}E_p + v_x\frac{\delta}{\delta x}E_p = \lambda_0\delta_M + \delta_U, \tag{A.1}$$

where

$$E_p = \rho_s h_p, \tag{A.2}$$

h_p being the specific enthalpy of the solid. The specific enthalpy is defined by:

$$h_p = T_p(c_{ps} + \alpha c_{pw}), \tag{A.3}$$

where c_{ps} and c_{pw} are the specific heat capacities of the solid and water respectively.

Separating the left side of (A.1) and substituting for E_p one gets:

$$\frac{\delta}{\delta t}Q_p = \frac{\delta}{\delta t}(\rho_s h_p) \tag{A.4}$$

$$= \frac{\delta}{\delta t}(\rho_s T_s(c_{ps} + \alpha c_{pw})) \tag{A.5}$$

$$= \rho_s\left[(c_{ps} + \alpha c_{pw})\frac{\delta T_p}{\delta t} + c_{pw}T_p\frac{\delta \alpha}{\delta t}\right], \tag{A.6}$$

and similarly

$$\frac{\delta}{\delta x}Q_p = \rho_s \left[(c_{ps} + \alpha c_{pw}) \frac{\delta T_p}{\delta x} + c_{pw} T_p \frac{\delta \alpha}{\delta x} \right]. \tag{A.7}$$

Inserting (A.6) and (A.7) in the original equation, (A.1), results in the following:

$$\frac{\delta}{\delta t}Q_p + v_x \frac{\delta}{\delta x}Q_p =$$
$$\rho_s \left[(c_{ps} + \alpha c_{pw}) \frac{\delta T_p}{\delta t} + c_{pw} T_p \frac{\delta \alpha}{\delta t} \right] + \rho_s v_x \left[(c_{ps} + \alpha c_{pw}) \frac{\delta T_p}{\delta x} + c_{pw} T_p \frac{\delta \alpha}{\delta x} \right] =$$
$$\rho_s \left[(c_{ps} + \alpha c_{pw}) \left(\frac{\delta T_p}{\delta t} + v_x \frac{\delta T_p}{\delta x} \right) + c_{pw} T_p \left(\frac{\delta \alpha}{\delta t} + v_x \frac{\delta \alpha}{\delta x} \right) \right],$$
$$\Downarrow$$

$$\frac{\delta}{\delta t}Q_p + v_x \frac{\delta}{\delta x}Q_p = \rho_s \left[(c_{ps} + \alpha c_{pw}) \left(\frac{\delta T_p}{\delta t} + v_x \frac{\delta T_p}{\delta x} \right) + c_{pw} T_p \left(\frac{\delta \alpha}{\delta t} + v_x \frac{\delta \alpha}{\delta x} \right) \right]. \tag{A.8}$$

Further by inserting the right hand side of (A.1) into the left hand side of (A.8), results in the following:

$$\frac{\lambda_0 \delta_M + \delta_U}{\rho_s} = (c_{ps} + \alpha c_{pw}) \left(\frac{\delta T_p}{\delta t} + v_x \frac{\delta T_p}{\delta x} \right) + c_{pw} T_p \left(\frac{\delta \alpha}{\delta t} + v_x \frac{\delta \alpha}{\delta x} \right). \tag{A.9}$$

Finally, the *solid phase mass transfer equation*, (A.10), is inserted in (A.9):

$$\frac{\delta \alpha}{\delta t} + v_x \frac{\delta \alpha}{\delta z} = \frac{\delta_M}{\rho_s}, \tag{A.10}$$

$$\frac{\lambda_0 \delta_M + \delta_U}{\rho_s} = (c_{ps} + \alpha c_{pw}) \left(\frac{\delta T_p}{\delta t} + v_x \frac{\delta T_p}{\delta x} \right) + c_{pw} T_p \frac{\delta_M}{\rho_s},$$
$$(c_{ps} + \alpha c_{pw}) \left(\frac{\delta T_p}{\delta t} + v_x \frac{\delta T_p}{\delta x} \right) = \frac{\lambda_0 \delta_M + \delta_U - c_{pw} T_p \delta_M}{\rho_s}$$
$$\Downarrow$$

$$\boxed{\frac{\delta T_p}{\delta t} + v_x \frac{\delta T_p}{\delta x} = \frac{(\lambda_0 - c_{pw} T_p)\delta_M + \delta_U}{\rho_s (c_{ps} + \alpha c_{pw})}} \tag{A.11}$$

which concludes the proof.

A.1.2 Gas Phase Heat Transfer Equation

The gas phase heat transfer equation is given by:

$$\frac{\delta}{\delta t}Q_g + v_z\frac{\delta}{\delta z}Q_g = -\lambda_0\delta_M - \delta_U, \tag{A.12}$$

where

$$Q_g = \rho_a h_g, \tag{A.13}$$

and

$$h_g = c_{pa}T_g + \gamma(\lambda_0 + c_{pv}T_g), \tag{A.14}$$

where c_{pa} and c_{pv} are the specific heat capacities of the gas and vapor respectively.

Next, the volumetric heat is substituted and differentiated:

$$\frac{\delta}{\delta t}Q_g = \frac{\delta}{\delta t}(\rho_a h_g) \tag{A.15}$$

$$= \frac{\delta}{\delta t}\left[\rho_a(c_{pa}T_g + \gamma(\lambda_0 + c_{pv}T_g))\right] \tag{A.16}$$

$$= \rho_a\left[(c_{pa} + \gamma c_{pv})\frac{\delta T_g}{\delta t} + (\lambda_0 + c_{pv}T_g)\frac{\delta\gamma}{\delta t}\right], \tag{A.17}$$

and similarly

$$\frac{\delta}{\delta z}Q_g = \rho_a\left[(c_{pa} + \gamma c_{pv})\frac{\delta T_g}{\delta z} + (\lambda_0 + c_{pv}T_g)\frac{\delta\gamma}{\delta z}\right], \tag{A.18}$$

Inserted in the left side of the original gas phase (A.12) leads to:

$$\frac{\delta}{\delta t}Q_g + v_z\frac{\delta}{\delta z}Q_g =$$

$$\rho_a\left[(c_{pa} + \gamma c_{pv})\frac{\delta T_g}{\delta t} + (\lambda_0 + c_{pv}T_g)\frac{\delta\gamma}{\delta t}\right] + \rho_a v_z\left[(c_{PA} + \gamma c_{pv})\frac{\delta T_g}{\delta z} + (\lambda_0 + c_{pv}T_g)\frac{\delta\gamma}{\delta z}\right] =$$

$$\rho_a\left[(c_{pa} + \gamma c_{pv})\left(\frac{\delta T_g}{\delta t} + v_z\frac{\delta T_g}{\delta z}\right) + (\lambda_0 + c_{pv}T_g)\left(\frac{\delta\gamma}{\delta t} + v_z\frac{\delta\gamma}{\delta z}\right)\right],$$

$$\Downarrow$$

$$\frac{\delta}{\delta t}Q_g + v_z\frac{\delta}{\delta z}Q_g = \rho_a\left[(c_{pa} + \gamma c_{pv})\left(\frac{\delta T_g}{\delta t} + v_z\frac{\delta T_g}{\delta z}\right) + (\lambda_0 + c_{pv}T_g)\left(\frac{\delta\gamma}{\delta t} + v_z\frac{\delta\gamma}{\delta z}\right)\right]. \tag{A.19}$$

Further by inserting the right hand side of (A.12) into the left hand side of (A.19), results in the following:

$$\frac{-\lambda_0\delta_M - \delta_U}{\rho_a} = (c_{pa} + \gamma c_{pv})\left(\frac{\delta T_g}{\delta t} + v_z\frac{\delta T_g}{\delta z}\right) + (\lambda_0 + c_{pv}T_g)\left(\frac{\delta \gamma}{\delta t} + v_z\frac{\delta \gamma}{\delta z}\right). \tag{A.20}$$

Finally, by inserting the gas phase mass transfer (A.21) in (A.20), the final heat equation is revealed:

$$\frac{\partial \gamma}{\partial t} + v_z\frac{\partial \gamma}{\partial z} = -\frac{\delta_M}{\rho_a}, \tag{A.21}$$

$$\frac{-\lambda_0\delta_M - \delta_U}{\rho_a} = (c_{pa} + \gamma c_{pv})\left(\frac{\delta T_g}{\delta t} + v_z\frac{\delta T_g}{\delta z}\right) - (\lambda_0 + c_{pv}T_g)\frac{\delta_M}{\rho_a},$$

$$(c_{pa} + \gamma c_{pv})\left(\frac{\delta T_g}{\delta t} + v_z\frac{\delta T_g}{\delta z}\right) = \frac{1}{\rho_a}\left[-\lambda_0\delta_M - \delta_U + (\lambda_0 + c_{pv}T_g)\delta_M\right],$$

$$\Downarrow$$

$$\boxed{\frac{\delta T_g}{\delta t} + v_z\frac{\delta T_g}{\delta z} = \frac{c_{pv}T_g\delta_M - \delta_U}{\rho_a(c_{pa} + \gamma c_{pv})}} \tag{A.22}$$

A.2 Differentiation of the Nonlinear Terms

The nonlinear parts of the ODE's defined in (4.22-4.25) are partially differentiated and the results are shown in this appendix. The reason for this differentiation is to calculate the Jacobian J defined in (4.57).

A.2.1 The Nonlinear Functions

Product humidity (r_1):

$$\frac{\partial r_1(\mathbf{x})}{\partial x_1} = -\frac{h\varepsilon}{\lambda_0\rho_s}(x_4 - T_{dp}(x_3))\frac{\partial}{\partial x_1}\zeta(x_1) \tag{A.23}$$

$$\frac{\partial r_1(\mathbf{x})}{\partial x_2} = 0 \tag{A.24}$$

$$\frac{\partial r_1(\mathbf{x})}{\partial x_3} = \frac{h\varepsilon}{\lambda_0\rho_s}\zeta(x_1)\frac{\partial}{\partial x_3}T_{dp}(x_3) \tag{A.25}$$

$$\frac{\partial r_1(\mathbf{x})}{\partial x_4} = -\frac{h\varepsilon}{\lambda_0\rho_s}\zeta(x_1) \tag{A.26}$$

Product temperature (r_2):

$$\frac{\partial r_2(\mathbf{x})}{\partial x_1} = \left[\left(\frac{(c_{ps}+x_1c_{pw})}{\zeta(x_1)}\frac{\partial}{\partial x_1}[\zeta(x_1)] - c_{pw}\right)(\lambda_0 - c_{pw}x_4)\delta_M \right. \tag{A.27}$$
$$\left. -\delta_U c_{pw}\right]\frac{1}{\rho_s(c_{ps}+c_{pw}x_1)^2}$$
$$\frac{\partial r_2(\mathbf{x})}{\partial x_2} = -\frac{c_{pw}\delta_M + h\varepsilon}{\rho_s(c_{ps}+c_{pw}x_1)} \tag{A.28}$$
$$\frac{\partial r_2(\mathbf{x})}{\partial x_3} = \frac{\lambda_0 - c_{pw}x_4}{\rho_s(c_{ps}+c_{pw}x_1)}\frac{h\varepsilon}{\lambda_0}\zeta(x_1)\frac{\partial}{\partial x_3}T_{dp}(x_3) \tag{A.29}$$
$$\frac{\partial r_2(\mathbf{x})}{\partial x_2} = \frac{h\varepsilon - (1-\frac{c_{pw}x_2}{\lambda_0})h\varepsilon\zeta(x_1)}{\rho_s(c_{ps}+c_{pw}x_1)} \tag{A.30}$$

Air humidity (r_3):

$$\frac{\partial r_3(\mathbf{x})}{\partial x_1} = \frac{h\epsilon}{\lambda_0\rho_a}(x_4 - T_{dp}(x_3))\frac{\partial}{\partial x_1}\zeta(x_1) \tag{A.31}$$
$$\frac{\partial r_3(\mathbf{x})}{\partial x_2} = 0 \tag{A.32}$$
$$\frac{\partial r_3(\mathbf{x})}{\partial x_3} = -\frac{h\epsilon}{\lambda_0\rho_a}\zeta(x_1)\frac{\partial}{\partial x_3}T_{dp}(x_3) \tag{A.33}$$
$$\frac{\partial r_3(\mathbf{x})}{\partial x_4} = \frac{h\epsilon}{\lambda_0\rho_a}\zeta(x_1) \tag{A.34}$$

Air temperature(r_4):

$$\frac{\partial r_4(\mathbf{x})}{\partial x_1} = \frac{c_{pv}x_4\delta_M}{\rho_a(c_{pa}+c_{pv}x_3)\zeta(x_1)}\frac{\partial}{\partial x_1}\zeta(x_1) \tag{A.35}$$
$$\frac{\partial r_4(\mathbf{x})}{\partial x_2} = \frac{h\varepsilon}{\rho_a(c_{pa}+c_{pv}x_3)} \tag{A.36}$$
$$\frac{\partial r_4(\mathbf{x})}{\partial x_3} = \frac{c_{pv}x_4}{\rho_a(c_{pa}+c_{pv}x_3)^2} \tag{A.37}$$
$$\left[\frac{h\varepsilon}{\lambda_0}\zeta(x_1)(c_{pa}+c_{pv}x_3)\frac{\partial}{\partial x_3}[T_{dp}(x_3)] - c_{pv}\delta_M + \frac{\delta_U}{x_4}\right]$$
$$\frac{\partial r_4(\mathbf{x})}{\partial x_4} = \frac{h\varepsilon}{\rho_a(c_{pa}+c_{pv}x_3)}\left[\frac{c_{pv}}{\lambda_0}\big(T_{dp}(x_3) - 2x_4\big)\zeta(x_1) - 1\right] \tag{A.38}$$

A.2.2 The Dew Point Temperature

The dew point temperature is given as

$$T_{dp}(x_3) = \frac{1}{\frac{1}{T_0} - \frac{R_v}{\lambda_0}ln(\frac{P_{atm}x_3}{P_{s,0}(\beta+x_3)})} \tag{A.39}$$

The differentiation of (A.39) with respect to x_3 is given as

$$\frac{\partial}{\partial x_3} T_{dp}(x_3) = \frac{\partial f(u_1)}{\partial u_1} \cdot \frac{\partial u_1}{\partial x_3} \tag{A.40}$$

where

$$f(u_1) = \frac{1}{u_1} \qquad u_1 = \frac{1}{T_0} - \frac{R_v}{\lambda_0} ln(\frac{P_{atm} x_3}{P_{s,0}(\beta + x_3)})$$

Further is

$$\frac{\partial u_1}{\partial x_3} = -\frac{R_v}{\lambda_0} \frac{\partial}{\partial x_3} ln\left(\frac{P_{atm} x_3}{P_{s,0}(\beta + x_3)}\right) \tag{A.41}$$

$$= -\frac{R_v}{\lambda_0} \frac{\partial f(u_2)}{\partial u_2} \cdot \frac{\partial u_2}{\partial x_3} \tag{A.42}$$

where

$$f(u_2) = ln(u_2) \qquad u_2 = \frac{P_{atm} x_3}{P_{s,0}(\beta + x_3)}$$

Further is

$$\frac{\partial u_2}{\partial x_3} = \frac{P_{atm}}{P_{s,0}} \frac{\beta}{(\beta + x_3)^2} \tag{A.43}$$

equation A.42 is now given as

$$\frac{\partial u_1}{\partial x_3} = -\frac{R_v}{\lambda_0} \frac{1}{u_2} \frac{P_{atm}}{P_{s,0}} \frac{\beta}{\beta + x_3} \tag{A.44}$$

equation A.40 can now be solved as

$$\frac{\partial}{\partial x_3} T_{dp}(x_3) = \frac{\lambda_0 R_v \beta {T_0}^2}{\left[\lambda_0 - R_v ln(\frac{P_{atm} x_3}{P_{s,0}(\beta + x_3)} T_0\right]^2 (\beta + x_3) x_3} \tag{A.45}$$

A.3 Linear Structuring of Multple-Zone Dryers

This appendix contains the details behind the structure used in the linear multiple zone-model (6.2). The structure was developed in [vD09], and in order for the reader to fully understand how to contruct the matrices in (6.2), the structuring is represented here.

The multiple-zone model is a linear combination of single zones with different characteristics and linearization points. While the product and air transfer between the zones in a real dryer could be rather complex, some simplifications has been made:

- The product and air transfer between zones is instant.

- If it is mixing of the product while transferring from one zone to the next, then the resulting product states is the average of the previous product states.

- When transferring air between two zones, the resulting air states is the average of the previous air states.

- The resolution of all zones is equal. This makes implementation more practical.

More spesific, the appendix contains the details of how to transfer the product and air from one zone to another, which includes mixing of the product between some zones. Further, there are two examples of how to assemble multiple-zone dryers, first a single-pass, and then a multiple-pass dryer.

A.3.1 Transfer Between Zones

In section 4.4 it was shown that we could represent each zone as a linear model. By indexing (4.59) with j, and defining $\boldsymbol{x}$=$\boldsymbol{x}_{lin}$ we can state the linear model for zone j as

$$\dot{\boldsymbol{x}}^j = \boldsymbol{A}^j\boldsymbol{x}^j + \boldsymbol{B}^j\boldsymbol{u}^j \tag{A.46}$$

where $\boldsymbol{A}^j$ and $\boldsymbol{B}^j$ are the system matrices for zone j defined in (4.60) and (4.61), respectlively. It follows from (4.62) that the input vector to zone j is given as

$$\boldsymbol{u^j} = \begin{bmatrix} \boldsymbol{x}^j_{1,in} \\ \boldsymbol{x}^j_{2,in} \\ \boldsymbol{x}^j_{3,in} \\ \boldsymbol{x}^j_{4,in} \end{bmatrix} \tag{A.47}$$

The structure of $\boldsymbol{x}_i$ and $\boldsymbol{x}_{i,in}$ defined in (4.51) and (4.52) are summarized for the reader such that the mapping between the zones are more easily understood:

$$\boldsymbol{x}_{i,in} = \begin{bmatrix} x_{i,in(1)} \\ \overline{\mathbf{0}} \\ x_{i,in(2)} \\ \overline{\mathbf{0}} \\ \vdots \\ x_{i,in(M)} \\ \overline{\mathbf{0}} \end{bmatrix} \; i \in 1,2 \qquad \boldsymbol{x}_{i} = \begin{bmatrix} x_{i,(1,1)} \\ x_{i,(2,1)} \\ x_{i,(3,1)} \\ \vdots \\ x_{i,(N,1)} \\ x_{i,(1,2)} \\ x_{i,(2,2)} \\ x_{i,(3,2)} \\ \vdots \\ x_{i,(N,2)} \\ x_{i,(1,3)} \\ x_{i,(2,3)} \\ x_{i,(3,3)} \\ \vdots \\ x_{i,(1,M-1)} \\ \vdots \\ x_{i,(N,M)} \end{bmatrix} \; i \in [1,4]$$

$$\boldsymbol{x}_{i,in} = \begin{bmatrix} x_{i,in(1)} \\ x_{i,in(2)} \\ \vdots \\ x_{i,in(N)} \\ \underline{\mathbf{0}} \end{bmatrix} \; i \in 3,4$$

where the zero series in $\boldsymbol{x}_{i,in}$; $\underline{\mathbf{0}}$ and $\overline{\mathbf{0}}$ are defined in (4.66) and (4.64) respectively.

A.3.1.1 Transfer of product between zones

The mapping of the product state i exiting zone $j-1$ at block-height m entering zone j is defined as

$$x^{j}_{i,in}(m) = x^{j}_{i}(1,m) = x^{j-1}_{i}(N,m) \qquad i \in 1,2 \tag{A.48}$$

and this mapping can also be described in matrix form:

$$\boldsymbol{x}^{j}_{i,in} = \boldsymbol{\Gamma}_s \boldsymbol{x}^{j-1}_{i} \qquad i \in 1,2 \tag{A.49}$$

where

$$\boldsymbol{\Gamma}_s = \begin{bmatrix} \boldsymbol{\phi}_s & 0 & 0 & \cdots & 0 \\ 0 & \boldsymbol{\phi}_s & 0 & \cdots & 0 \\ 0 & 0 & \boldsymbol{\phi}_s & \cdots & 0 \\ \vdots & \vdots & \vdots & \ddots & \vdots \\ 0 & 0 & 0 & \cdots & \boldsymbol{\phi}_s \end{bmatrix} \qquad \boldsymbol{\phi}_s = \begin{bmatrix} 0 & 0 & \cdots & 1 \\ 0 & 0 & \cdots & 0 \\ \vdots & \vdots & \ddots & \vdots \\ 0 & 0 & \cdots & 0 \end{bmatrix} \tag{A.50}$$

$$dim(\boldsymbol{\Gamma}_s) = (N \cdot M) \times (N \cdot M)$$
$$dim(\boldsymbol{\phi}_s) = N \times N$$

A.3.1.2 Mixing of the product between the zones

When a multiple-zone dryer is used, it is normal to mix the product between some of the zones. This can be done just by dropping the product from an elevated zone down to a lowered zone, or sometimes the mixing can be more mechanical.

In this thesis it is assumed that when it is mixing of the product between some of the zones, then the product is completely mixed. It is also assumed that the time used to mix the product is zero.

When there is mixing between the zones, the mapping of the product state i exiting zone $j-1$ entering zone j at block-height m is defined as

$$x^j_{i,in}(m) = x^j_i(1,m) = \frac{1}{M}\sum_{k=1}^{M} x^{j-1}_i(N,k) \qquad i \in 1,2 \tag{A.51}$$

which is the average of the product states exiting the previous zone. If we want to implement this function we need a mapping matrix like we had in (A.49). This new mapping matrix, which correspond to (A.51) is defined as

$$\boldsymbol{x}^j_{i,in} = \boldsymbol{\Gamma}_{\overline{s}}\boldsymbol{x}^{j-1}_i \tag{A.52}$$

where

$$\boldsymbol{\Gamma}_{\overline{s}} = \begin{bmatrix} \boldsymbol{\phi}_{\overline{s}} & \boldsymbol{\phi}_{\overline{s}} & \cdots & \boldsymbol{\phi}_{\overline{s}} \\ \boldsymbol{\phi}_{\overline{s}} & \boldsymbol{\phi}_{\overline{s}} & \cdots & \boldsymbol{\phi}_{\overline{s}} \\ \vdots & \vdots & \ddots & \vdots \\ \boldsymbol{\phi}_{\overline{s}} & \boldsymbol{\phi}_{\overline{s}} & \cdots & \boldsymbol{\phi}_{\overline{s}} \end{bmatrix} \qquad \boldsymbol{\phi}_{\overline{s}} = \begin{bmatrix} 0 & 0 & \cdots & \frac{1}{M} \\ 0 & 0 & \cdots & 0 \\ \vdots & \vdots & \ddots & \vdots \\ 0 & 0 & \cdots & 0 \end{bmatrix} \tag{A.53}$$

$$dim(\boldsymbol{\Gamma}_{\overline{s}}) = (N \cdot M) \times (N \cdot M)$$
$$dim(\boldsymbol{\phi}_{\overline{s}}) = N \times N$$

A.3.1.3 Transfer of used air between zones

In multiple pass dryers the used air from one zone is often the input to another zone. In the following it is assumed that the air transported between the zones is completely mixed, which is not necessarily a simplification, but rather as a result of the natural way that air travel.

When mixing the air between the zones, the mapping of the air state i exiting zone h entering zone j is defined as

$$x^j_{i,in}(n) = x^j_i(n,1) = \frac{1}{N}\sum_{k=1}^{N} x^h_i(k,M) \qquad i \in 3,4 \tag{A.54}$$

which is the average of the air states exiting zone h. If we want to implement this function we need a mapping matrix like we had in (A.49) and (A.52). This new mapping matrix, which correspond to (A.54) is defined as

$$\boldsymbol{x}_{i,in}^{j} = \boldsymbol{\Gamma}_g \boldsymbol{x}_i^h \tag{A.55}$$

where

$$\boldsymbol{\Gamma}_g = \begin{bmatrix} 0 & 0 & \cdots & \boldsymbol{\phi}_g \\ 0 & 0 & \cdots & 0 \\ \vdots & \vdots & \ddots & \vdots \\ 0 & 0 & \cdots & 0 \end{bmatrix} \qquad \boldsymbol{\phi}_g = \begin{bmatrix} \frac{1}{N} & \frac{1}{N} & \cdots & \frac{1}{N} \\ \frac{1}{N} & \frac{1}{N} & \cdots & \frac{1}{N} \\ \vdots & \vdots & \ddots & \vdots \\ \frac{1}{N} & \frac{1}{N} & \cdots & \frac{1}{N} \end{bmatrix} \tag{A.56}$$

$$dim(\boldsymbol{\Gamma}_g) = (N \cdot M) \times (N \cdot M)$$
$$dim(\boldsymbol{\phi}_g) = N \times N$$

A.3.2 Structure of the Input Vector

Here we construct the input vector (A.47) to zone j . This vector depends on the configuration of the zone. Several configurations of product transfer between the zones is possible:

1. The zone is the first zone of the dryer and therefore there is no product transfer from previous zones.
2. Transfer of product from the previous zone.
3. Transfer of product from the previous zone with mixing included.

for each of the configurations stated above, there is also a configuration of air input/transfer to the zone:

- Air input to the zone is fresh air, i.e. it is a manipulated variable for the dryer.
- Air input to the zone is used air, i.e. it is transferred from another zone.

All together this makes 6 possible configurations of transfer to the zone. We can now construct the input vector as a combination of product transfer and air transfer:

$$\boldsymbol{u}^j = \boldsymbol{x}_{s,in}^j + \boldsymbol{x}_{g,in}^j \tag{A.57}$$

where $\boldsymbol{u}^j$ is the input vector to zone j. This vector is a combination of the input vector of the product $\boldsymbol{x}_{s,in}^j$ and the air $\boldsymbol{x}_{g,in}^j$.

A.3.2.1 Product and Air Configurations

The two vectors in (A.57) will now be defined for the different configurations mentioned above.

If the product is transfered from the previous zone, i.e. if this is not the first zone of the dryer, then we can state the product input vector for zone j as

$$\boldsymbol{x}_{s,in}^{j} = \boldsymbol{\Phi}_s \boldsymbol{x}^{j-1} \tag{A.58}$$

where $\boldsymbol{x}^{j-1}$ is the states of zone $j-1$ where the product is transferred from. $\boldsymbol{\Phi}_s$ is the product transition matrix between the systems, and is defined as

$$\boldsymbol{\Phi}_s = \begin{bmatrix} \boldsymbol{\Gamma}_s & 0 & 0 & 0 \\ 0 & \boldsymbol{\Gamma}_s & 0 & 0 \\ 0 & 0 & 0 & 0 \\ 0 & 0 & 0 & 0 \end{bmatrix} \tag{A.59}$$

If there is mixing of the product between the zones, then $\boldsymbol{\Phi}_s$ in (A.58) can be replaced by

$$\boldsymbol{\Phi}_{\overline{s}} = \begin{bmatrix} \boldsymbol{\Gamma}_{\overline{s}} & 0 & 0 & 0 \\ 0 & \boldsymbol{\Gamma}_{\overline{s}} & 0 & 0 \\ 0 & 0 & 0 & 0 \\ 0 & 0 & 0 & 0 \end{bmatrix} \tag{A.60}$$

$$dim(\boldsymbol{\Phi}_s) = dim(\boldsymbol{\Phi}_{\overline{s}}) = (N \cdot M \cdot 4) \times (N \cdot M \cdot 4)$$

where $\boldsymbol{\Gamma}_s$ and $\boldsymbol{\Gamma}_{\overline{s}}$ is given in (A.50) and (A.53), respectively.

If the zone is the first zone of the dryer $(j = 1)$, we can state the product input vector as

$$\boldsymbol{x}_{s,in}^{1} = \boldsymbol{B}_s \boldsymbol{u}_s \tag{A.61}$$

where

$$\boldsymbol{B}_s = \begin{bmatrix} \boldsymbol{\delta} & 0 \\ 0 & \boldsymbol{\delta} \\ 0 & 0 \\ 0 & 0 \end{bmatrix} \qquad \boldsymbol{u}_s = \begin{bmatrix} \alpha_{in} \\ T_{s,in} \end{bmatrix} \tag{A.62}$$

α_{in}^{j} and $T_{s,in}^{j}$ is the humidity and the temperature of the product entering the dryer. $\boldsymbol{\delta}$ is defined in (4.64)

If the air input to the zone is a manipulated variable for the dryer, we can state the air input vector for zone j as

$$\boldsymbol{x}_{g,in}^{j} = \boldsymbol{B}_g \boldsymbol{u}_j \tag{A.63}$$

where

$$\boldsymbol{B}_g = \begin{bmatrix} 0 & 0 \\ 0 & 0 \\ \boldsymbol{\sigma} & 0 \\ 0 & \boldsymbol{\sigma} \end{bmatrix} \qquad \boldsymbol{u}_j = \begin{bmatrix} \gamma_{in}^{j} \\ T_{g,in}^{j} \end{bmatrix} \tag{A.64}$$

γ_{in}^{j} and $T_{g,in}^{j}$ is the humidity and the temperature of the air entering zone j. $\boldsymbol{\sigma}$ is defined in (4.66)

If the air input to the zone is used air from another zone, we can state the air input vector for zone j as

$$\boldsymbol{x}_{g,in}^{j} = \boldsymbol{\Phi}_g \boldsymbol{x}^h \tag{A.65}$$

where $\boldsymbol{x}^h$ is the states of zone h where used air is transferred from. $\boldsymbol{\Phi}_g$ is the air transition matrix between the systems, and is defined as

$$\boldsymbol{\Phi}_g = \begin{bmatrix} 0 & 0 & 0 & 0 \\ 0 & 0 & 0 & 0 \\ 0 & 0 & \boldsymbol{\Gamma}_g & 0 \\ 0 & 0 & 0 & \boldsymbol{\Gamma}_g \end{bmatrix} \tag{A.66}$$

$$dim(\boldsymbol{\Phi}_g) = (N \cdot M \cdot 4) \times (N \cdot M \cdot 4)$$

where $\boldsymbol{\Gamma}_g$ is given in (A.56).

A.3.2.2 Two Input Vector Examples

If both product and air is transferred from other zones, we can state (A.57) as

$$\boldsymbol{u}^j = \boldsymbol{\Phi}_s \boldsymbol{x}^{j-1} + \boldsymbol{\Phi}_g \boldsymbol{x}^h \tag{A.67}$$

where $\boldsymbol{x}^{j-1}$ is the states of zone $j-1$ where the product is transferred from, and $\boldsymbol{x}^h$ is the states of zone h where the used air is transferred from.

If the first zone of the dryer uses fresh air, the input vector is not dependent on the other zones of the dryer, and can therefore be stated as the sum of two external inputs:

$$\boldsymbol{u}^j = \boldsymbol{B}_s \boldsymbol{u}_s + \boldsymbol{B}_g \boldsymbol{u}_1 \tag{A.68}$$

where $\boldsymbol{u}_s$ and $\boldsymbol{u}_1$ is defined in (A.62) and (A.64), respectively.

A.3.3 Assembling the Multiple Zone System

We now want to describe the multiple zone dryer as one linear system. By utilizing the input vector in (A.57) to gather the zones defined in (A.46) into one system, a dryer containing L zones and K external air inputs can be defined as

$$\dot{\hat{\boldsymbol{x}}} = \hat{\boldsymbol{A}}\hat{\boldsymbol{x}} + \hat{\boldsymbol{B}}\hat{\boldsymbol{u}} \tag{A.69}$$

where

$$\hat{\boldsymbol{x}} = \begin{bmatrix} \boldsymbol{x}^1 \\ \boldsymbol{x}^2 \\ \boldsymbol{x}^3 \\ \vdots \\ \boldsymbol{x}^L \end{bmatrix} \qquad \hat{\boldsymbol{u}} = \begin{bmatrix} \boldsymbol{u}_s \\ \boldsymbol{u}_1 \\ \boldsymbol{u}_2 \\ \boldsymbol{u}_3 \\ \vdots \\ \boldsymbol{u}_K \end{bmatrix} \tag{A.70}$$

$$dim(\hat{\boldsymbol{A}}) = (N \cdot M \cdot 4 \cdot L) \times (N \cdot M \cdot 4 \cdot L)$$
$$dim(\hat{\boldsymbol{B}}) = (N \cdot M \cdot 4 \cdot L) \times (2 \cdot K)$$

and $\hat{\boldsymbol{A}}$ and $\hat{\boldsymbol{B}}$ are the dryer configuration matrices. Since these are dependent on the configuration of the dryer, we need example systems to construct these matrices.

A.3.3.1 Example 1: single pass/multiple-stage dryer

Here the dryer is a single pass/multiple-stage dryer with 4 zones. The dryer is illustrated in Figure A.1. The product is mixed two times during the drying. The first mixing takes place between zone 1 and 2, while the second mixing takes place between zone 3 and 4. The dryer has four external air inputs, e.g. there is no air transfer between the zones.

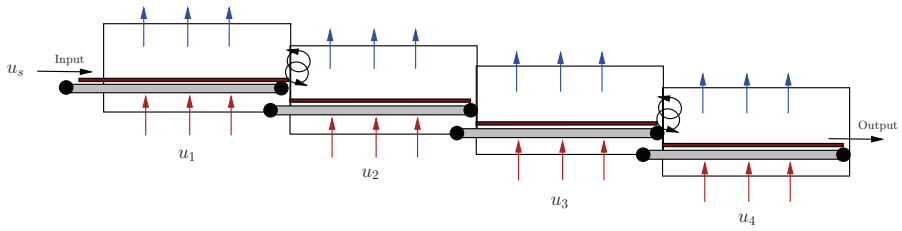

Figure A.1: Illustration of the configuration of the single pass dryer used in Example 1.

We can state the total system as:

$$\dot{\hat{\boldsymbol{x}}} = \hat{\boldsymbol{A}}\hat{\boldsymbol{x}} + \hat{\boldsymbol{B}}\hat{\boldsymbol{u}} \tag{A.71}$$

where

$$\hat{\boldsymbol{x}} = \begin{bmatrix} \boldsymbol{x}^1 \\ \boldsymbol{x}^2 \\ \boldsymbol{x}^3 \\ \boldsymbol{x}^4 \end{bmatrix} \qquad \hat{\boldsymbol{u}} = \begin{bmatrix} \boldsymbol{u}_s \\ \boldsymbol{u}_1 \\ \boldsymbol{u}_2 \\ \boldsymbol{u}_3 \\ \boldsymbol{u}_4 \end{bmatrix} \tag{A.72}$$

where the input vector to zone j was defined in (A.57). The dryer configuration matrices are given as

$$\hat{\boldsymbol{A}} = \begin{bmatrix} \boldsymbol{A}^1 & 0 & 0 & 0 \\ \boldsymbol{B}^2\boldsymbol{\Phi}_{\overline{s}} & \boldsymbol{A}^2 & 0 & 0 \\ 0 & \boldsymbol{B}^3\boldsymbol{\Phi} & \boldsymbol{A}^3 & 0 \\ 0 & 0 & \boldsymbol{B}^4\boldsymbol{\Phi}_{\overline{s}} & \boldsymbol{A}^4 \end{bmatrix} \tag{A.73}$$

$$\hat{\boldsymbol{B}} = \begin{bmatrix} \boldsymbol{B}^1\boldsymbol{B}_s & \boldsymbol{B}^1\boldsymbol{B}_g & 0 & 0 & 0 \\ 0 & 0 & \boldsymbol{B}^2\boldsymbol{B}_g & 0 & 0 \\ 0 & 0 & 0 & \boldsymbol{B}^3\boldsymbol{B}_g & 0 \\ 0 & 0 & 0 & 0 & \boldsymbol{B}^4\boldsymbol{B}_g \end{bmatrix} \tag{A.74}$$

where $\boldsymbol{A}^j$, $\boldsymbol{B}^j$, $\boldsymbol{B}_s$, $\boldsymbol{B}_g$, $\boldsymbol{\Phi}_s$ and $\boldsymbol{\Phi}_{\overline{s}}$ were defined in (4.60), (4.61), (A.62), (A.64), (A.59) and (A.60) respectively.

A.3.3.2 Example 2: multiple pass dryer

Here the dryer is a multiple pass/multiple-stage dryer with 4 zones. The dryer is illustrated in Figure A.2. The product is mixed once during the drying and it takes place between zone 2 and 3. The dryer has external air inputs in zone 3 and zone 4. The used air from zone 3 and 4 is reused in zone 2 and 1, respectively.

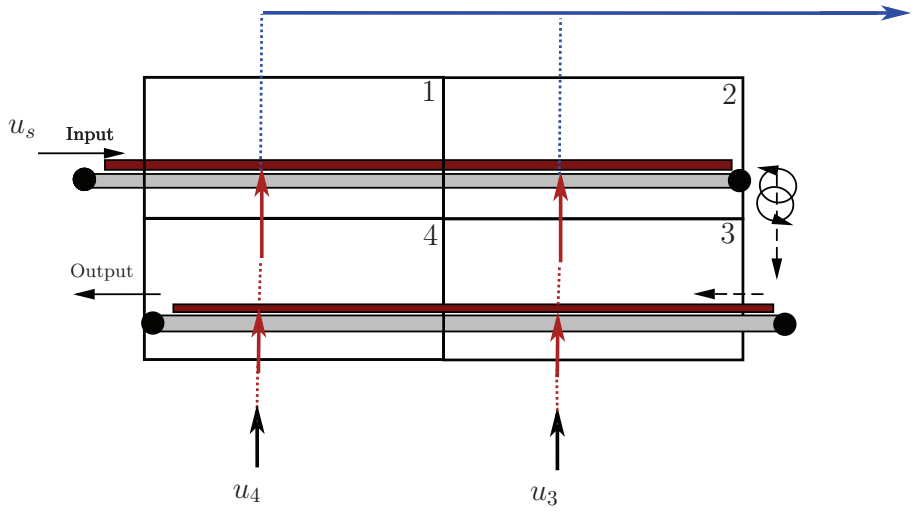

Figure A.2: Illustration of the configuration of the multiple pass dryer used in Example 2.

We can state the total system as:

$$\dot{\hat{\boldsymbol{x}}} = \hat{\boldsymbol{A}}\hat{\boldsymbol{x}} + \hat{\boldsymbol{B}}\hat{\boldsymbol{u}} \tag{A.75}$$

where

$$\hat{\boldsymbol{x}} = \begin{bmatrix} \boldsymbol{x}^1 \\ \boldsymbol{x}^2 \\ \boldsymbol{x}^3 \\ \boldsymbol{x}^4 \end{bmatrix} \qquad \hat{\boldsymbol{u}} = \begin{bmatrix} \boldsymbol{u}_s \\ \boldsymbol{u}_3 \\ \boldsymbol{u}_4 \end{bmatrix} \tag{A.76}$$

where the input vector to zone j was defined in (A.57). The dryer configuration matrices are given as

$$\hat{\boldsymbol{A}} = \begin{bmatrix} \boldsymbol{A}^1 & 0 & 0 & \boldsymbol{B}^1\boldsymbol{\Phi}_g \\ \boldsymbol{B}^2\boldsymbol{\Phi}_s & \boldsymbol{A}^2 & \boldsymbol{B}^2\boldsymbol{\Phi}_g & 0 \\ 0 & \boldsymbol{B}^3\boldsymbol{\Phi}_{\overline{s}} & \boldsymbol{A}^3 & 0 \\ 0 & 0 & \boldsymbol{B}^4\boldsymbol{\Phi}_s & \boldsymbol{A}^4 \end{bmatrix} \tag{A.77}$$

$$\hat{\boldsymbol{B}} = \begin{bmatrix} \boldsymbol{B}^1\boldsymbol{B}_s & 0 & 0 \\ 0 & 0 & 0 \\ 0 & \boldsymbol{B}^3\boldsymbol{B}_u & 0 \\ 0 & 0 & \boldsymbol{B}^4\boldsymbol{B}_u \end{bmatrix} \tag{A.78}$$

where $\boldsymbol{A}^j$, $\boldsymbol{B}^j$, $\boldsymbol{B}_s$, $\boldsymbol{B}_g$, $\boldsymbol{\Phi}_s$, $\boldsymbol{\Phi}_{\overline{s}}$ and $\boldsymbol{\Phi}_g$ were defined in (4.60), (4.61), (A.62), (A.64), (A.59), (A.60) and (A.66) respectively.

A.3.4 Defining the Output Vector

In the previous section the linear model which described the multiple zone dryer was defined as

$$\dot{\hat{\boldsymbol{x}}} = \hat{\boldsymbol{A}}\hat{\boldsymbol{x}} + \hat{\boldsymbol{B}}\hat{\boldsymbol{u}} \tag{A.79}$$

If the linear model is to be used in a control application, all the states will not be needed. So we define our output for the linear system as

$$\boldsymbol{y} = \hat{\boldsymbol{C}}\hat{\boldsymbol{x}} \tag{A.80}$$

Here $\boldsymbol{C}$ will be defined in such a way, that $\boldsymbol{y}$ will contain the information that a control application would need. It is assumed that the control application would only need the average exit value of each state from each zone. While there are four states, the length of y becomes $dim(\boldsymbol{y}) = (4 \cdot L) \times 1$ where L is the number of zones the dryer consist of.

If we define the scalar variables α_m^j, $T_{s,m}^j$, γ_m^j, $T_{g,m}^j$ as the average exit values of zone j for the product moisture, product temperature, air moisture

and air temperature, respectively. Then the output vector can be defined as:

$$\boldsymbol{y} = \begin{bmatrix} \alpha_m^1 \\ T_{s,m}^1 \\ \gamma_m^1 \\ T_{g,m}^1 \\ \vdots \\ \alpha_m^L \\ T_{s,m}^L \\ \gamma_m^L \\ T_{g,m}^L \end{bmatrix} = \begin{bmatrix} \boldsymbol{C} & 0 & \cdots & 0 \\ 0 & \boldsymbol{C} & \cdots & 0 \\ \vdots & \vdots & \ddots & \vdots \\ 0 & 0 & \cdots & \boldsymbol{C} \end{bmatrix} \begin{bmatrix} \boldsymbol{x}^1 \\ \boldsymbol{x}^2 \\ \vdots \\ \boldsymbol{x}^L \end{bmatrix} = \hat{\boldsymbol{C}}\hat{\boldsymbol{x}} \tag{A.81}$$

where

$$\boldsymbol{C} = \begin{bmatrix} \boldsymbol{C}_s & 0 & 0 & 0 \\ 0 & \boldsymbol{C}_s & 0 & 0 \\ 0 & 0 & \boldsymbol{C}_g & 0 \\ 0 & 0 & 0 & \boldsymbol{C}_g \end{bmatrix} \qquad \begin{aligned} \boldsymbol{C}_s &= \underbrace{\begin{bmatrix} \boldsymbol{\varphi} & \boldsymbol{\varphi} & \cdots & \boldsymbol{\varphi} \end{bmatrix}}_{N \cdot M} \\ \boldsymbol{C}_g &= \begin{bmatrix} \underbrace{0 \quad \cdots \quad 0}_{N \cdot (M-1)} & \underbrace{\frac{1}{N} \quad \cdots \quad \frac{1}{N}}_{N} \end{bmatrix} \end{aligned} \tag{A.82}$$

$$\boldsymbol{\varphi} = \underbrace{\begin{bmatrix} 0 & \cdots & 0 & \frac{1}{M} \end{bmatrix}}_{N} \tag{A.83}$$

$$\begin{aligned} dim(\hat{\boldsymbol{C}}) &= (4 \cdot L) \times (N \cdot M \cdot 4 \cdot L) \\ dim(\boldsymbol{C}) &= 4 \times (N \cdot M \cdot 4) \end{aligned}$$

Nomenclature

Background theory nomenclature:

m_p = mass, product [kg]
m_s = mass, solid [kg]
m_w = mass, water [kg]
m_g = mass, product [kg]
m_a = mass, air [kg]
m_v = mass, vapor [kg]
α = humidity ratio, product [kg/kg]
γ = humidity ratio, air [kg/kg]
M_p = mass per volume unit, product [kg/m^3]
M_g = mass per volume unit, gas [kg/m^3]
T_{dp} = temperature, dew point [°C]
T_0 = reference temperature, gas [K]
p_a = partial pressure, air [hPa]
p_v = partial pressure, vapor [hPa]
$p_{s,0}$ = saturated partial pressure at reference temperature [hPa]
R_v = specific gas constant [J/kg K]
λ_0 = heat of vaporization, water [J/kg]
β = spesific mass ratio, steam/dry air [1]
$\zeta(\alpha)$ = falling rate multiplicator of the drying rate [1]
θ = order of the polynomial fit used in the falling rate

E_p = energy, product [J]
E_g = energy, gas [J]
T_p = temperature, product [°C]
T_g = temperature, gas [°C]
w_p = mass flow, product [kg/s]
w_s = mass flow, solid [kg/s]
w_g = mass flow, gas [kg/s]
w_a = mass flow, air [kg/s]
ρ_s = mass density, dry solid [kg/m^3]
ρ_a = mass density, dry air [kg/m^3]
v_p = velocity, conveyor-belt [m/s]
v_g = velocity, air stream [m/s]
c_{pp} = specific heat capacity, product [J/kg °C]
c_{pg} = specific heat capacity, gas [J/kg °C]
c_{pa} = specific heat capacity, air [J/kg °C]
c_{pv} = specific heat capacity, vapor [J/kg °C]
c_{ps} = specific heat capacity, solid [J/kg °C]
c_{pw} = specific heat capacity, water [J/kg °C]

Case study nomenclature:

$pT_{i,in}$ = input product temperature, zone i [°C]
$pT_{i,out}$ = output product temperature, zone i [°C]
$gT_{i,in}$ = input gas temperature, zone i [°C]
$gT_{i,out}$ = output gas temperature, zone i [°C]
$\alpha_{i,in}$ = input product moisture, zone i [kg/kg]
$\alpha_{i,out}$ = output product moisture, zone i [kg/kg]
$\gamma_{i,in}$ = input gas moisture, zone i [kg/kg]
$\gamma_{i,out}$ = output gas moisture, zone i [kg/kg]
H_u = Input prediction horizon for the MPC [timesteps]
T_s = sampling time for the MPC [s]

Nonlinear model nomenclature:

T_p = temperature, product [°C]
T_g = temperature, gas [°C]
α = humidity ratio, product [kg/kg]
γ = humidity ratio, air [kg/kg]
δ_M = Drying rate [kg/m^3/s]
δ_U = Heat transfer [J/m^3/s]
T_{dp} = temperature, dew point [°C]
$\zeta(\alpha)$ = falling rate multiplicator of the drying rate [1]
c_{pa} = specific heat capacity, air [J/kg °C]
c_{pv} = specific heat capacity, vapor [J/kg °C]
c_{ps} = specific heat capacity, solid [J/kg °C]
c_{pw} = specific heat capacity, water [J/kg °C]
ρ_s = mass density, dry solid [kg/m^3]
ρ_a = mass density, dry air [kg/m^3]
v_x = velocity, conveyor-belt [m/s]
v_z = velocity, air stream [m/s]
h = heat transfer coefficient [J/s m^2 °C]
ε = evaporation area/product volume ratio [1/m]
λ_0 = heat of vaporization, water [J/kg]
M_p = total mass per volume unit, product [kg/m^3]
M_g = total mass per volume unit, gas [kg/m^3]
Q_p = total energy per volume unit, product [J/m^3]
Q_g = total energy per volume unit, gas [J/m^3]
h_p = enthalpy, product [J/kg]
h_g = enthalpy, gas [J/kg]
T_0 = reference temperature, gas [K]
$p_{s,0}$ = partial pressure at reference temperature [hPa]
R_v = specific gas constant [J/kg K]
p_θ = polynomial coefficient in the falling rate
θ = order of the polynomial fit used in the falling rate
p_a = partial pressure, air [hPa]
p_v = partial pressure, vapor [hPa]
$P_{atm} = p_a + p_v$

Bibliography

[ASM07] editor Arun S. Mujumdar. Handbook of industrial drying. *CRC/Taylor & Francis, 3 edition*, 2007.

[Che99] Chi-Tsong Chen. Linear system theory and design. *Oxford, 3 edition*, 1999.

[CTK94] Z. B. Maroulis & D. Marios-Kouris C. T. Kiranoudis. Modeling and design of conveyor belt dryers. *Journal of Food Engineering 23, Department of Chemical Engineering, NAtional Techincal University, Athens, Greece*, 1994.

[EG03] O. Egeland and J. T. Gravdahl. Modeling and simulation for automatic control. *Marine Cybernetics*, 2003.

[Hov08] Morten Hovd. Dr. ing. process control, b.sc. (hons) natural gas engineering. *The Norwegian University of Sciece and Technology, Department of Engineering Cybernetics*, e-mail 2010 19th of March 13:08.

[Hwa97] R. G. Brown & Patrick Y. C. Hwang. Introduction to random signals and applied kalman filtering, third edition. *John Wiley & Sons*, 1997.

[Lyd85] Aksel L. Lydersen. Mass transfer in engineering practice. *John Wiley & Sons*, 1985.

[Mac02] J. M. Maciejowski. Predictive control with constrains. *Prentice Hall*, 2002.

[MB02] K. R. Muske and T. A. Badgwell. Disturbance modeling for offset-free linear model predictive control. *Journal of Process Control*, 2002.

[MGV01] Gary L. Barker Mathew G.Pelletier, Joseph W. Laird and Suhas V.Patankar. Engineering & ginning, analysis and design of a dryer model for use in the design of starch-coated cottonseed dryers. *The journal of Cotton Science, The Cotton Foundation*, 2001.

[Mus97] K. R. Muske. Steady-state target optimization in linear model predictive control. *Proceedings of the American Control Conference*, 1997.

[RR98] S. J. Wright Rao, C. V. and J. B. Rawlings. Application of interior-point methods to model predictive control. *Journal of Optimization Theory and Applications 99*, 1998.

[Sal08a] John Paul Salvador. Dynamic control and simulation of conveyor-belt dryers. *Master thesis, The Norwegian University of Science and Technology*, 2008.

[Sal08b] John Paul Salvador. Regulering av fuktighetsinnhold i fiskefòr. en analyse av båndtørking av fiskefòr. *Final year project, The Norwegian University of Science and Technology*, 2008.

[Shi94] F.G. Shinskey. Feedback controllers for the process industries. *McGraw-Hill*, 1994.

[SP05] S. Skogestad and I. Postlethwaite. Multivariable feedback control. *John Wiley & Sons, 2nd edition*, 2005.

[SR99] P. O. M. Scokaert and J. B. Rawlings. Feasibility issues in linear model predictive control. *AIChE Journal 45*, 1999.

[vD09] Tord van Delft. Modeling of conveyor-belt dryers. *Final year project, The Norwegian University of Sciece and Technology*, 2009.